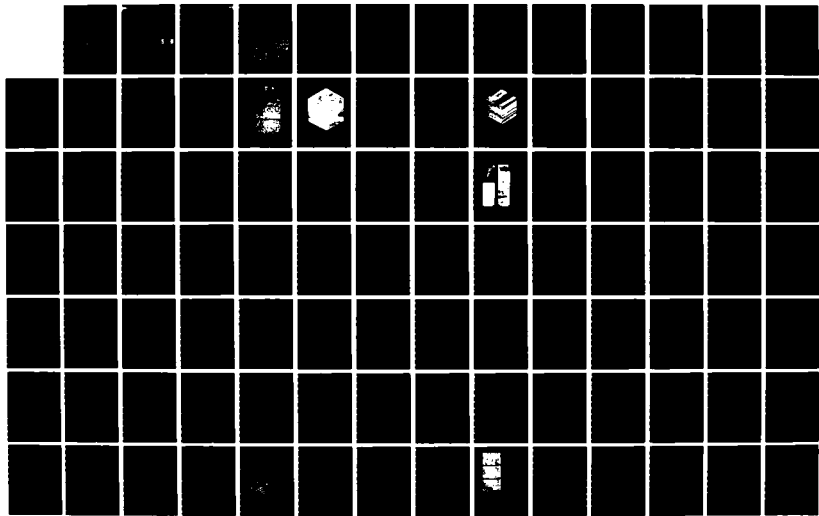AD-A169 980   FATIGUE BEHAVIOR OF LONG AND SHORT CRACKS IN WROUGHT   1/2
              AND POWDER ALUMINUM..(U) CALIFORNIA UNIV BERKELEY DEPT
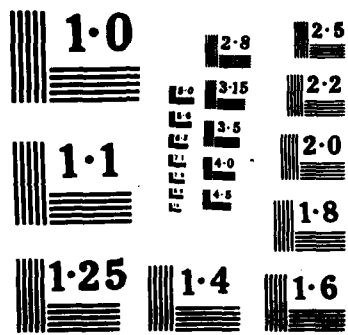   OF MATERIALS SCIENCE AND MINERA..   R O RITCHIE ET AL.
UNCLASSIFIED 01 MAY 86 UCB/RP/86/A1040 AFOSR-TR-86-0447 F/G 11/6   NL

AD-A169 980

ENTATION PAGE

1a. REPORT SECURITY	1b. RESTRICTIVE MARKINGS
Unclassified	None

2a. SECURITY CLASSIFICATION AUTHORITY	3. DISTRIBUTION / AVAILABILITY OF REPORT
Not Applicable	
2b. DECLASSIFICATION / DOWNGRADING SCHEDULE	Not Applicable
Not Applicable	

4. PERFORMING ORGANIZATION REPORT NUMBER(S)	5. MONITORING ORGANIZATION REPORT NUMBER(S)
UCB/RP/86/A1040	AFOSR-TR- 86-0447

6a. NAME OF PERFORMING ORGANIZATION	6b. OFFICE SYMBOL (If applicable)	7a. NAME OF MONITORING ORGANIZATION
Robert O. Ritchie, Dept. of Mat. Sci. & Minl. Eng.		Air Force Office of Scientific Research AFOSR/NE

6c. ADDRESS (City, State, and ZIP Code)	7b. ADDRESS (City, State, and ZIP Code)
University of California Hearst Mining Building Berkeley, California 94720	Bldg. 410, Bolling AFB Washington, D.C. 20322 ATTN: Dr. A. H. Rosenstein, AFOSR/NE

8a. NAME OF FUNDING / SPONSORING ORGANIZATION	8b. OFFICE SYMBOL (If applicable)	9. PROCUREMENT INSTRUMENT IDENTIFICATION NUMBER
AFOSR	NE	AFOSR-82-0181

8c. ADDRESS (City, State, and ZIP Code)	10. SOURCE OF FUNDING NUMBERS			
Bolling AFB DC 20332-6448	PROGRAM ELEMENT NO.	PROJECT NO.	TASK NO.	WORK UNIT ACCESSION NO.
	61102	2306	A1	

11. TITLE (Include Security Classification)
FATIGUE BEHAVIOR OF LONG AND SHORT CRACKS IN WROUGHT AND POWDER ALUMINUM ALLOYS (Unclassified)

12. PERSONAL AUTHOR(S)
RITCHIE, Robert O. and YU, Weikang

13a. TYPE OF REPORT	13b. TIME COVERED	14. DATE OF REPORT (Year, Month, Day)	PAGE COUNT
Annual	FROM 85/4/15 TO 86/4/14	1986 May 1	

16. SUPPLEMENTARY NOTATION

DTIC
ELECTE
S
JUL 2 3 1986
D

17.	COSATI CODES		18. SUBJECT TERMS (Continue on reverse if necessary and identify by block number)
FIELD	GROUP	SUB-GROUP	Fatigue; Defect-tolerant fatigue design; Variable amplitude loading; Fatigue in aluminum alloys; Fatigue behavior of long and short cracks; Fatigue cracks: crack closure

19. ABSTRACT (Continue on reverse if necessary and identify by block number)

The fatigue behavior of short cracks, which are small compared to the scale of the microstructure, small compared to the scale of local plasticity or simply physically small (i.e., ≤ 1 mm), must be considered as one of the major factors limiting the application of defect-tolerant fatigue design for airframe and engine components. Accordingly, the current program is aimed at identifying factors which govern the growth of such short cracks (in contrast to long cracks) in a series of commercial aluminum alloys, with specific reference to behavior at near-threshold levels (below $\sim 10^{-6}$ mm/cycle). In this annual report, the status of the program is described in terms of i) a description of results on the role of compression overloads in influencing fatigue crack growth in a new aluminum-lithium alloy (2090) and a comparison of behavior with results in 2124 and 7150, ii) an evaluation of the role of crack tip shielding in controlling the growth of short (50 to 400 μm) through-thickness cracks and small (10 to 400 μm) surface cracks in 2124, and iii) a general assessment of the small crack problem. It is concluded that the near-

20. DISTRIBUTION / AVAILABILITY OF ABSTRACT	21. ABSTRACT SECURITY CLASSIFICATION
☒ UNCLASSIFIED/UNLIMITED ☐ SAME AS RPT. ☐ DTIC USERS	Unclassified

22a. NAME OF RESPONSIBLE INDIVIDUAL	22b. TELEPHONE (Include Area Code)	22c. OFFICE SYMBOL
Dr. Alan Rosenstein	(202) 767-4933	AFOSR/NE

DD FORM 1473, 84 MAR   83 APR edition may be used until exhausted.   All other editions are obsolete.

86

SECURITY CLASSIFICATION OF THIS PAGE
Unclassified

threshold behavior of long cracks and the near- and sub-threshold behavior of small cracks is strongly influenced by considerations of crack tip shielding, specifically from crack deflection and crack closure mechanisms. Other factors responsible for "anomalous" small crack behavior, however, can be identified and are discussed in the report.
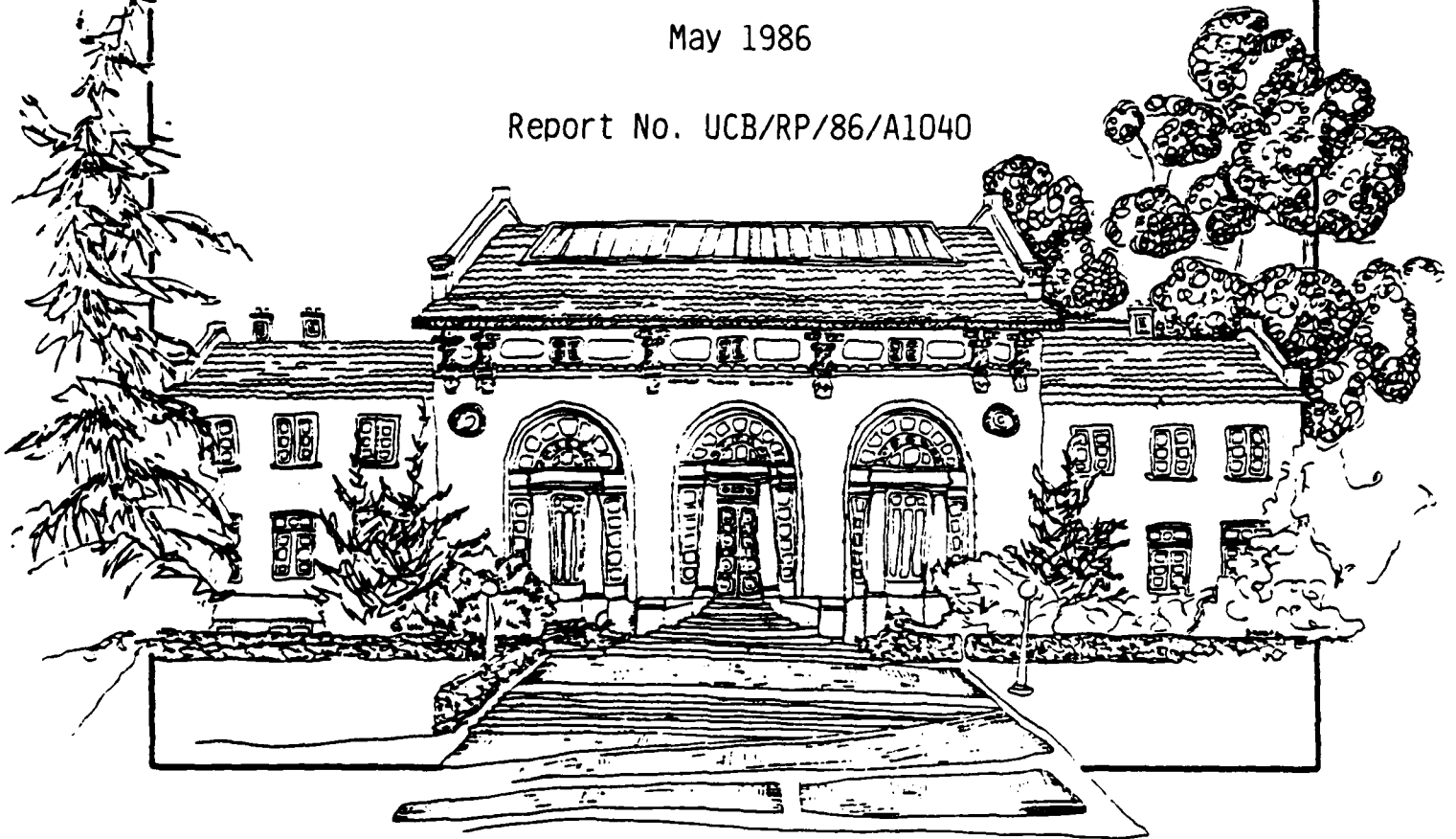
Annual Report
to
U.S. Air Force Office of Scientific Research

on

FATIGUE BEHAVIOR OF LONG AND SHORT CRACKS IN WROUGHT AND POWDER ALUMINUM ALLOYS

Grant AFOSR-82-0181

for period 15 April 1985 to 14 April 1986

by

R. O. Ritchie and W. Yu

May 1986

Report No. UCB/RP/86/A1040

Department of Materials Science and Mineral Engineering
University of California, Berkeley, CA 94720

Annual Report

to

U.S. Air Force Office of Scientific Research

on

FATIGUE BEHAVIOR OF LONG AND SHORT CRACKS

IN WROUGHT AND POWDER ALUMINUM ALLOYS

Grant AFOSR-82-0181

for period 15 April 1985 to 14 April 1986

submitted to

U.S. Air Force Office of Scientific Research
Bldg. 410, Bolling Air Force Base
Washington, D.C.   20322
Attention: Dr. Alan H. Rosenstein

submitted by

R. O. Ritchie and W. Yu
Department of Materials Science and Mineral Engineering
University of California
Berkeley, California   94720

May 1986

TABLE OF CONTENTS

-ii-

FATIGUE BEHAVIOR OF LONG AND SHORT CRACKS
IN WROUGHT AND POWDER ALUMINUM ALLOYS

R. O. Ritchie

(Grant No. AFOSR-82-0181)

FORWARD

Accesion For		
NTIS CRA&I	☑	
DTIC TAB	☐	
Unannou:ced	☐	
Justification		
By		
Distribution /		
Availability Codes		
Dist	Avail and / or Special	
A-1		

QUALITY INSPECTED 4

-iv-

ABSTRACT

The fatigue behavior of short cracks, which are small compared
to the scale of the microstructure, small compared to the scale of
local plasticity or simply physically small (i.e., $\leq$ 1 mm), must be
considered as one of the major factors limiting the application of
defect-tolerant fatigue design for airframe and engine components.
Accordingly, the current program is aimed at identifying factors
which govern the growth of such short cracks (in contrast to long
cracks) in a series of commercial aluminum alloys, with specific
reference to behavior at near-threshold levels (below $\sim 10^{-6}$
mm/cycle). In this annual report, the status of the program is
described in terms of i) a description of results on the role of
compression overloads in influencing fatigue crack growth in a new
aluminum-lithium alloy (2090) and a comparison of behavior with
results in 2124 and 7150, ii) an evaluation of the role of crack tip
shielding in controlling the growth of short (50 to 400 μm) through-
thickness cracks and small (10 to 400 μm) surface cracks in 2124, and
iii) a general assessment of the small crack problem. It is
concluded that the near-threshold behavior of long cracks and the
near- and sub-threshold behavior of small cracks is strongly
influenced by considerations of crack tip shielding, specifically
from crack deflection and crack closure mechanisms. Other factors
responsible for "anomalous" small crack behavior, however, can be
identified and are discussed in the report.

1. INTRODUCTION

The objective of this program is to identify mechanical, microstructural and environmental factors governing the fatigue crack growth of long ($\gtrsim$ 25 mm) and short ($\lesssim$ 1 mm) cracks in commercial aluminum alloys with specific reference to behavior at ultralow, near-threshold growth rates below typically 10^{-6} mm/cycle. This report covers the fourth year of the program of research where attention has been focussed on studies of a new aluminum-lithium alloy (2090) and specifically on its fatigue crack growth behavior under periodic compression overloads, and on small through-thickness and surface flaws (10 to 400 μm) in 2124 alloy. Based on these results, an overall assessment of the small crack problem is presented, and suggestions are made for its potential solution, both with respect to defect-tolerant life prediction and alloy design.

2. REVIEW OF PREVIOUS RESEARCH

2.1 Introduction

Despite an increasing interest, both academically and technologically, in conventional long crack fatigue crack propagation, particularly at near-threshold levels (e.g., ref. 1), a major limitation in the application of such information to defect-tolerant design must be regarded as the problem of short flaws. By short flaws, it is implied that flaws are i) small compared with the

scale of microstructure, ii) small compared with the scale of local plasticity, or iii) simply physically small (i.e., $\leq$ 0.5 to 1 mm). Design codes at present attempt to predict the growth rates of in-service flaws based on data collected in the laboratory with specimens containing crack sizes of the order of 25 mm. In service, however, initial defects sizes are often far smaller than this. This leads to a potential for non-conservative defect-tolerant lifetime predictions since the vast majority of experimental observations[2-18] on the behavior of short cracks has shown that their growth rates are in excess of long cracks at the same nominal driving force (e.g., at the same stress intensity range ΔK) and furthermore that such short cracks can initiate and propagate at ΔK levels **below** the "long crack" fatigue threshold ΔK_{TH} (Fig. 2.1).

Studies in prior years have involved i) an extensive review of all aspects,[19] including environmental,[20] of the behavior of small fatigue cracks, ii) a study of the role of aging treatment/microstructure in influencing near-threshold crack growth and closure behavior in 7150 aluminum alloys,[21] iii) a study of the effect of wake machining and the development of crack closure with crack extension in underaged, peak aged and overaged 7150,[22,23] and iv) an evaluation of the role of compression overloads in influencing near-threshold fatigue crack growth in 7150.[24-26] This work has been described in detail in previous Annual Reports and has been reported in the literature.[21-26] Papers published on these topics in the past
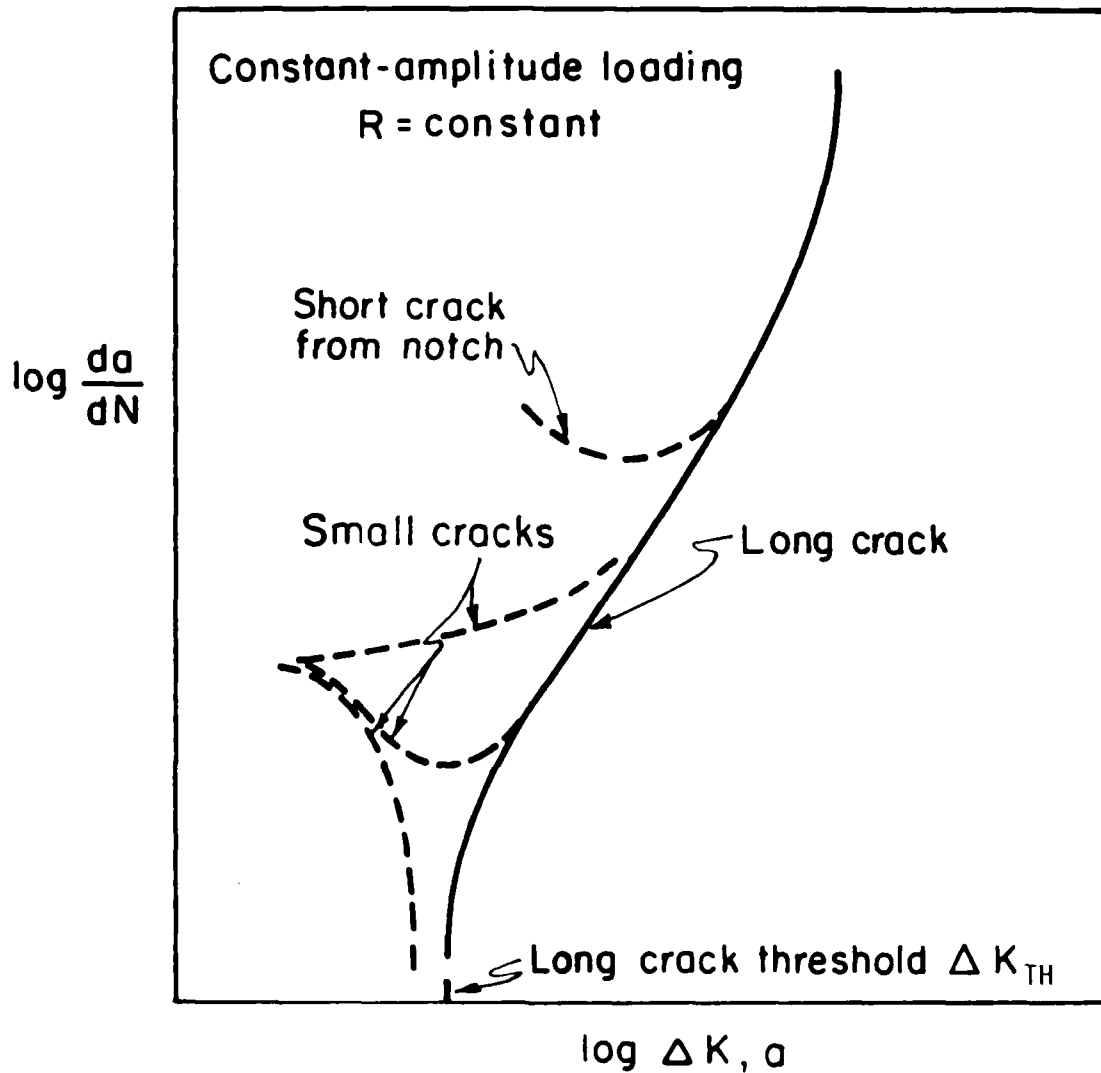
Fig. 2.1: Schematic representation of the typical variation in fatigue crack growth rates da/dN, with the nominal cyclic stress intensity factor ΔK, or crack length a, for "long" and "small" cracks. ΔK_{TH} is the nominal threshold stress intensity range below which long cracks remain dormant.

year are appended to this report. For completeness, summaries are
presented below.

2.2 Long Crack Studies in 7150 Aluminum Alloys[21]
   (E. Zaiken)

Studies were made of the role of aging treatment/microstructure
in influencing fatigue crack propagation and crack closure behavior
in a high purity I/M 7150 aluminum alloy, with specific reference to
crack growth at low and high load ratios in the near-threshold
regime. A trend of increasing growth rates and decreasing threshold
ΔK_{TH} values with increased aging was seen to be consistent with lower
measured levels of crack closure and a decreasing tortuosity in crack
path. Based on crack growth measurements in moist room air, where
closure due to corrosion product formation (Fig. 2.2) was found to be
negligible in this alloy, the superior fatigue resistance of
underaged microstructures (compared to overaged structures of similar
strength and peak aged structures of higher strength) was attributed
to greater slip reversibility and to enhanced roughness-induced crack
closure (Fig. 2.2) and deflection from the more tortuous crack paths.
Such factors are found to be promoted in alloy systems hardened by
coherent, shearable precipitates where the mode of deformation is one
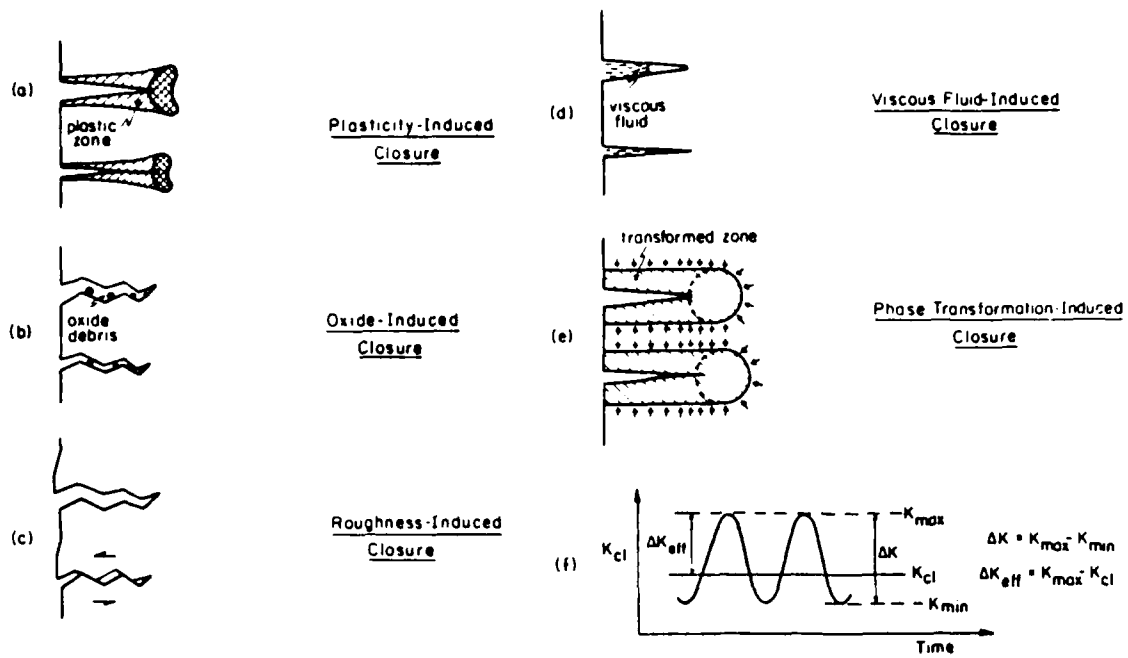of non-homogeneous planar slip.

Fig. 2.2: Schematic illustration of primary mechanisms of fatigue crack closure and the nomenclature required in the definition of stress intensities representative of the fatigue cycle.

2.3 Development of Crack Closure and the Threshold Condition for Short and Long Fatigue Cracks in 7150 Aluminum Alloy[22,23] (E. Zaiken)

In an attempt to analyze the behavior of physically "short" cracks, studies were made of the development, location and effect of crack closure on the behavior of fatigue cracks arrested at the "long" crack threshold stress intensity range, ΔK_{TH}, in under, peak and overaged microstructures in an I/M 7150 aluminum alloy. By monitoring the change in closure stress intensity, K_{cl}, during the in situ removal of material left in the wake of arrested threshold cracks, approximately 50 pct of the closure was found to be confined to a region within ~ 500 μm of the crack tip. Following wake removal, previously arrested threshold cracks recommenced to propagate at low load ratios even though nominal stress intensity ranges did **not** exceed ΔK_{TH}, representing the behavior of physically short cracks emanating from notches. No such behavior was seen at high load ratios. With subsequent crack extension, crack closure was observed to re-develop leading to a deceleration in growth rates. The development of such closure was found to occur over crack extensions comparable with microstructural dimensions, rather than those associated with local crack tip plasticity. Such results provide confirmation that the existence of a fatigue threshold and the growth of physically short cracks are controlled primarily by crack closure.

2.4 Role of Compression Overloads in Influencing Crack Closure and Near-Threshold Fatigue Crack Growth in 7150 Aluminum Alloy[24-26] (E. Zaiken, P. Donehoo, W. Yu)

Studies were made of the effect of periodic single compression cycles on near-threshold fatigue crack propagation in an I/M 7150 aluminum alloy. Based on experiments at a load ratio of R = 0.10 on cracks arrested at the fatigue threshold (ΔK_{TH}) in under-, peak and overaged microstructures, large compression overload cycles, of magnitude 5 times the peak tensile load, were found to cause immediate re-initiation of crack growth, even though the applied stress intensity range **did not exceed** ΔK_{TH}. Following an initial acceleration, subsequent crack advance was observed to take place at progressively decreasing growth rates until re-arrest occurred. Such behavior was attributed to measured changes in crack closure which vary the effective near-tip driving force for crack extension (ΔK_{eff}). Specifically, roughness-induced closure primarily was reduced by the application of compressive cycles via a mechanism involving crack surface abrasion which causes flattening and cracking of fracture surface asperities. Closure, however, was re-generated on subsequent propagation resulting in the re-arrest. Such observations provide further confirmation that the existence of a fatigue threshold is controlled principally by the development of crack closure.

3. EXPERIMENTAL PROCEDURES AND MATERIALS

3.1 Materials

The following commercial wrought aluminum alloys, namely 7150, 2024, 2124, and lithium-containing 2090, were obtained from ALCOA in the solution treated, quenched and stretched (2%) conditions. Nominal chemical compositions are shown below in Table 3.1. All alloys were received in the form of 25 mm thick plate, except the 2090 which was 13 mm plate.

Table 3.1: Nominal Chemical Compositions in wt% of Alloys

	Si	Fe	Cu	Li	Mn	Mg	Cr	Zn	Ti	Zr	Al
2024	0.50	0.50	4.50	--	0.50	1.50	0.10	0.25	0.15	--	balance
2124	0.20	0.30	4.50	--	0.50	1.50	0.10	0.25	0.15	--	balance
7150	0.07	0.11	2.10	--	--	2.16	--	6.16	0.02	0.13	balance
2090	0.12	0.10	2.70	2.20	0.05	0.25	--	--	0.15	0.12	balance

Fatigue tests were performed on 6.4 mm thick compact C(T) test-pieces, heat-treated in the 2124 and 7150 alloys to yield peak-aged (PA) microstructures and underaged (UA) and overaged (OA) microstructures at the same approximate yield strength. The rationale for this was to examine, at constant yield strength, the influence of different plastic flow mechanisms, i.e., underaged (i.e., T3) structures are associated primarily with deformation via planar slip due to the coherent nature of the hardening precipitates

whereas overaged (i.e., T7) structures are associated with a more homogeneous wavy slip from incoherent particle hardening mechanisms.

Specific heat treatment schedules and room temperature mechanical properties are listed in Tables 3.2 and 3.3, respectively. The nature of these microstructures has been discussed elsewhere.[21] Briefly, in the 7150 alloy, underaged structures were characterized by coherent GP zones ($\sim$ 4-8 nm diameter), which were replaced in the T6 condition by semi-coherent η' precipitates (Fig. 3.1). T7 structures were hardened by coarsened η' in the matrix and by predominately incoherent η precipitates in both matrix and grain boundaries, the latter resulting in small precipitate-free-zones ($\sim$ 30 nm half width), as shown in Fig. 3.1c. Grains were pancake-shaped with an approximate size of 15 by 5 μm.

In the 2124 and 2024 alloys, in addition to the widely distributed second phase inclusions, the naturally (underaged) structures were also strengthened by G-P zones. At the peak aged condition, the major strengthening particles include the Al-Cu θ'' and the magnesium-containing S' phase, both semi-coherent. The overaged structures were characterized by the formation of incoherent θ' and θ phases in the matrix and, most noticeably, along the grain boundaries. The precipitate-free zones were readily found. The grains were pancake shaped with an approximate diameter of 350 μm and thickness of 50 μm (Fig. 3.2).

Corresponding heat-treatments and mechanical properties for 2024 and 2124 alloys also are listed in Tables 3.2 and 3.3.

Fig. 3.1: Transmission electron micrographs of a) underaged, b) peak aged (T6) and c) overaged (T7) I/M 7150 aluminum alloy.
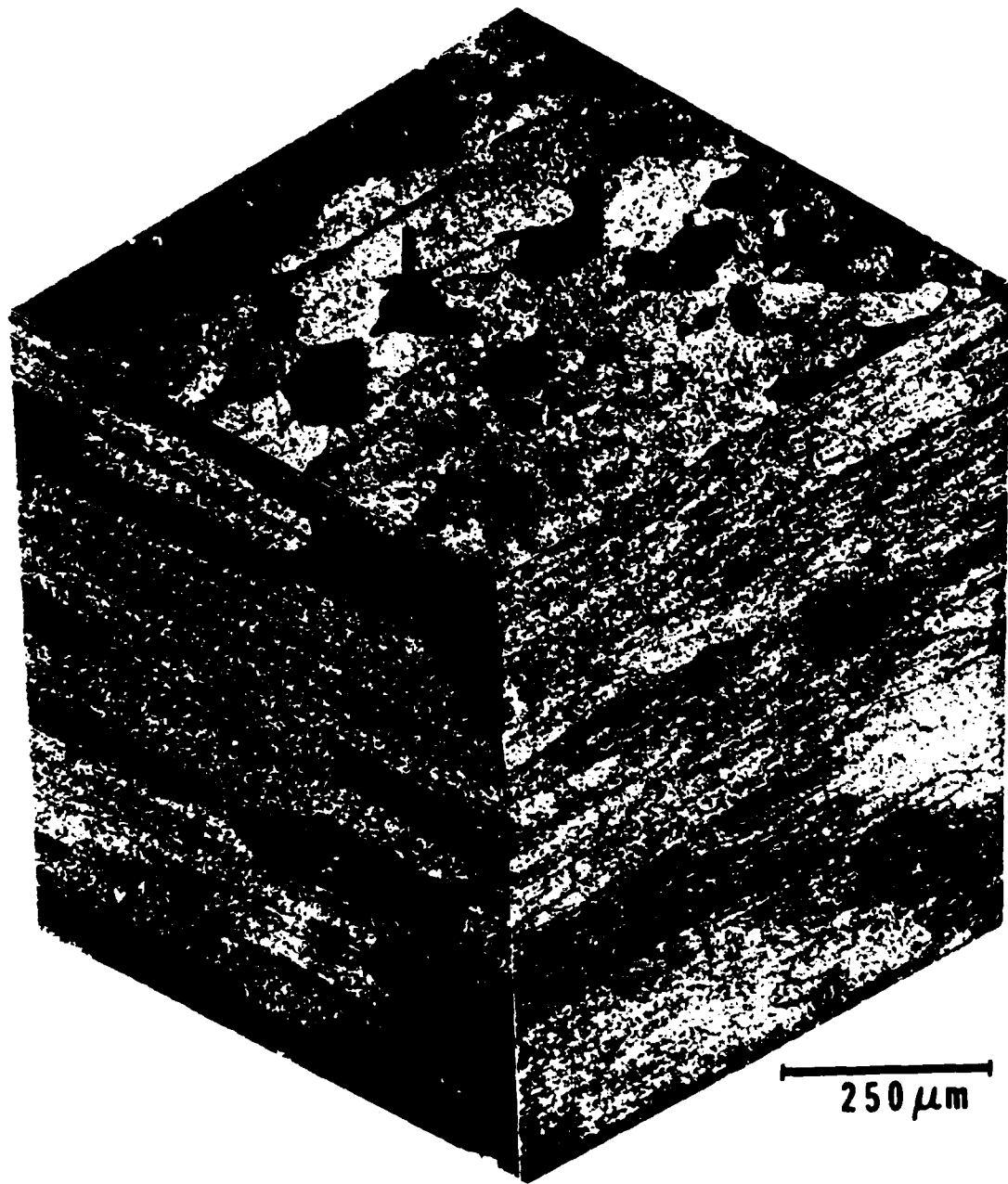
Fig. 3.2: Three-dimensional grain structure of aluminum alloy 2125-T351 (Keller's reagent etch).

Table 3.2: Heat-Treatments Utilized

	7150 Alloy	2024 and 2124 Alloys
Underaged	ST* + 1½ hr at 121°C	ST* + naturally aged (ambient)
Peak Aged	ST* + 100 hr at 121°C	ST* + 12 hr at 190°C
Overaged	ST* + 24 hr at 121°C + 40 hr at 163°C	ST* + 48 hr at 190°C

*ST = solution treated, stretched 2%

Table 3.3: Room Temperature Mechanical Properties of Alloys Tested

	Yield Strength (MPa)	U.T.S. (MPa)	Elong.* (%)	Redn. Area (%)	Work Hardening Exponent
7150					
Underaged	371	485	6.8	12.1	0.055
Peak Aged (T6)	404	480	6.0	10.3	0.046
Overaged (T7)	372	478	7.1	12.5	0.058
2024					
Underaged (T351)	360	471	17.6	24.3	-
Peak Aged (T851)	432	473	8.4	22.6	-
Overaged	340	471	9.0	22.8	-
2124					
Underaged (T351)	360	488	17.8	26.7	-
Peak Aged (T851)	447	479	10.0	23.3	-
Overaged	370	440	10.2	21.9	-
2090					
Peak Aged (T851)	535	565	11.0	-	-

*On 25 mm gauge length.

In addition, specimens were taken from a plate of commercial lithium-containing aluminum alloy 2090. The material was furnished by ALCOA in the T8-E41 condition. The alloy was hot-rolled to a thickness of 13 mm, solution heat-treated to near-peak conditions, quenched, and then stretched $\sim 8\%$ prior to aging. The term E41 refers to a processing treatment which is proprietary to ALCOA. The chemical composition of 2090 is listed in Table 3.1; mechanical properties (longitudinal orientation) are listed in Table 3.3.

The microstructure of 2090 consists of large, unrecrystallized grains with planar, elongated shape (Fig. 3.3). Grains are of approximate size 20 μm thick in the short direction, 500 μm wide in the transverse direction, and a few millimeters long in the rolling direction. The microstructure of 2090 has been characterized by Rioja and Ludwiczak.[27] They note that the alloy contains four metastable phases, δ', β', T_1', and T_2', which are thought to be precursors to the equilibrium β, T_1, and T_2 phases. The δ' phase (Al_3Li) normally exists as spherical precipitates, but small precipitates can also wet the surfaces of the β' (Al_3Zr) and T_1' (Al_5CuLi_3) phases. It is thought that the δ' phase is responsible for the strongly-directional mechanical properties of this alloy.

3.2 Test Procedures

To obtain a comparison between long and short crack near-threshold behavior and to demonstrate experimentally that the anomalous behavior of through-thickness short cracks results from a
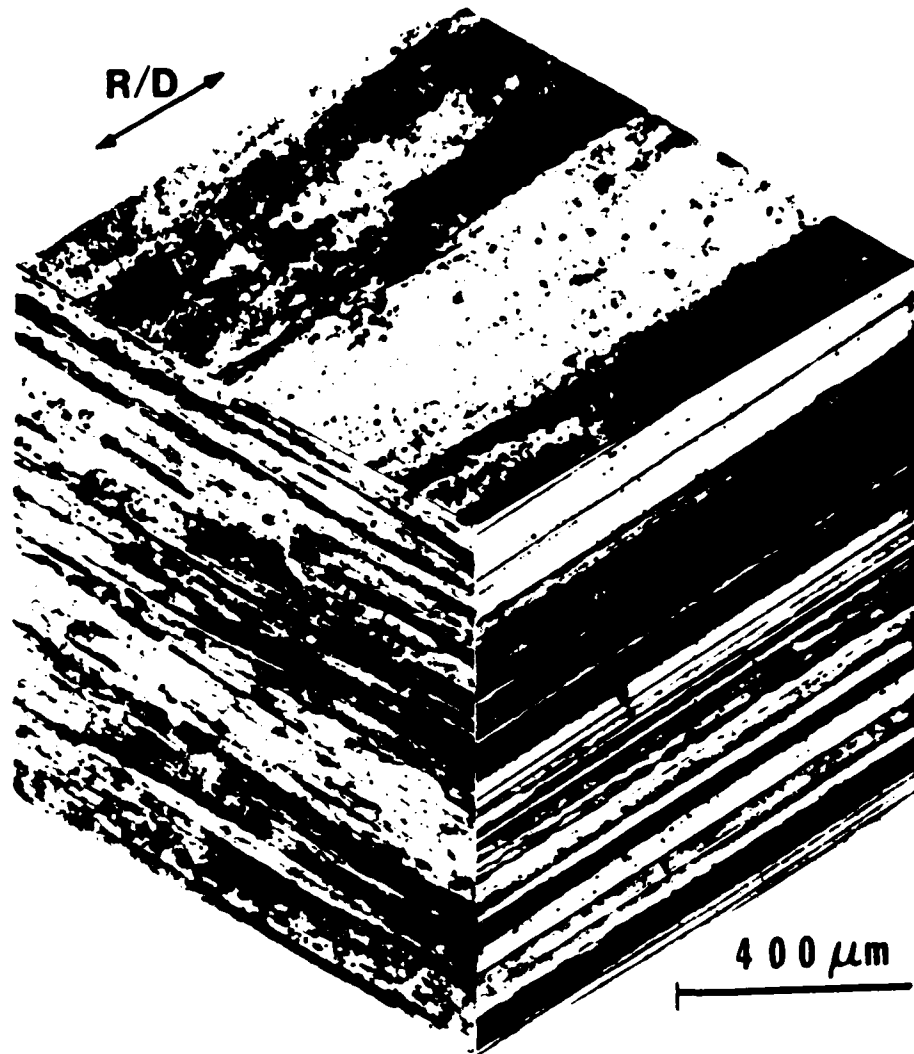
Fig. 3.3: Three-dimensional optical micrograph showing the grain structure of aluminum-lithium alloy 2090-T8E41 (Keller's reagent etch).

lesser effect of closure in the wake of the crack tip, the "3-in-1" test specimen/procedure is being utilized, shown schematically in Fig. 3.4.

Starting with a conventional 1-T compact C(T) test-piece, 6.4 mm thick, long crack threshold tests are performed at 50 Hz using standard load shedding procedures to determine the near-threshold crack growth behavior and the value of the fatigue threshold range ΔK_{TH} for long cracks[1] (A). To demonstrate the effect of closure in the wake of the crack tip, two procedures are then adopted for the long crack arrested at ΔK_{TH}. In certain specimens, material is machined away behind the crack tip to "remove" closure in the wake. This has been performed using a jeweler's saw to machine a 0.3 mm width cut. Conversely, closure is "removed" by applying a single compression overload. In either case, following such procedures, the subsequent growth of the formerly arrested long crack is monitored, under nominally constant ΔK conditions, until closure has once again developed with increase in crack length to approach crack arrest (B). The third stage of the test is then to carefully machine away the majority of the test-piece to leave a (two-dimensionally) small crack in a strip of metal (C), which is then tested in four-point bend to investigate near- (and sub-) threshold short crack behavior (D).

In addition, tests were performed to examine the behavior of naturally-occurring (three-dimensionally) small surface cracks, using replication techniques. The replication was performed with cellulose acetate tape and acetone on the top (tensile) surface of rectangular

A. Long Crack Threshold Test
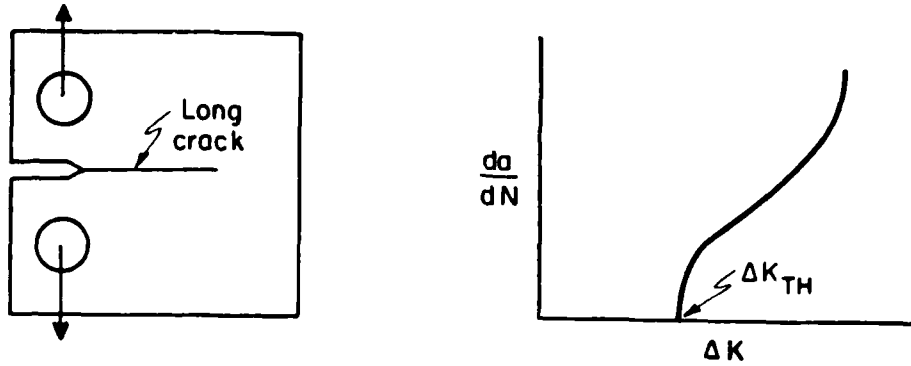
B. Removal of Wake
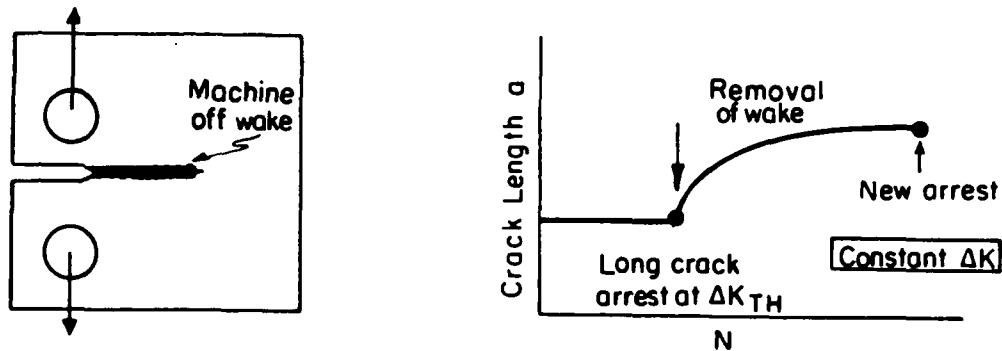
C. Machine Off to Leave Short Crack
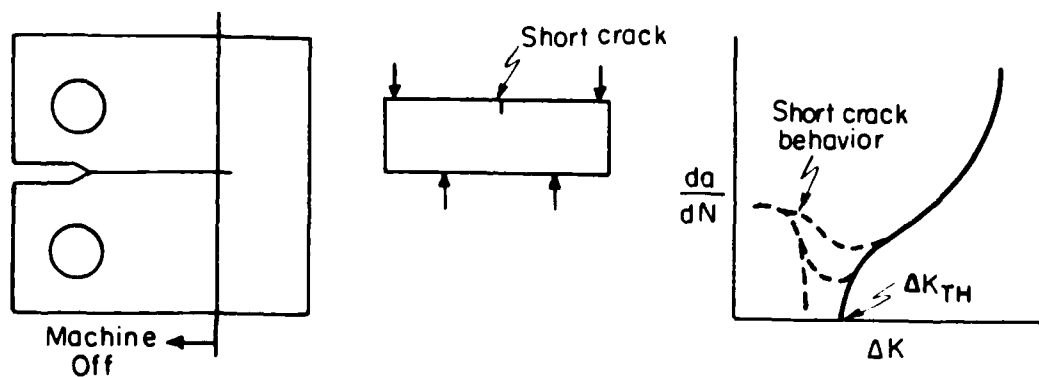
D. Short Crack Threshold Test

Fig. 3.4: Test geometries, procedures, and expected results for the "3-in-1" specimen developed to experimentally demonstrate the role of closure and the differences between long and short crack behavior.

bend specimens (64 mm x 13 mm x 6.4 mm), tested in four-point bending. Tests were carried out at a load ratio of R = 0.1 such that the maximum stress due to bending was 0.9 times the yield stress of the material. Prior to testing, specimens were metallographically polished and etched to reveal the grain structure.

4. IN-SITU CRACK CLOSURE MEASUREMENT

4.1 Introduction

Despite the widespread adoption of the concept of fatigue crack closure, there remains much uncertainty as to the most reliable methods of measurement. The majority of procedures involve the use of gauges to obtain a compliance curve for the cracked specimen and determining the point of deviation from linearity during elastic unloading along this curve.[28-35] Other methods involve laser inferometry techniques,[35] electrical potential measurements,[36] ultrasonics[37] and surface replication.[10]

Although perhaps the most accurate of all procedures, at least for surface measurements, the laser inferometry technique for detecting crack closure requires special instrumentation.[35] Electrical potential techniques, although widely used for crack length measurement, suffer from the presence of crack surface oxide films which can result in uncertainty on the exact point of crack surface contact. Replica techniques are accurate, but provide only a surface measurement and do not lend themselves to automation. For

standard automated testing, compliance gauge measurements offer the most practical solution. The gauges can be mounted at the crack mouth (e.g., clip gauges), on the side surfaces (e.g., Elber gauges) or on the back-face. Location on the side surfaces is not preferred as measurements become strongly sensitive to the position of the crack in relation to the gauge. Of the remaining locations, the back-face strain approach was selected as it offered substantially greater resolution than the use of a crack mouth-mounted clip gauge.

4.2 Experimental Details and Discussion

The back-face strain method,[28-30] used to evaluate crack closure,[30-32] is based on compliance measurements from a strain gauge mounted on the back face of the specimen. The closure stress intensity, K_{cl}, which is defined at first contact between mating crack surfaces on unloading, is measured at the point of deviation from linearity of the elastic unloading compliance curve.

In order to monitor crack closure continuously in real time during a high frequency (e.g., 50 Hz) fatigue test, an algorithm was developed with the present system to automate the process of deriving the point of closure from compliance data. Load and back-face strain signals were first amplified with two identical amplifiers and digitized to feed into a PDP-11 computer. Although care was taken to keep the signals in-phase, due to the nature of the amplifiers some phase difference between the load and strain signals was found to exist. Since this can introduce false hysteresis and cause error in

the closure measurement, a phase shifting circuit was used for compensation. Active filter circuits are also used to remove the high frequency noise in the measurement system.

In order to automate detection of the closure point at first deviation in linearity from the unloading compliance curve, the straight line portion of the curve was defined and the correlation coefficient used as an indicator for linearity. First, starting from maximum load, points from 5 to 10% of the total curve were used to determine the baseline correlation coefficient. Points were then added one by one to the data set and correlation coefficients calculated. Since the correlation coefficient will decrease if the next point deviates from linearity, and increase if it falls on the straight line, the closure point was defined where the correlation coefficient had the highest value, i.e., at the end of the straight line portion of the curve.

This technique is relatively immune to signal noise because the correlation coefficient is itself an indicator of noise. Moreover, its use removes the ambiguities inherent in the manual determination of closure. Accuracy depends primarily on the accuracy of the digitizing process and the noise level. Sensitivity and the speed of the analog-to-digital converter are also crucial to the success of the method. In the present system, where the speed of the algorithm was a strong function of the computation speed, the unloading compliance curve was digitized into about 350 points within a half fatigue cycle, and involved a computation process of about 10

seconds. This readily permitted closure measurements to be made automatically during the test approximately once every 30 seconds.

5. ROLE OF COMPRESSION OVERLOADS IN 2090 ALLOY

5.1 Introduction

Compression cycles are often a common occurrence in service, particularly for aerospace applications, and are known to be of importance in the process of crack initiation in smooth specimens. Their effect on the propagation of (long) fatigue cracks, however, at least at intermediate to high ΔK levels, has long been considered to be minimal (e.g., ref. 38). Although data are limited, several authors have found growth rates to be slightly faster at negative load ratios compared to R = 0 in both steels and aluminum alloys,[38-40] although the effect is negligible in certain alloys such as 7075-T6.[38] Under variable amplitude fatigue loading, however, cyclic compressive stresses immediately following tensile overloads are known to lessen the post overload retardation in growth rates which usually accompanies single tensile overloads.[41-43] Moreover, under certain conditions of cracks initiating from notches, fatigue crack growth has been demonstrated under purely cyclic compressive loading (e.g., ref. 44). In fact, the technique has been used as a reliable means of producing small flaws for short crack experiments.[12,16]

Unlike behavior at higher growth rates where effects are small, recent studies at near-threshold levels have highlighted a significant role of compressive cycling on crack extension behavior.[24-26,39,40] Not only are threshold ΔK_{TH} values lower at R = -1 compared to R = 1, but large periodic compressive cycles (of the order of one half the yield stress) applied during positive R cycling have been shown to dramatically reduce the threshold and to accelerate crack growth rates in both ferrous and aluminum alloys. Physical explanations for these effects have been suggested in terms of the redistribution of residual stresses **ahead** of the crack tip and reduced closure forces due to a diminished deformation zone left **behind** the crack tip,[40,45] and the flattening of fracture surface asperities and a compacting of corrosion debris on crack faces, both processes leading to a reduction in closure.[24-26]

Previous studies[24-26] have examined the role of compression cycling by applying compression overloads to cracks arrested at the threshold ΔK_{TH}, principally in the 7150 alloy. Here it was found that the compaction of fracture surface asperities was a primary mechanism. Accordingly, the objective of the present work was to examine this effect in an alloy known for its dependence upon asperity-induced crack closure.

The alloy chosen for study was the lithium-containing 2090-T8E41 alloy, where it was found that **crack growth at** ΔK_{TH} could be promoted through the application of periodic compression cycles, of magnitude two times the peak tensile load. Similar to 2124 and 7150 aluminum

alloys, such compression-induced crack growth at the threshold decelerates progressively until the crack re-arrests, consistent with the reduction and subsequent re-generation of crack closure. The compressive loads required to cause such behavior, however, were far smaller in the 2090 alloy. Such diminished resistance of aluminum-lithium alloys to compression cycles was related to their enhanced "extrinsic" crack growth resistance (from crack path deflection and resultant crack closure), and the reduction in this shielding due to compacting of fracture surface asperities by moderate compressive stresses.

5.2 Experimental Procedures

Results on the 2090-T8E41 aluminum-lithium alloy were compared with results on 2124-T351 and previous reported results[24] on 7150 alloy in the under-, peak and overaged conditions.

Fatigue crack propagation testing was conducted with 6.4 mm thick compact C(T) test pieces, machined from the center of the plate in the T-L orientation. Tests were performed in controlled room temperature air ($22^{\circ}C$, 45% relative humidity) using computer-controlled electro-servo-hydraulic testing machines operating at a frequency of 50 Hz (sine wave) and load ratio ($R = K_{min}/K_{max}$) of 0.1. Direct current electrical potential methods were used to continuously monitor crack length. Corresponding measurement of crack closure was achieved using an automated back-face strain compliance technique. To minimize the inherent experimental difficulties and ambiguity in

such closure stress intensity K_{cl} measurements, the system was programmed to monitor closure continuously by determining the highest load where the elastic unloading compliance curve deviated from linearity.[46] Data are presented both in terms of the nominal stress intensity range, defined as $\Delta K = K_{max} - K_{min}$, and, after allowing for crack closure, the effective stress intensity range, defined as $\Delta K_{eff} = K_{max} - K_{cl}$.

Compression overload experiments were performed by first propagating a crack to arrest at the fatigue threshold, ΔK_{TH}, operationally defined at a growth rate less than 10^{-9} mm/cycle. The approach to the threshold was performed using an automated load-shedding scheme of $\Delta K = \Delta K_0 \exp[C(a - a_0)]$, where ΔK and a are the instantaneous values of stress intensity and crack length, ΔK_0 and a_0 are their initial values and C is the K-gradient set to -0.1 mm^{-1}. Single (spike) compressive overloads were then applied to the arrested crack at ΔK_{TH}. The magnitudes of the compressive overloads were varied between one and four times the maximum tensile load in the cycle; the absolute values were between 0.3 and 2.2 kN, corresponding to fictitious "negative" stress intensities of 3.5 to 14 MPa√m. The length of the arrested fatigue cracks was about 5 to 9 mm beyond the initial notch, to give a total length between 22 and 28 mm. Following application of the compression cycle, subsequent crack extension and the development of closure were continuously monitored, with the loading conditions maintained at a constant $\Delta K = \Delta K_{TH}$.

5.3 Baseline Fatigue Behavior of 2090-T8E41

Fatigue crack propagation rate (da/dN) data for 2090-T8E41 are plotted in Fig. 5.1 as a function of the nominal and effective stress intensity ranges, ΔK and ΔK_{eff}, respectively. Corresponding closure K_{cl} values are given by the data points in Fig. 5.2. At R = 0.1, the alloy shows a nominal fatigue threshold of ΔK_{TH} = 3.4 MPa$\sqrt{m}$, which is comparable with other high strength aluminum alloys, such as 2124 and 7150, in their commercial tempered conditions (Fig. 5.3a). Despite having at least 30% higher strength than the other alloys, crack advance in 2090 can be seen to be consistently slower over the entire range of growth rates (except for near-threshold growth in 2124-T351), and to show a particular superiority above 10^{-6} mm/cycle. The latter observations are not associated solely with an increased elastic modulus, as 2090 still shows lower growth rates compared to 2124 and 7150 when the data are replotted in terms of ΔK, normalized with respect to Young's modulus (Fig. 5.3b). Conversely, the improved crack growth properties appear to be consistent with the fact that, unlike 2124, crack closure levels in 2090 do not decay rapidly with increasing stress intensity range above the threshold; rather K_{cl} values remain above 50% K_{max} out to ΔK levels about 7 MPa$\sqrt{m}$ (Fig. 5.2).

The higher levels of crack closure, which give rise to a lower ΔK_{eff} and hence to slower growth rates, are consistent with the highly crystallographic nature of the crack path in 2090, compared to 2124, as illustrated in Fig. 5.4. Similar to that reported for other
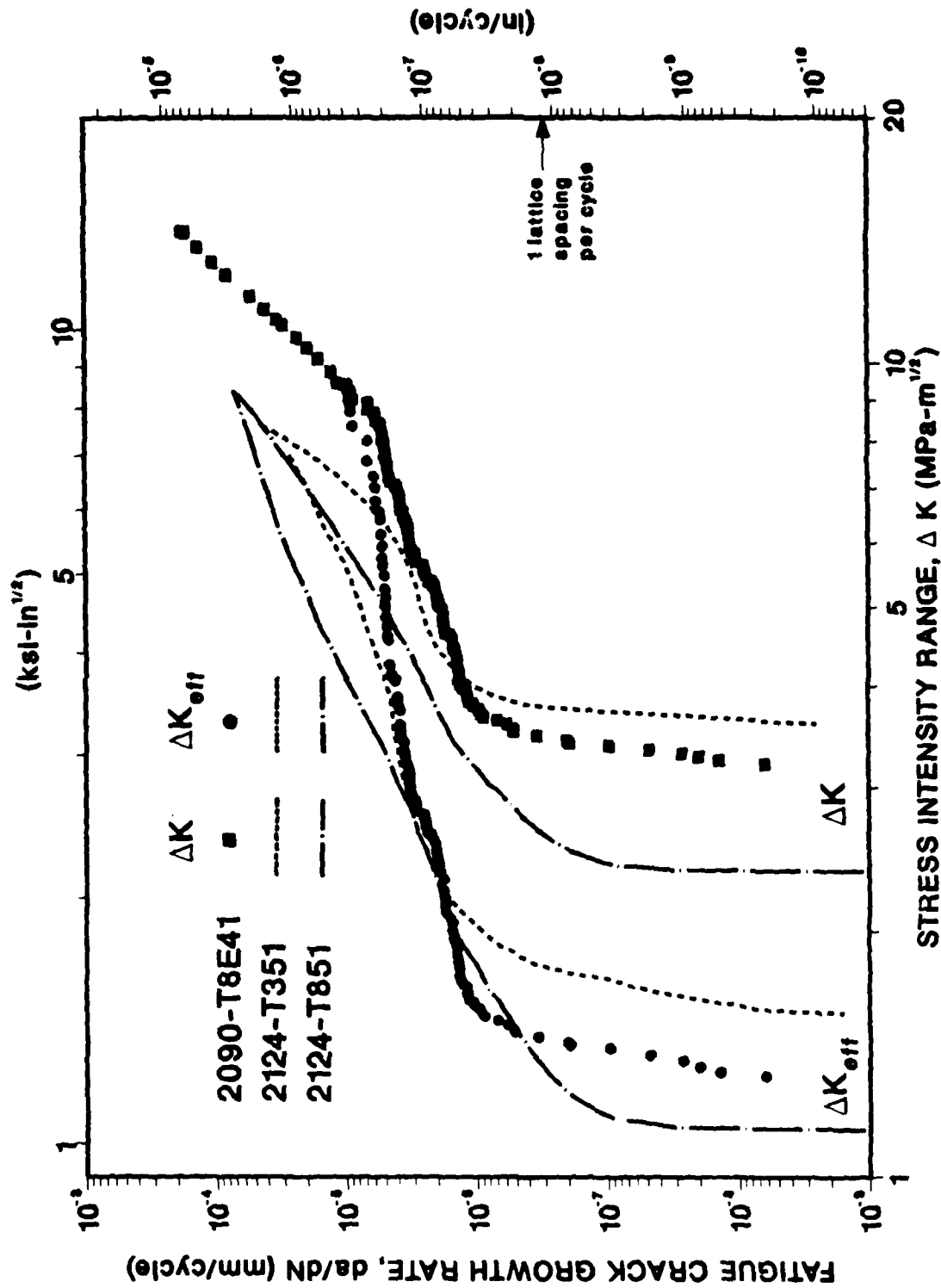
Fig. 5.1: Fatigue crack propagation behavior of 2090-T8E41 at R = 0.1 in moist air, plotted as a function of the nominal and effective stress intensity range, ΔK and ΔK_{eff}, respectively. ΔK_{eff} values are based on crack closure measurements shown in Fig. 5.2.
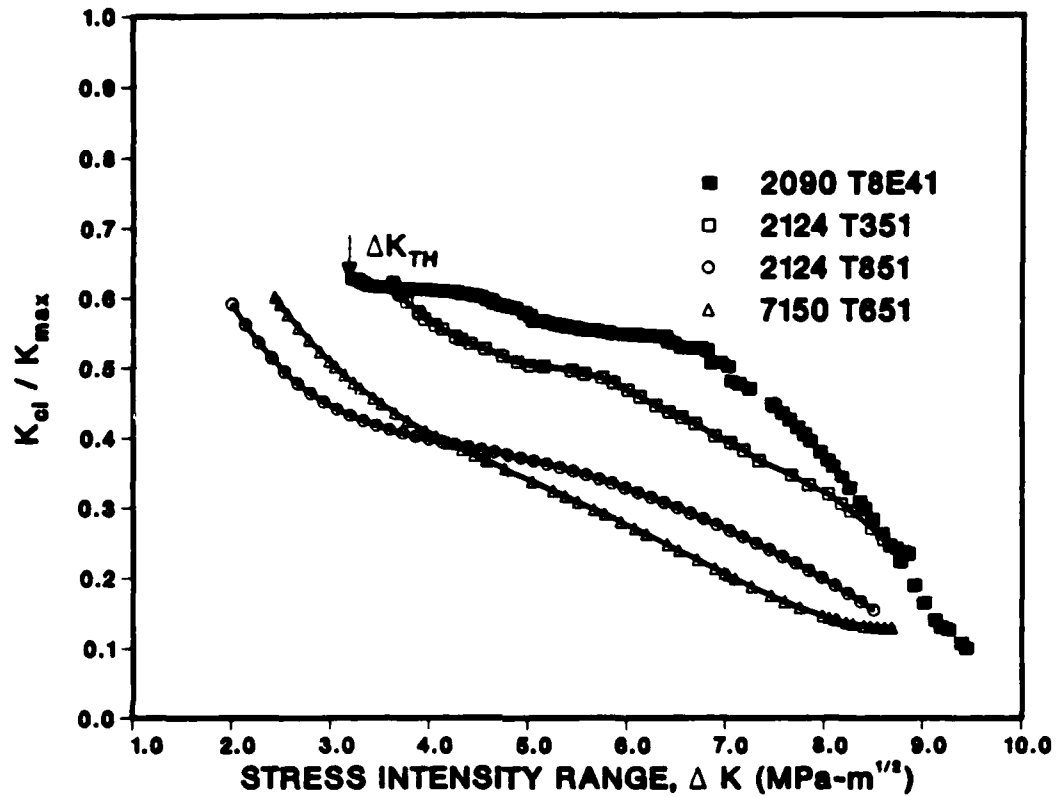
Fig. 5.2: Variation in closure stress intensity, K_{cl}, normalized with respect to K_{max}, with nominal stress intensity range, ΔK, for 2090-T8E41 alloy at $R = 0.1$. For comparison, crack closure data are also shown for 2124 and 7150 alloys.
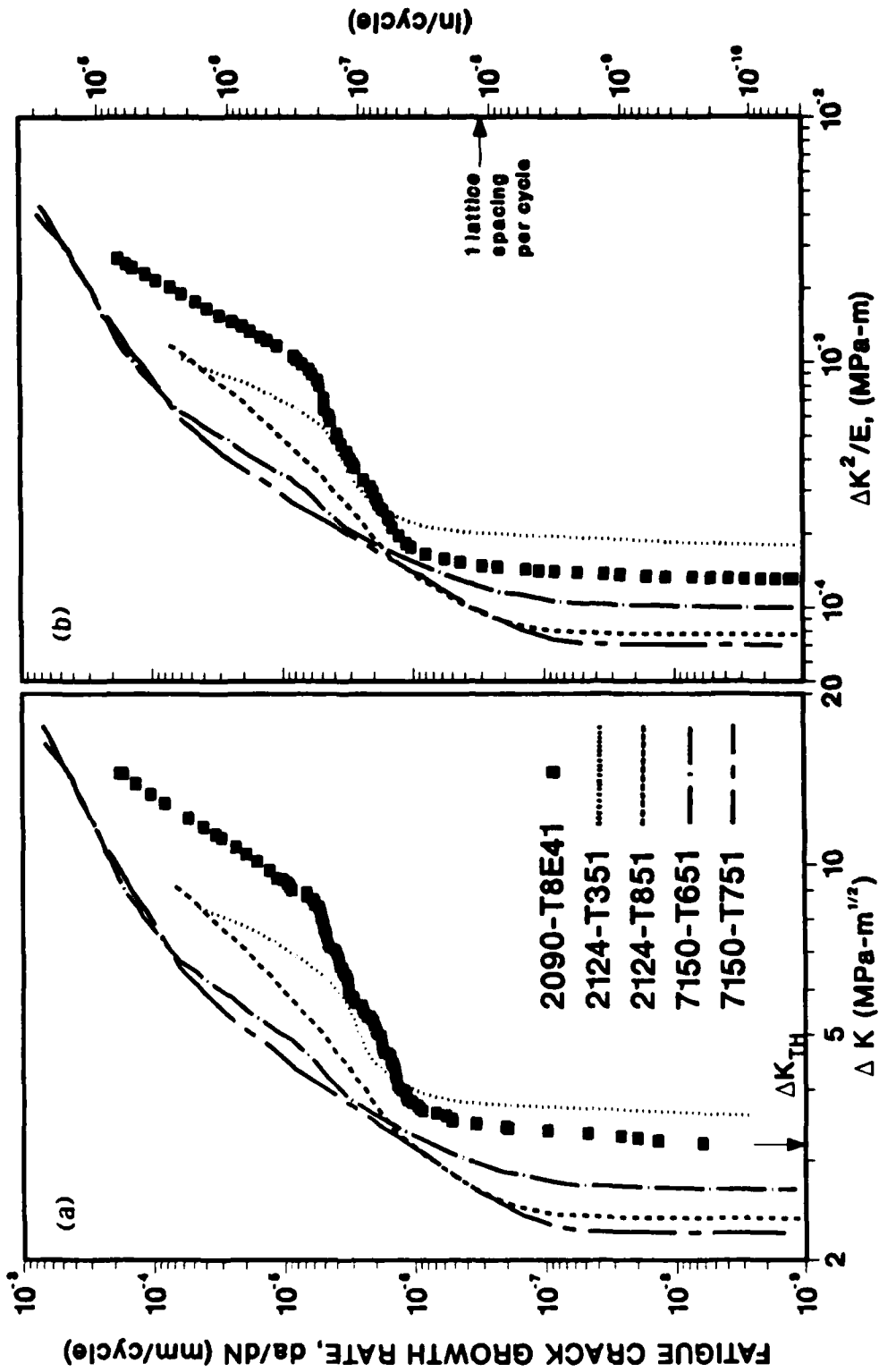
Fig. 5.3: Comparison of fatigue crack propagation behavior at R = 0.1 in 2090-T8E41 alloy with behavior 2124 and 7150 alloys. Growth rates are compared on the basis of a) the nominal stress intensity range, ΔK, and b) ΔK normalized with respect to Young's modulus, E.

Fig. 5.4: Morphology of the fatigue crack path in a) 2090-T8E41 alloy, compared to b) 2124-T3 alloy tested under similar conditions. Note the strongly crystallographic and deflected crack path in the aluminum-lithium alloy. Crack path profiles are derived from metallographic sections, taken perpendicular to the crack surface at the center of the specimen.

aluminum-lithium alloys (e.g., ref. 47), the crack path shows frequent deflections at both near-threshold and particularly higher ΔK levels, giving it a marked "zig-zag" appearance from propagation along slip bands. Resulting fracture surfaces are thus characterized by numerous "cleavage-like" facets, with additional evidence of secondary cracking. Although such crystallographic crack path morphologies are not uncommon in precipitation-hardened aluminum alloys, particularly at near-threshold levels in coherent particle-hardened (planar slip) microstructures (e.g., ref. 21), behavior in Al-Li alloys is striking in that this mode persists to much higher growth rates, accounting for the higher levels of closure and much slower growth rates above 10^{-6} mm/cycle.

5.4 Compression Overload Testing

The effect of single (spike) compressive overloads on cracks in 2090 arrested at ΔK_{TH} is shown in Fig. 5.5, in terms of post-overload crack extension as a function of number of cycles. The application of a 100% compression cycle (corresponding to a compressive load of equal magnitude to the peak tensile load at threshold) showed no detectable effect on either crack closure or crack growth. Compression cycles of 200% and above, however, resulted in rapid crack extension, following short dormant periods, even though conditions were maintained at a constant ΔK equal to the threshold. Above 400% compression, cracking commenced immediately following the overload, without any dormant period.
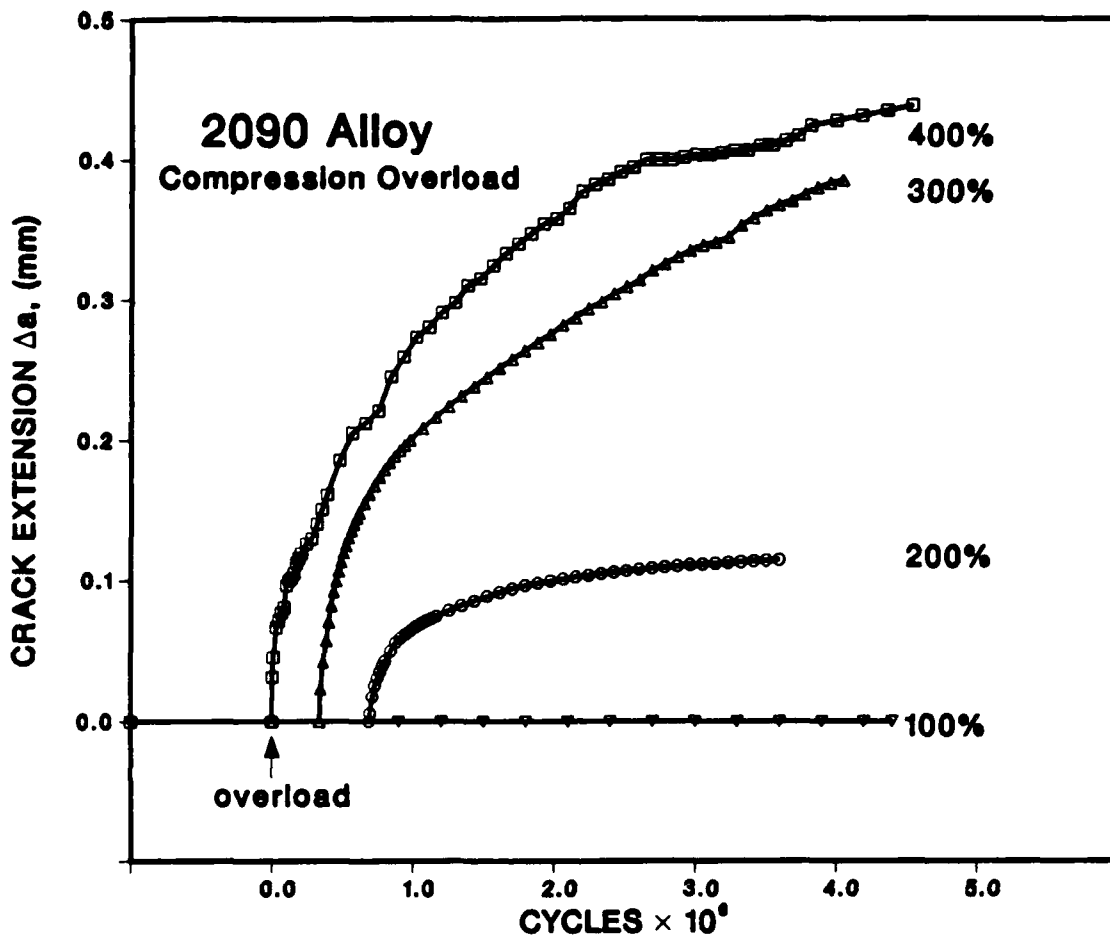
Fig. 5.5: Fatigue crack extension at constant $\Delta K = \Delta K_{TH}$ in 2090-T8E41 alloy, as a function of the number of cycles following the application of 100, 200, 300 and 400% single compression overload cycles. Compression overloads are applied to cracks arrested at the threshold ΔK_{TH} at R = 0.1.

For comparison, data for 2124-T351, 7150-T651 and 7150-T751, measured under identical test conditions, are included in Fig. 5.6. Whereas 200% compression overloads are required to re-initiate cracking at ΔK_{TH} in 2090, at least 300% overloads are required in 2124 and 500% overloads in 7150.

The initial acceleration at ΔK_{TH}, which is shown in Fig. 5.6 as function of compressive load amplitude, was followed by a progressive deceleration in growth rates until re-arrest. Post-overload crack extensions to re-arrest ranged from 110 μm, following 200% compression, to 410 μm, following 400% compression. Such behavior was found to be concurrent with a measured reduction in K_{cl} at the overload, and the subsequent re-generation in closure with further crack extension. Quantitative estimates of the consequent increase in local "crack driving force," ΔK_{eff}, at the overload, and its decay with crack extension, are plotted in Fig. 5.7. Fractographically, the reduction in closure following compression overload cycles could be attributed to signs of fretting debris and specifically to compaction of asperities and abrasion on fracture surfaces, similar to behavior reported previously in 7150.[24]

It is apparent that, although the aluminum-lithium alloy shows much improved crack growth properties under constant amplitude conditions, in the presence of periodic compression loading, the growth of arrested threshold cracks can occur far more readily. Paradoxically, both features are a consequence of the same phenomenon, i.e., the tortuous crack paths and resultant crack
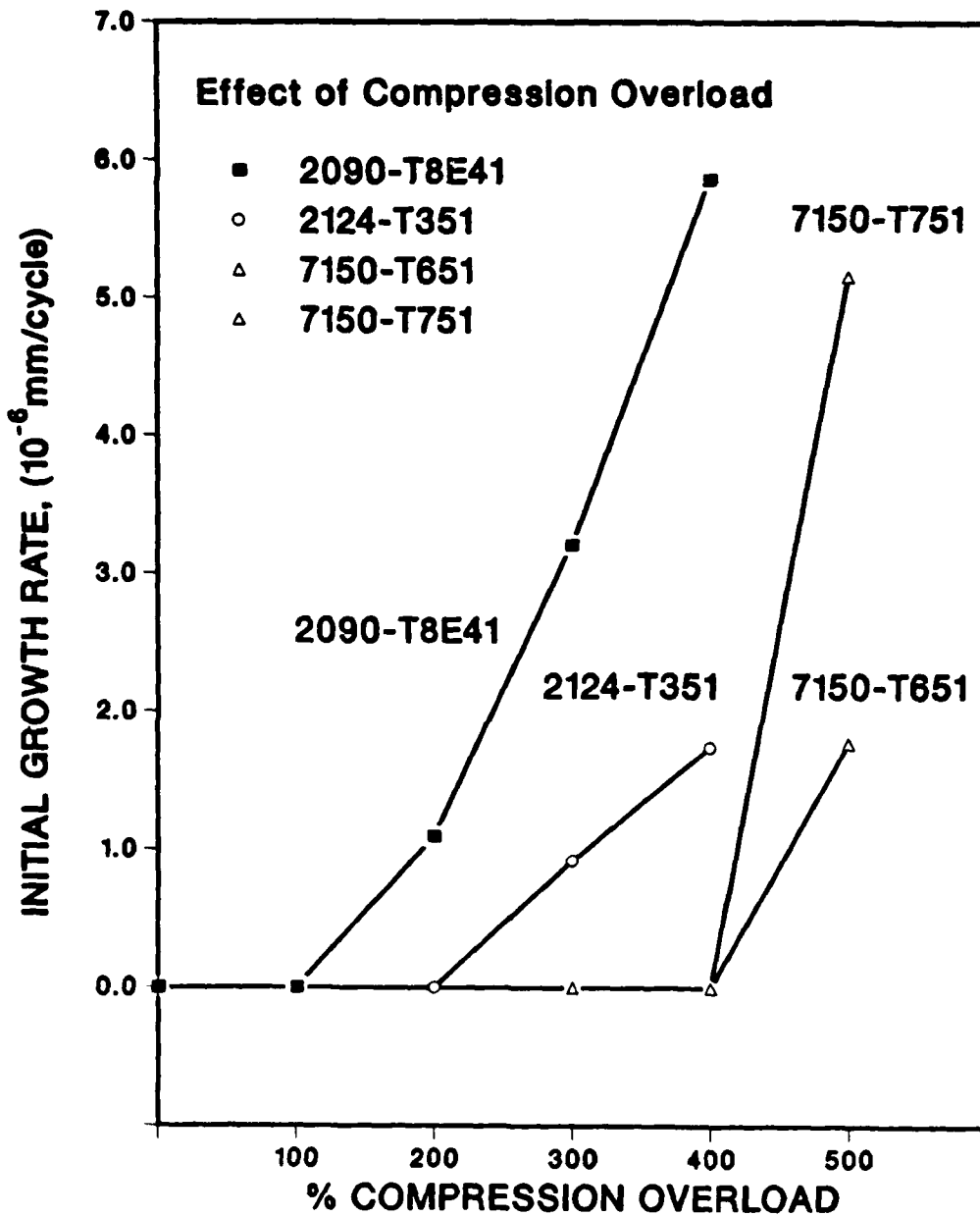
Fig. 5.6: Comparison of compre-sion overload results for 2090-T8E41 with results for 2124 and 7150, showing initial crack growth rate, following the compression cycle, as a function of the magnitude of the overload. Note the increased sensitivity of the aluminum-lithium alloy to the compression cycles.
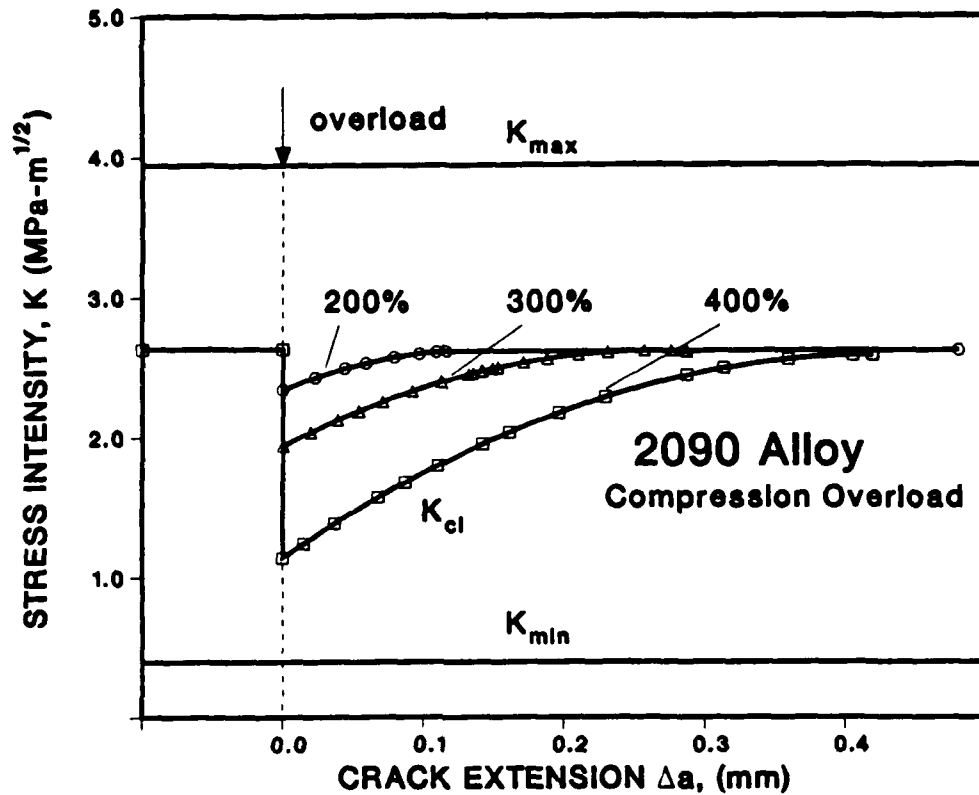
Fig. 5.7: Variation in ΔK $(= K_{max} - K_{min})$ and ΔK_{eff} $(= K_{max} - K_{cl})$ with crack extension at ΔK_{TH} for fatigue crack growth following compressive overloads on arrested threshold cracks in 2090-T8E41 alloy. ΔK_{eff} values are computed from K_{cl} data, measured using the back-face strain compliance technique.

closure from asperity wedging, which are characteristic of coherent particle-hardened microstructures and particularly of aluminum-lithium alloys.[47,48] The crack deflection and roughness-induced closure certainly provide enhanced crack tip shielding to impede crack extension, yet, by the same token, the increased dependence on crack closure due to any wedging mechanism inside the crack will necessarily make the alloy prone to "damage" (i.e., reduced shielding in a higher ΔK_{eff}) in the presence of compressive loads from the potential break-up of the wedge.

5.5 Conclusions

Based on a study of fatigue crack propagation behavior at R = 0.1 in 12.7 mm plate of the aluminum-lithium-copper alloy 2090-T8E41, with specific emphasis on the effect of compressive overload cycles, the following conclusions can be made:

1. Crack growth rates in 2090, over the range 10^{-9} to 10^{-4} mm/cycle, were found to be lower than in 2124 and 7150, when compared at peak strength or at their respective commercial tempers. The superiority of 2090 was particularly evident above 10^{-6} mm/cycle.

2. Such behavior was attributed primarily to the strongly crystallographic and tortuous nature of the crack path, which promoted crack tip shielding from crack deflection and consequent roughness-induced crack closure, and not solely to the increased elastic modulus of 2090. Unlike 2124 and 7150, shielding persisted into the mid-range of growth rates above 10^{-6} mm/cycle.

3. The application of single compression overloads, of magnitude two times the tensile peak load, was sufficient to cause the extension of cracks arrested at the threshold ΔK_{TH} in 2090, even though the applied ΔK level was maintained at ΔK_{TH}. Such growth at ΔK_{TH} was concomitant with a reduction in crack closure following the compression cycle, apparently resulting from the crushing of fracture surface asperities and compacting of fretting debris.

4. Post-overload crack growth rates were found to decay progressively until re-arrest, concurrent with the re-generation of (roughness-induced) crack closure with crack extension.

5. Due to an increased dependence on crack tip shielding, 2090-T8E41 shows a higher sensitivity to periodic compressive load cycles, compared to traditional high strength aluminum alloys. Specifically, the compressive loads required to cause crack growth at ΔK_{TH} were over a factor of two smaller in 2090, than in 2124 or 7150.

6. SHORT CRACK GROWTH IN 2124 ALLOY

6.1 Introduction

There are many factors which contribute to differences in behavior between long and short cracks.[2-20,35,46,49-63] The problem of microstructurally-small flaws, for example, may simply result from the inappropriate use of continuum mechanics involving the preferential initiation and growth of flaws in "soft spots" in the microstructure. Conversely, where crack sizes are comparable with

the extent of crack tip plasticity, or where cracks are embedded within the plastic zone of a notch, differences may result simply from the inappropriate use of LEFM in characterizing crack tip fields.[8,52] Other major differences have been related to the three-dimensional nature of crack growth,[53-55] anomalously higher plastic strains at the tips of microstructurally-small cracks,[49,56] and environmental effects.[15,18,20] However, in essence, the problem is one of a breakdown in similitude[57] and thus in defining the appropriate "crack driving force" for small crack growth. Such a driving force must account for excessive plasticity ahead of the crack tip and more importantly crack tip shielding behind it.[16,46]

The so-called anomalous behavior of small fatigue cracks is studied here with reference to the phenomenon of crack tip shielding, i.e., where the "effective crack driving force" actually experienced in the near-tip region is reduced from the applied (far-field) value. Sources of shielding are described in terms of mechanisms which act primarily on the wake of the crack, and rely on the production of elastically constrained zones which envelop the crack (zone shielding), on the generation of wedging, bridging or sliding forces between the crack surfaces (contact shielding), and on crack path deflection and meandering. It is shown that the general implications of shielding are resistance-curve toughness behavior, contrasting microstructural factors controlling crack initiation and crack growth, reduced growth rates, and "small crack" effects.[46] The latter notions are illustrated by experimental studies on near-

threshold fatigue behavior in a 2124 aluminum alloy, where shielding arises predominantly from crack closure induced by fracture surface asperity contact. By comparing the crack propagation and closure data for long cracks (of length $\sim$ 25 mm) and physically-short cracks (of length $\sim$ 50 to 400 μm), it is shown that shielding becomes increasingly more effective with increase in size of the short crack, resulting in crack size-dependent behavior. For two-dimensional short cracks, it is concluded that the lack of shielding provides the dominant mechanism for the growth of cracks below the long crack threshold stress intensity range. Moreover, the development of shielding with initial crack extension can result in progressively decreasing growth rate behavior as the threshold is approached.

6.2 Experimental Procedures

The material used was the commercial 2124-T351 25 mm thick plate discussed in Section 3. The heat treatment and room temperature mechanical properties were also listed in that section (Tables 3.1-3.3).

All fatigue testing was performed in controlled room temperature air (22°C, 45% relative humidity) using electro-servo-hydraulic testing machines operating at a frequency of 50 Hz (sine wave) with load ratios ($R = K_{min}/K_{max}$) 0.1, 0.5 and 0.75. D.C. electrical potential methods were used to monitor crack length, whereas a back-face strain technique provided continuous (macroscopic) measurements of crack closure.

In order to isolate the role of shielding and minimize problems from non-uniform growth, experiments were confined to the two-dimensional physically-short flaw, of a length no greater than 400 μm (large compared to computed plastic zone sizes). To compare the near-threshold crack growth and closure behavior of such flaws with long cracks, a "3-in-1" test procedure was utilized, as described in Section 3.

C(T) specimens, machined in the T-L orientation from the plate mid-section, were used to determine long crack growth rates and fatigue threshold values ΔK_{TH} for crack lengths between 17.5 and 38 mm. Thresholds were approached using an automated load-shedding scheme. After arrest at threshold, the distribution of closure along the crack length was examined by progressively removing material from the crack wake and monitoring the change in K_{cl} at each step. With the specimen at minimum load, material was slowly removed to within 250 μm of the tip using a ~ 0.3 mm wide jeweler's saw cut. Following wake removal to leave a small crack emanating from a (sharp) machined notch, cycling at threshold levels was resumed and the subsequent growth rate and closure behavior closely followed. Finally, after a further load shedding sequence to re-arrest the crack at the threshold, the major portion of the specimen was carefully machined off to leave a rectangular bend specimen (12 mm wide by 6 mm thick) containing a short crack. Initial crack lengths between 50 and 250 μm could be readily obtained with this procedure. Short crack growth

rate and closure data were then established in four-point bending under progressively increasing loads.

6.3 Long Crack Behavior

Fatigue crack growth rate data at R = 0.1 for underaged and overaged microstructures in 2124 alloy are shown in Fig. 6.1 for 17.5 to 38 mm long cracks over the range 5×10^{-11} to 10^{-7} m/cycle. Growth rates (da/dN) are plotted as a function of both the nominal stress intensity range, ΔK, and, after allowing for crack closure (Fig. 6.2), the effective stress intensity range, ΔK_{eff}, defined as $K_{max} - K_{cl}$. Specific threshold data are listed in Table 6.1.

Table 6.1: Long Crack Fatigue Threshold Data for 2124 Alloy

	R	K_{cl}	ΔK_{TH}	$\Delta K_{TH,eff}$	CTOD		Plastic Zone	
					$\Delta \delta$	δ_{max}	r_Δ	r_{max}
		(MPa√m)	(MPa√m)	(MPa√m)	(nm)	(μm)	(μm)	(μm)
Underaged	0.10	2.43	3.58	1.42	126.9	0.31	4.02	19.9
	0.50	0.67	1.97	1.52	37.6	0.30	1.91	19.1
	0.75	0.23	1.53	1.48	22.7	0.73	0.72	46.0
Overaged	0.10	1.04	1.97	1.04	36.6	0.09	1.13	5.6

Similar to long crack results in 7000 series alloys (e.g., ref. 24), underaged structures show lower near-threshold fatigue crack propagation rates and higher threshold ΔK_{TH} values compared to
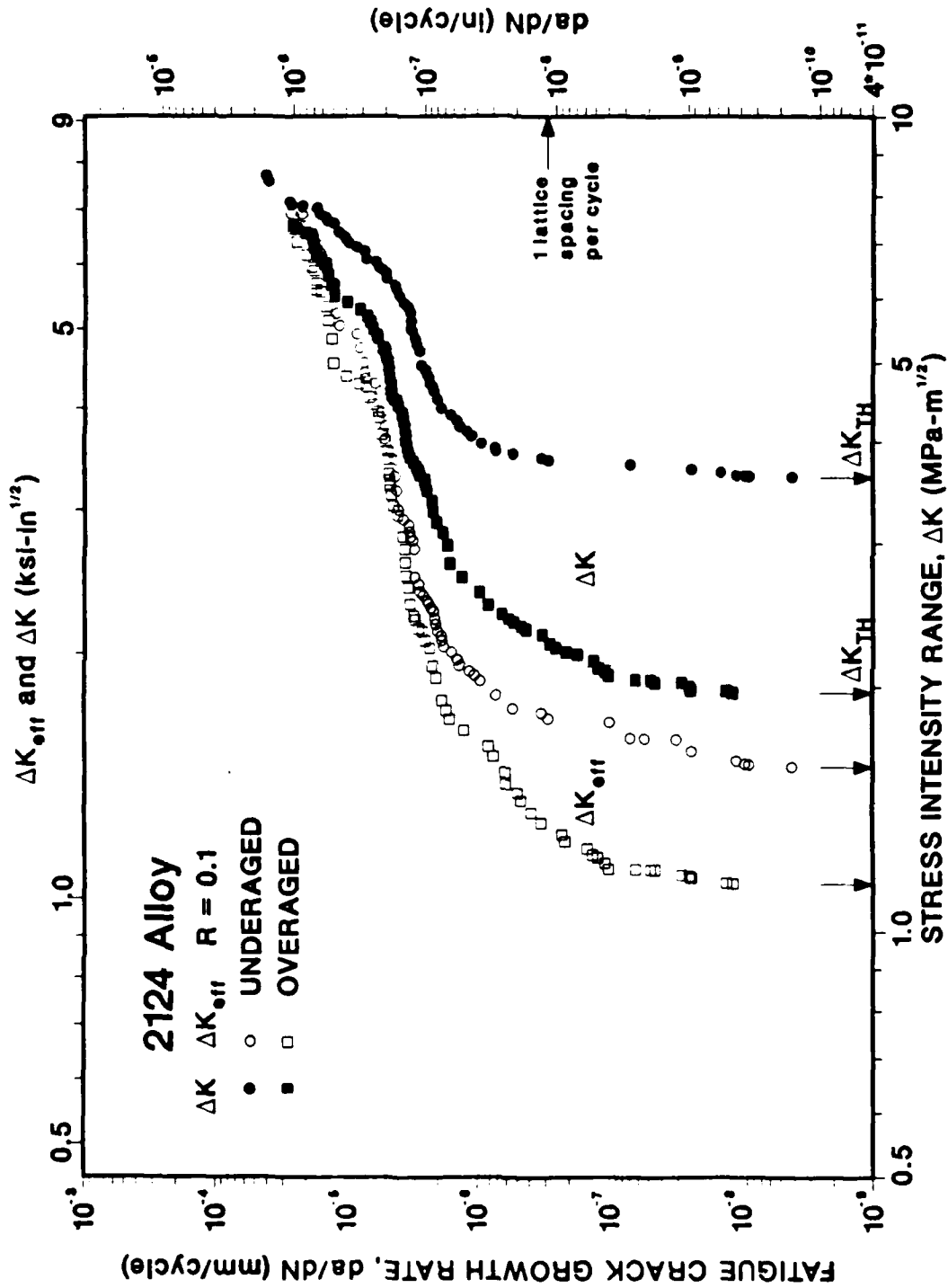
Fig. 6.1: Fatigue crack propagation behavior of long cracks in underaged (T351) and overaged 2124 alloy at R = 0.1. Growth rates are plotted as a function of the nominal stress intensity range, ΔK, and ΔK_{eff} after correcting for crack closure.

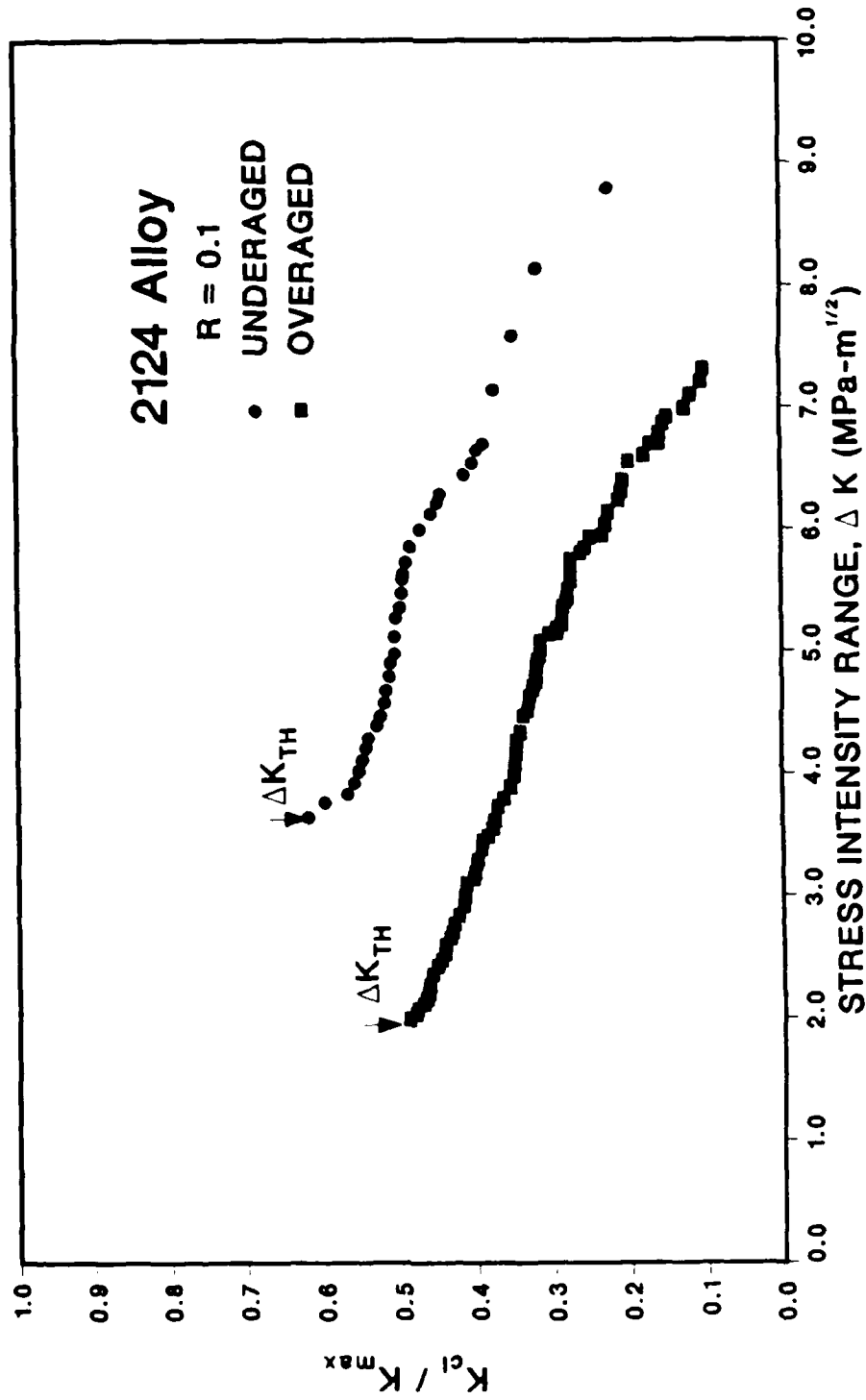Fig. 6.2: Variation in fatigue crack closure with nominal stress intensity range for long cracks in underaged (T351) and overaged 2124 alloy at R = 0.1. Results, plotted as the ratio of closure to maximum stress intensity, K_{cl}/K_{max}, are based on back-face strain measurements and correspond to the growth rate behavior presented in Fig. 6.1.

overaged structures. Such superior crack growth properties have been associated with the planar slip characteristics of coherent particle hardened microstructures. This results in greater slip reversibility and hence less crack tip damage per cycle, and in higher levels of crack closure from the more faceted (crystallographic) crack path, crack deflection and the consequent enhancement in roughness-induced closure from fracture surface asperity contact (e.g., refs. 24 and 47).

Following removal of their wake, threshold cracks arrested at $R = 0.1$ were observed to propagate when cycling resumed at the threshold ΔK_{TH}, similar to behavior reported for 7090, 7150 aluminum alloys and A508 steel.[22,23,34,64] Such observations of crack growth at the threshold provide confirmation that experimentally measured values of ΔK_{TH} are associated primarily with the build-up of closure, and do not necessarily represent an intrinsic material threshold. Consequently, where shielding mechanisms are inhibited, such as with small flaws or cracks at notches, or in the presence of compressive overload cycles,[24] the consequent increase in near-tip driving force may result in crack growth at or below ΔK_{TH}, and in general to growth rates which exceed those of long cracks at the same stress intensity level.

6.4 Short Crack Behavior of Notches

The experiment described above, where crack extension at ΔK_{TH} was observed following removal of the wake of an arrested threshold

crack, additionally provides an example of the accelerated growth of short cracks at notches, i.e., a fatigue crack (of length 250 μm) growing from a notch (of root radius $\sim$ 300 μm) in a region well beyond the notch field. Under constant load conditions with ΔK initially at ΔK_{TH}, cracks at $R = 0.75$ remain stationary, whereas at $R = 0.1$ they commence to propagate in both structures. Even though the nominal ΔK levels are marginally increasing, such growth occurs at a progressively decreasing growth rate over the first 300 μm, displaying the "trough-like" behavior characteristic of small cracks at near-threshold levels (Fig. 6.3).

Such behavior can be readily accounted for by considerations of crack tip shielding, specifically through characterization in terms of a local driving force (see also refs. 22,23,34,64). Concurrent back-face strain measurements of K_{cl}, over the 1 mm of growth following wake removal, show a steady increase in closure with initial short crack extension (Fig. 6.4). The value of K_{cl} approaches an apparent saturation value, after roughly 400 μm of crack extension, comparable with the long crack K_{cl} value at threshold (Table 6.1). As indicated in the figure, when such K_{cl} data are incorporated into the calculation of an effective stress intensity range, it can be seen that the initial progressive reduction in growth rates shown by the short crack is directly consistent with a corresponding progressive decrease in ΔK_{eff}.

It should be noted that the "small crack effect" observed in this experiment was achieved with a short crack of length 200 to
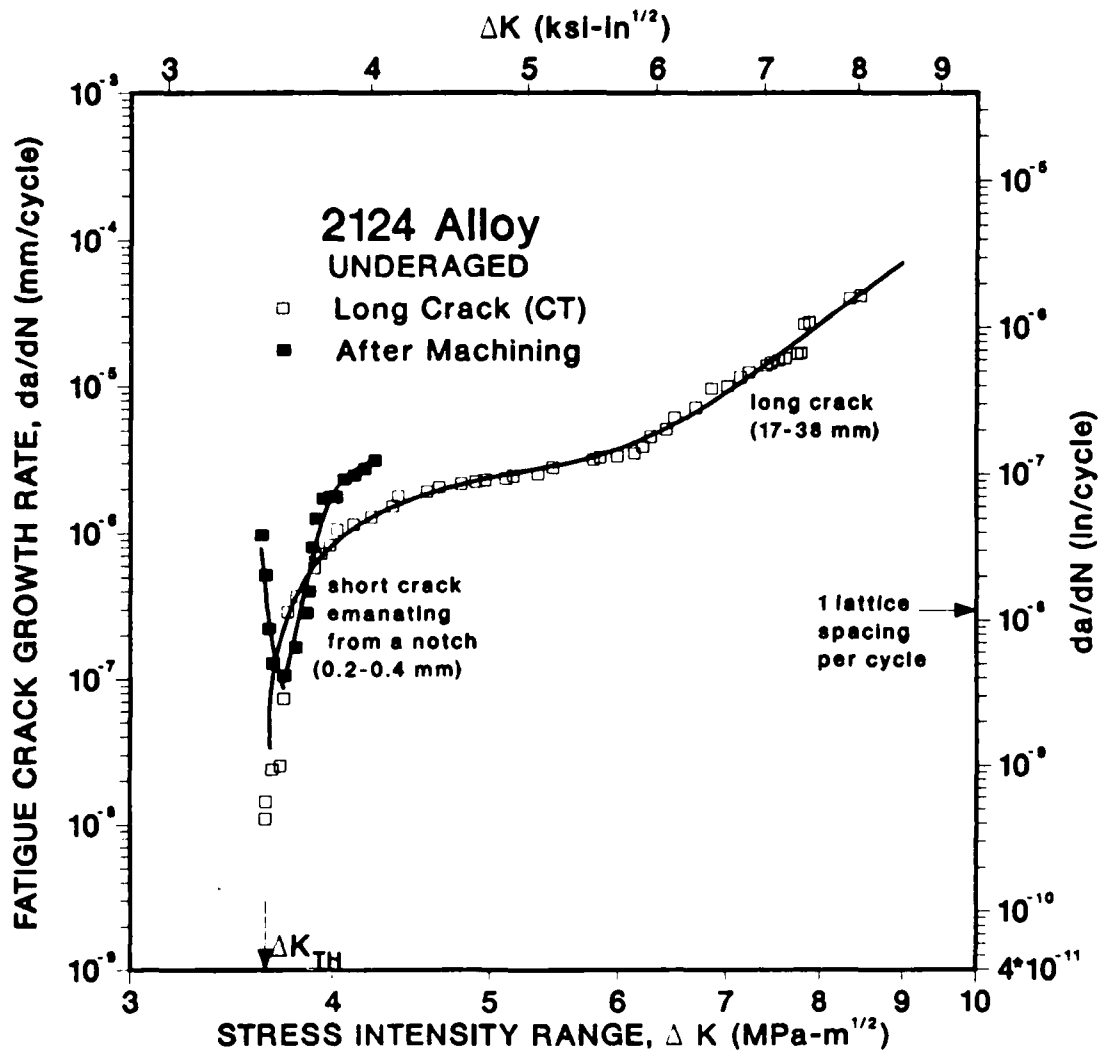
Fig. 6.3: Comparison of fatigue crack propagation data in underaged (T351) 2124 aluminum alloy at R = 0.1, showing results for long cracks (a = 17-38 mm) and physically-short cracks (a = 200-400 µm) emanating from a machined notch.
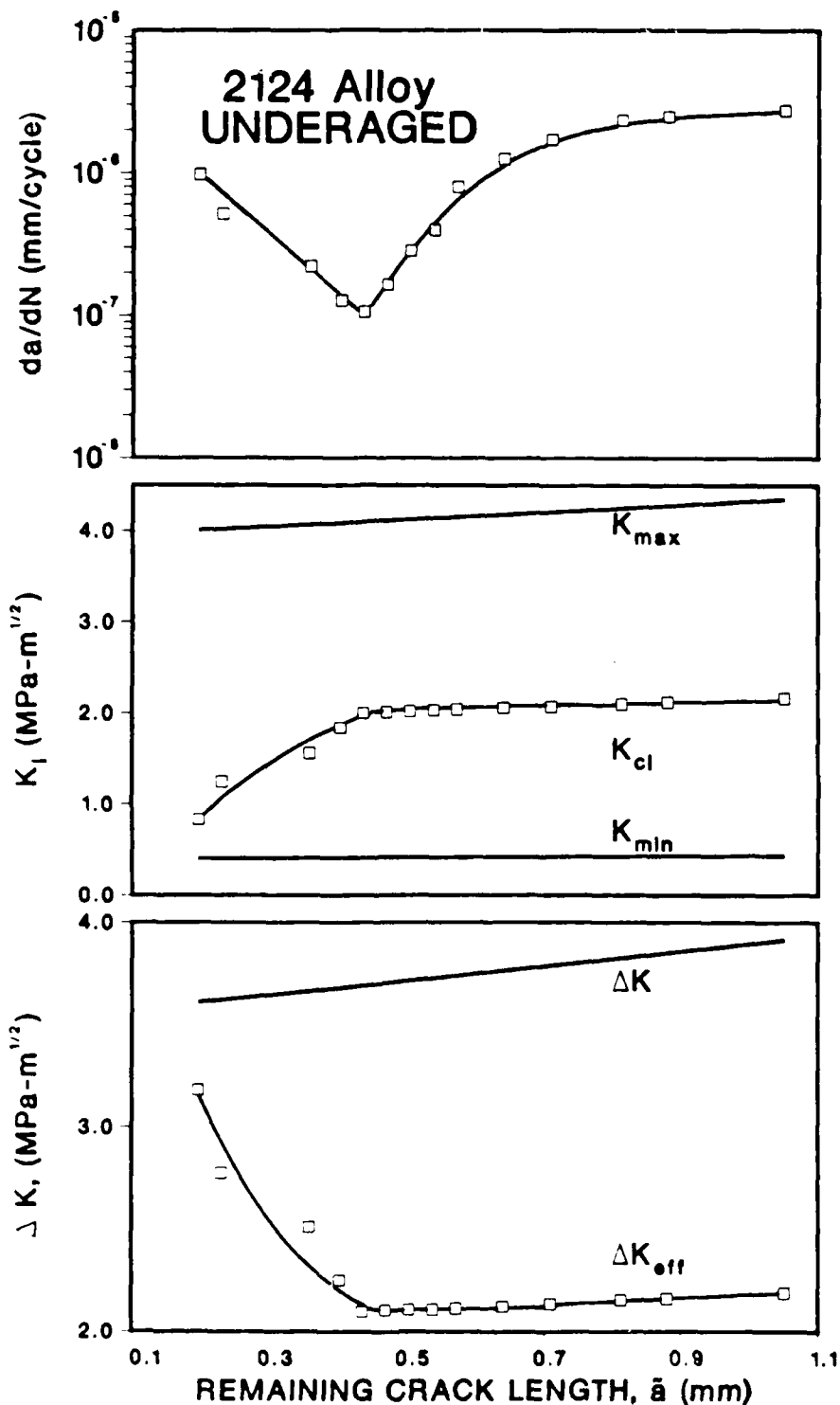
Fig. 6.4: Variation in growth rate, K_{cl}, and nominal and local crack driving forces, ΔK and ΔK_{eff}, respectively, with initial crack extension at $\Delta K = \Delta K_{TH}$ for physically-short cracks (a = 200-400 μm) emanating from a machined notch in 2124-T351 alloy at R = 0.1.

400 µm; length dimensions which are large compared to the scale of local plasticity (maximum plastic zone sizes do not exceed 20 µm). Thus, so-called "anomalous" behavior of small flaws does not necessarily result simply from a breakdown of linear elastic fracture mechanics, but rather from differences in the **local** crack driving force due to the varying influence of crack tip shielding with crack length.

6.5 Physically-Short Crack Behavior

Results for the behavior of physically-short cracks growing from a free surface are shown in Figs. 6.5-6.7 for the underaged (T351) microstructure. Specimens were cycled at a series of stepwise increasing ΔK levels starting well below the threshold ΔK_{TH}. As shown in Fig. 6.5, for an initial crack length of approximately 50 µm, short crack growth commences with a rate initially exceeding 10^{-8} m/cycle at a ΔK level as low as 0.58 MPa$\sqrt{m}$, only to decelerate progressively until arrest at 0.67 MPa$\sqrt{m}$ after an extension of roughly 140 µm. After an increase in applied load, cracking abruptly re-starts, again followed by progressive deceleration to arrest. This sequence of events is repeated several times until the crack length reaches 450 µm, whereupon the short crack data merges with long crack results following a characteristic minimum in growth rates.

During each deceleration and arrest event for the short crack, the development of crack closure with crack extension was closely
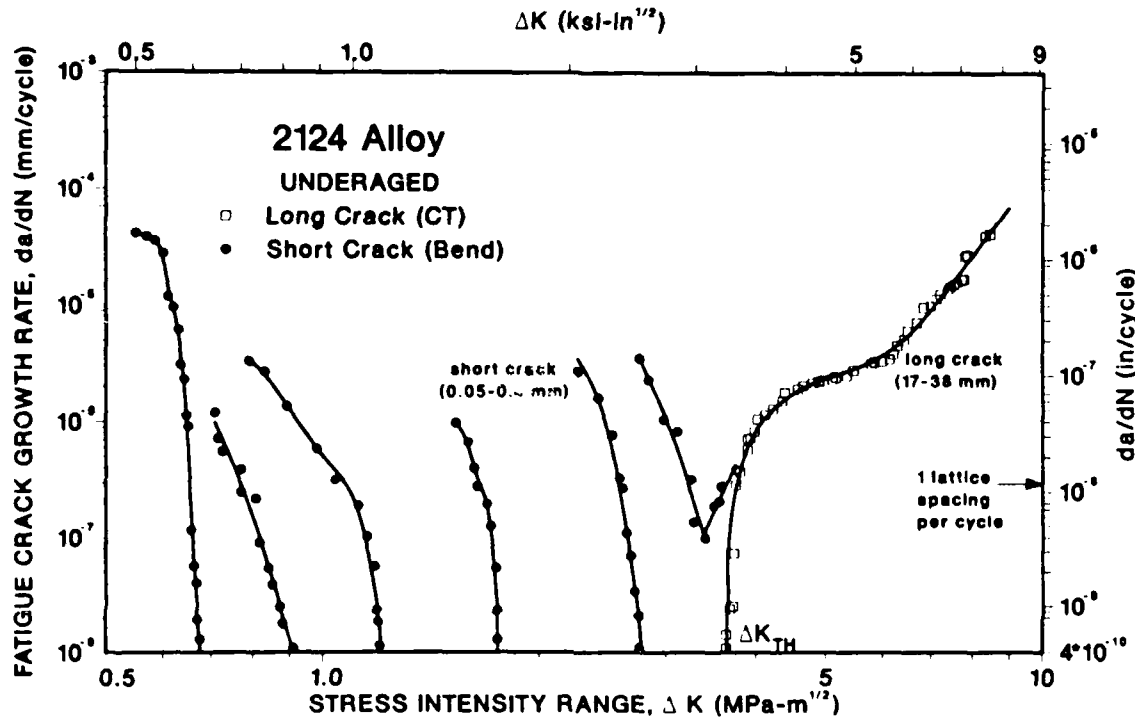
Fig. 6.5: Variation in fatigue crack growth rates in 2124-T351 alloy at R = 0.1, showing a comparison of results for long cracks (a = 17-38 mm) and physically-short cracks (a = 50-400 μm) emanating from a free surface. Note how the short crack grows at sub-threshold stress intensities at progressively decreasing growth rates, arresting after each decay sequence until finally merging with long crack data.

SUB-THRESHOLD CRACK GROWTH
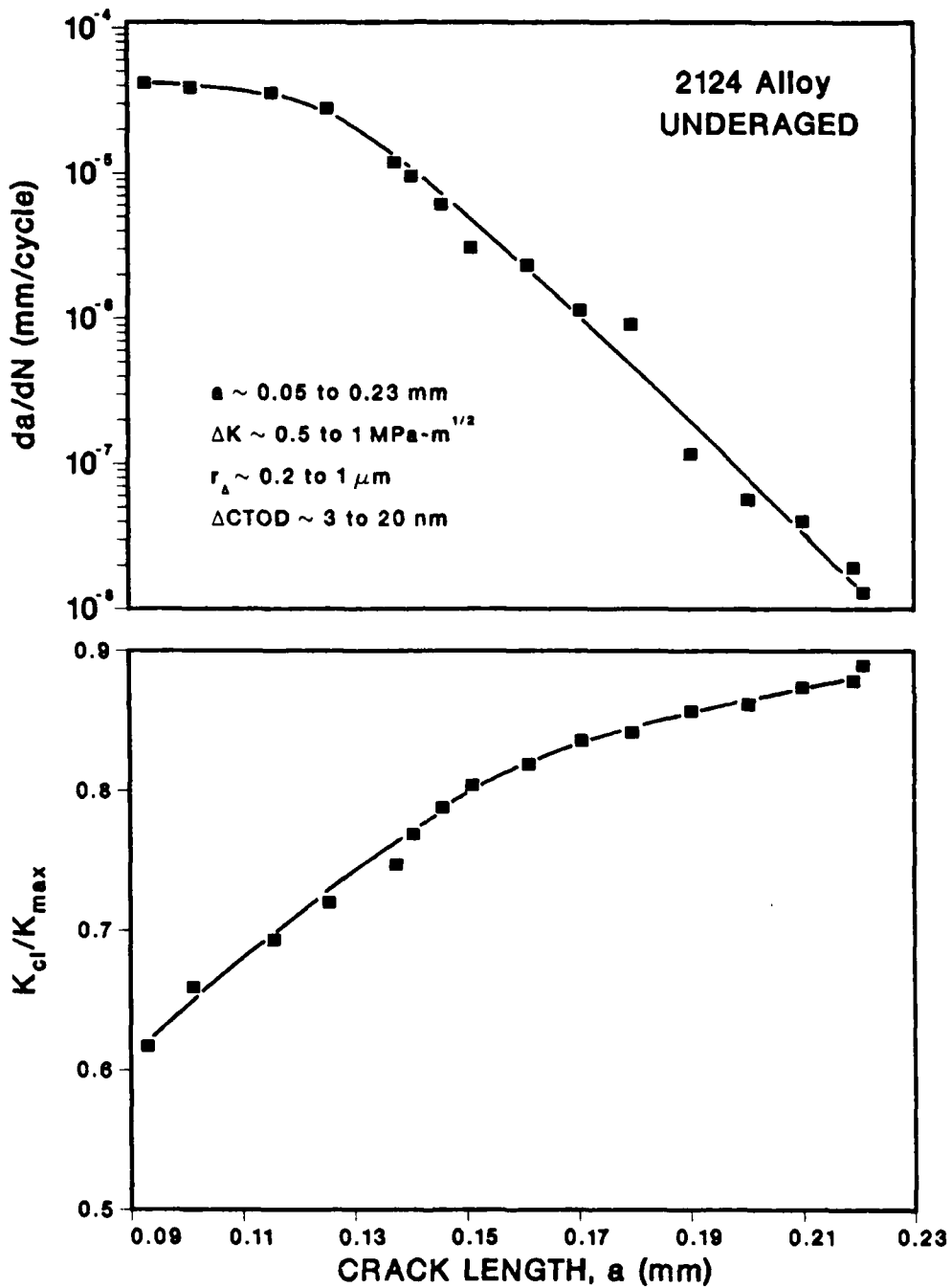
Fig. 6.6: Variation in da/dN and K_{cl}/K_{max} with crack extension during sub-threshold propagation of physically-short cracks in 2124-T351 alloy, corresponding to data in Fig. 6.5. Note how crack closure is generated during initial crack extension (a = 90 to 230 μm), concurrent with the progressive decay in growth rates to crack arrest.
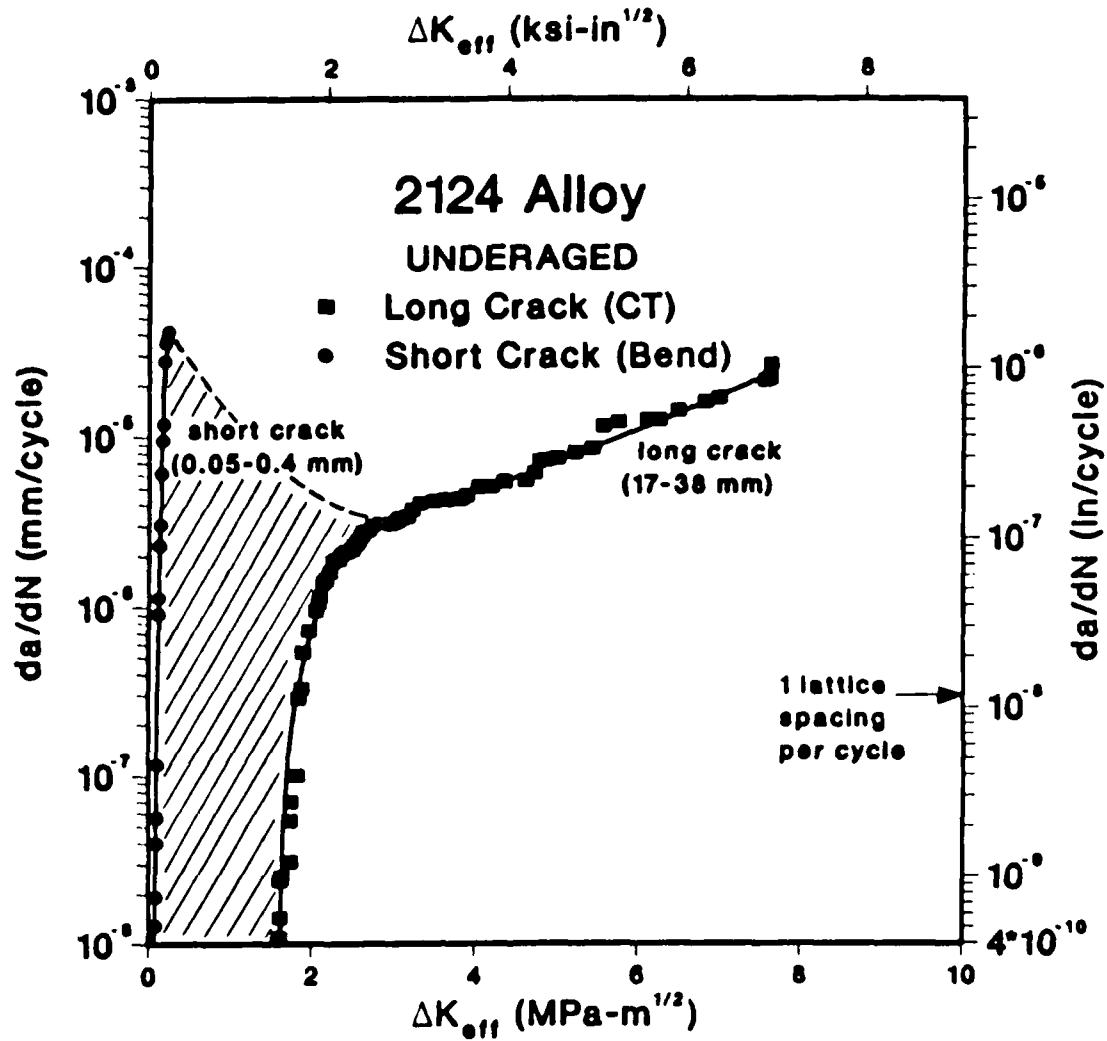
Fig. 6.7: Variation in fatigue crack growth rates in 2124-T351 alloy at R = 0.1 for long cracks (a = 17-38 mm) and physically-short cracks (a = 90-400 μm), plotted as a function of ΔK_{eff} (after allowing for crack closure). Note that physically-short cracks propagate below the effective threshold, indicating that differences in behavior between long and short cracks may not be solely attributable to closure effects.

monitored. Results for one such event, involving the extension of a 90 μm long crack to 230 μm, are shown in Fig. 6.6. **The progressive reduction in growth rates leading to arrest can be seen to be associated directly with a concurrent increase in crack closure,** which results in a corresponding reduction in ΔK_{eff}. The magnitude of this increase is associated with very high levels of K_{cl}/K_{max} approaching 0.9, far in excess of those for long cracks. Although closure data were not measured during every arrest event in Fig. 6.5, it was apparent that, since the crack retained closure generated from previous load steps, there was a cumulative increase in K_{cl} throughout the entire sequence. These results are plotted as a function of ΔK_{eff} in Fig. 6.6.

Similar sub-threshold behavior has been reported for naturally-occurring small cracks, specifically for 15-30 μm deep, semi-elliptical surface flaws initiated at graphite nodules in nodular cast iron.[55] Here, the deceleration and arrest phenomenon was attributed qualitatively to the three-dimensional nature of cracking, involving initial preferential growth at the surface before an equilibrium crack shape was formed.[53-55] While certainly a mechanism for the apparent initial retardation of small surface cracks, close fractographic examination of the through-thickness cracks in the present study revealed no such evidence of non-uniform growth.

6.6 Discussion

The current experimental results provide quantitative evidence of the dominant role of crack tip shielding, specifically from fatigue crack closure, in influencing the near-threshold behavior of both long and physically-short fatigue cracks. First, with respect to long cracks, wake machining experiments clearly show that i) the existence of a threshold stress intensity range for no crack growth, ΔK_{TH}, and ii) the effect of load ratio in influencing ΔK_{TH}, can be attributed to variations in the magnitude of the closure stress intensity, K_{cl}. The commonality of threshold values for each structure, when computed in terms of ΔK_{eff}, would appear to suggest that some intrinsic threshold does exist for long cracks.

Second, for (two-dimensional) physically-short cracks, both emanating from a sharp notch or at a free surface, observations of crack growth at stress intensities below ΔK_{TH}, at rates which progressively decay to arrest or merge with long crack data, have been shown to be associated quantitatively with an initial lack of shielding and its subsequent development with crack extension. Specifically, the sub-threshold decay in short crack growth rates has been related to a concurrent increase in K_{cl}, such that the local driving force, ΔK_{eff}, sees a minimum.

Although care must be exercised in interpreting growth rate data plotted as a function of ΔK_{eff}, due to experimental uncertainties in the measurement of K_{cl}, it is apparent from the present results that, even after allowing for crack closure, **physically-short cracks can**

propagate below the long crack (ΔK_{eff}) threshold (Fig. 6.7). Thus, similar to conclusions reported for microstructurally-small cracks in aluminum alloys,[56] shielding via crack closure apparently does not provide a complete rationalization for the enhanced growth rates of small flaws, although it clearly provides a major contribution. The nature of the other contributing mechanisms is currently uncertain, although in-situ surface measurements on microstructurally-small cracks in 2024 and 7075 alloys have shown higher plastic strain levels at the tips of the small flaws,[49,56] conceivably resulting from reduced zone shielding associated with the limited plastic wake.

Finally, with respect to the practical problem of dealing with the small crack effect in fatigue design and life prediction, it would appear that the damage-tolerant methodology of integrating growth rate data between the limits of initial and final crack size can be extended into the physically-small crack regime through the use of a driving force which accounts for crack tip shielding (principally from closure and possibly deflection) and, where necessary, excessive plasticity ahead of the tip. Parameters based on ΔK_{eff} and perhaps ΔJ may be considered appropriate here. This approach, however, cannot be extended indefinitely to account for the behavior of microstructurally-small flaws, which may initiate and grow from local "soft spots" in the microstructure. Since the size scales in this regime are below the continuum approximation, any deterministic analysis based on a presumed material parameter must be considered questionable. It would seem that a probabilistic approach

here will be most useful which, when added to the extended damage-
tolerant analysis, can yield more realistic estimates of total
fatigue life.

6.7 Conclusions

Based on an investigation into the role of crack tip shielding
in influencing the behavior of long and small fatigue cracks,
involving an experimental study of long ($\sim$ 25 mm) and physically-
short ($\sim$ 50-400 μm) near-threshold cracks in 2124 aluminum alloy, the
following conclusions can be made:

1. The existence of a threshold stress intensity range ΔK_{TH} for
the dormancy of long cracks was found to be associated with high
levels of crack closure, with values of K_{cl}/K_{max} approaching 0.7. By
accounting for such closure through the use of the ΔK_{eff} parameter,
the influence of load ratio, but not microstructure, in affecting
long crack growth rates and threshold values became minimal.

2. Through removal of material from the wake of long cracks,
arrested at the threshold, to discern the distribution of shielding,
over 60% of the closure was found to be located within 900 μm of the
crack tip.

3. Through-thickness physically-short cracks, both emanating
from a sharp notch or from a free surface, were observed to propagate
at nominal stress intensity ranges at, or below, ΔK_{TH}. Short crack
growth rates were observed to decay progressively until arrest (or

before merging with long crack data), concurrent with a measured increase in K_{cl} and consequent reduction in ΔK_{eff}.

4. Differences in behavior between long and physically-short cracks appear to be rationalized largely by the variation in crack closure with the extent of crack wake. However, as short cracks were still observed to propagate **below** the effective threshold stress intensity range (after accounting for closure), other factors, such as enhanced crack tip plastic strains, must be involved.

7. ASSESSMENT OF THE SMALL CRACK PROBLEM

7.1 Introduction

The total fatigue life of engineering structures and components is often dominated by the time (or number of cycles) during which incipient cracks are small (typically less than 1 mm) and propagating at low growth rates. However, it is in this regime that the behavior of such cracks may become non-unique, and exhibit growth rates far in excess of those of long cracks (typically larger than 10 mm) subjected to the same nominal "driving force," e.g., the same stress intensity range.[2-20,35,46,49-72]

In this section, the salient features of the problem are evaluated with respect to the various classes of small flaws. In addition, some thoughts are offerred on the incorporation of small crack methodology into current design and fatigue life prediction

analyses and on the development of new materials with superior resistance to the growth of microcracks by fatigue.

7.2 The Small Crack Problem

The small crack problem is in essence one created by fracture mechanics through a breakdown in the similitude concept at small crack sizes.[57] For example, it has been shown[65] that crack tip strain fields for large and microstructurally-small fatigue cracks, driven by nominally equivalent cyclic stress intensities, are qualitatively and quantitatively dissimilar. It is thus a problem of defining a flaw size-independent "crack driving force" to account for observations that small cracks can propagate at rates different from those of corresponding long cracks at the same nominal driving force. In the large majority of cases, small crack growth rates exceed those of long cracks, although there is evidence in steels of a mild reverse effect.[66,67] Following initiation, small cracks are observed to grow at stress intensities below the long crack threshold; some extend with decaying growth rates until arrest, while others propagate quite rapidly to merge with long crack behavior (Fig. 2.1). The problem therefore has practical significance, because damage-tolerant fatigue lifetime computations are invariably based on long crack data. As overall life is most influenced by low growth rate behavior, the accelerated and sub-threshold extension of small flaws can lead to potentially dangerous over-predictions of life.

7.3 Definition of a Small Crack

Adjectives describing various types of small crack currently abound, although some consensus is emerging. For example, the distinction between (three-dimensional) small flaws and (two-dimensional) short flaws, the latter being small in all but one dimension, clearly is of importance.[53,56] Short flaws are generally through-thickness cracks, no smaller than 50 µm, which are created artificially by removing the wake material from long through cracks. Their behavior appears to be dominated, like that of large cracks, by the cyclic stress intensity factor ΔK (for small-scale yielding), corrected by considerations of crack closure.[46,53] Naturally-occurring small flaws, conversely, often approach microstructural dimensions, and although their behavior is still largely affected by closure, several other factors, including crack shape,[53,54] enhanced crack tip plastic strains,[56] and local arrest at grain boundaries,[68,69] are of comparable significance.

Useful qualifiers remain microstructurally-, mechanically- and physically-small (or short), which pertain respectively to cracks small compared to microstructural dimensions, to the scale of local plasticity, and simply to cracks of a size less than 0.5 to 1 mm.[19] In addition, fatigue cracks have also been described, with reference to environmental effects, as chemically-small,[15,18,20,70] as described below. Each of these classes of small flaw is associated with particular phenomena which primarily distinguish it from long crack behavior (Table 7.1). For example, for mechanically-small

Table 7.1: <u>Classes of Small Fatigue Cracks</u>

Type of Small Crack	Dimension	Responsible Mechanism	Potential Solution
Mechanically-small	$a \lesssim r_y{}^a$	excessive (active) plasticity	use of ΔJ, ΔS $\Delta CTOD$
Microstructurally-small	$a \lesssim d_g{}^b$ $2c \lesssim 5\text{-}10\ d_g$	crack tip shielding enhanced $\Delta \varepsilon_p$ crack shape	probabilistic approach
Physically-small	$a \lesssim 1$ mm	crack tip shielding (crack closure)	use of ΔK_{eff}
Chemically-small	up to ~ 10 mm^c	local crack tip environment	

$^a r_y$ is plastic zone size or plastic field of notch.

$^b d_g$ is critical microstructural dimension, e.g., grain size, a is the crack depth and 2c the surface length.

^{c}Critical size is a function of frequency and reaction kinetics.

flaws, characterization in terms of elastic-plastic fracture mechanics (e.g., through the use of $\Delta CTOD$ or ΔJ^7), or even in terms of the strain energy density ΔS,[71] may help resolve differences in growth rates behavior between long and small cracks. On the other hand, for physically-small flaws, allowance for differences in the magnitude of crack closure (e.g., through the use of ΔK_{eff}) appears to be the predominant correlating factor.[16,19,46,72] In the case of microstructurally-small flaws, all these factors may be important, plus others associated with local inhomogeneities in the

microstructure, non-uniform growth, retardation at grain boundaries, and so forth.[56,66,68]

In particular, the microstructurally-small, rapidly growing crack corresponds to a three-dimensional crack whose plastic zone is less than the key microstructural dimension, which in most cases is the grain size. Thus, the crack tip tends to operate as it would in a single crystal preferentially oriented for operation of the relevant crack extension mechanism. In addition, the crack front encompasses relatively few grains, so that growth is not averaged over many disadvantageously oriented grains. The latter is probably a major factor in distinguishing small cracks from short through-thickness cracks, whose fronts must necessarily sample many grains. It further provides an explanation why crack tip shielding alone is generally sifficient to rationalize behavior of the short through crack.

7.4 Origins of Differences Between Long and Small Crack Behavior

Several major factors have been identified which are primarily responsible for differences in long and small crack behavior (Table 7.1). Of particular significance is the varying contribution of crack tip shielding, with size of the crack wake, in locally reducing the effective driving force experienced at the tip.[46] Such shielding arises in fatigue from crack closure (e.g., refs. 19,71), and to a lesser extent from crack deflection,[73] and has been shown to be diminished at small crack sizes.[46,53] However, for

microstructurally-small cracks, it is now apparent that closure does
not provide the entire solution (although uncertainties in
experimental measurement make this question difficult to resolve).
There is now considerable evidence that, additionally, such flaws are
impeded locally by grain boundaries,[68,69] influenced by non-uniform
growth,[53,54] and may experience higher cyclic plastic strains at
their tips.[56] Finally, differences in local crack tip environment
with crack size provide the source of the chemically-short
effect,[15,18,20,70] as described in Section 7.5.

7.5 Environmental Effects

One of the most complex issues involved in the small crack
problem is associated with (liquid) environmental effects.[15,18,20,70]
As outlined by Gangloff and Wei,[70] the chemically-short crack may
still propagate 1.5 to several hundred times faster than long cracks
subjected to the same mechanical driving force. Moreover, it may be
somewhat larger than the microstructurally- or mechanically-short
flaw, as short crack behavior has been reported for crack sizes
upwards of ~ 10 mm. (Precise statement of the size range for
chemically-short cracks cannot be defined; it depends upon several
factors and is principally controlled by frequency and reaction
kinetics.) The discrepancy in behavior is attributed to differences
in local crack tip chemical environment and conditions.[15,18,20,70]
The critical issues thus pertain to the determination of crack tip
conditions, as a function of crack length, in terms of the coupled

processes of fluid transport and chemical/electrochemical reactions within the crack, and the determination of the origin of the environmentally-enhanced cracking rates in relation to the hydrogen embrittlement and film rupture/dissolution mechanisms.

7.6 "Driving Force" for Small Crack Propagation

Several authors (e.g., refs. 7,19,46,50,53,70) have sought improved field characterizing parameters to describe the driving force for small crack advance (Table 7.1). Although parameters such as $\Delta\sigma$ and $\Delta\epsilon_p$ have been suggested,[50] only those parameters that can be measured globally, yet define (at least nominally) local conditions, are reviewed here. For mechanically-small cracks, where the extent of local plasticity is comparable with crack size, elastic-plastic fracture mechanics solutions have been proposed through the use of ΔJ[7] and ΔS.[71] While certainly appropriate for taking account of excessive plasticity **ahead** of the tip, it should be noted that J is a nonlinear elastic parameter, and thus cannot account for the vital influence of wake plasticity (prior plastic) zones **behind** the tip. Similarly, the use of ΔS cannot account for the varying contribution from wake-related crack tip shielding. To allow for such wake effects, which principally cause crack closure, the adoption of a closure-corrected ΔK_{eff} appears to be a suitable approach for physically-small cracks[46,53] and cracks emanating from notches.[13] For microstructurally-small flaws, however, such deterministic treatments may simply not apply, as initial cracking

may center on local preferential growth sites ("soft spots") in the microstructure.[56] Here a probabilistic approach may be the optimum treatment to describe the behavior of such tiny flaws.

7.7 Intrinsic Thresholds

There is now good evidence that intrinsic threshold cyclic stress intensities may exist for long fatigue cracks. By subtracting out the contribution from crack closure through the use of the ΔK_{eff} parameter, threshold values at low load ratios approach those at high load ratios where closure effects are minimal (e.g., refs. 16,46). Similarly, intrinsic thresholds may exist for physically- and mechanically-short cracks, of magnitude comparable with the effective long crack value.[46,51,53] For microstructurally-small cracks, however, the question of an intrinsic threshold may not be meaningful. Here the "fatal" flaws are the ones that initiate first at local "soft spots" in the microstructure. As their dimensions are well below any continuum approximation, characterization in terms of a material parameter clearly would be inappropriate. Further, in light of evidence[56] suggesting the invalidity of ΔK within this flaw size regime, it may be more appropriate to consider a threshold stress, rather than a stress intensity, for microstructurally-small flaws (i.e., akin to the fatigue limit).

7.8 Small Crack Methodology in Life Prediction and Design

For physically- or mechanically-small cracks, the adoption of small crack methodology in life prediction analyses would appear to be feasible by mere extension of the current damage-tolerant procedures to smaller crack sizes through the use of ΔK_{eff}, or an equivalent elastic-plastic characterizing parameter. Such an approach would greatly enhance projected lifetimes, as computations are dominated by the regimes where the crack is small and advancing slowly. Conversely, for the reasons outlined above, descriptions of the extension of microstructurally-small flaws will not be generally amenable to deterministic analyses which rely on (continuum) material parameters, and should be treated with probabilistic approaches.

7.9 Small Crack Considerations in Alloy Design

From an alloy design perspective, the study of small cracks and associated long crack thresholds has resulted in a far clearer understanding of the various contributions to fatigue resistance. Moreover, it has led to the realization that microstructural features which benefit resistance to the growth of (long) cracks may have an entirely different influence on crack initiation and small crack growth. To impede long crack growth, the primary mechanisms are **extrinsic**, whereby mechanical, microstructural, and even environmental mechanisms are utilized to reduce locally the crack driving force.[46] Here, promotion of crack tip shielding, principally through crack closure and deflection, provides the most potent effect

under cyclic loading. Conversely, to impede crack initiation and the early growth of microstructurally-small cracks, where shielding effects are minimized, the primary mechanisms are **intrinsic**. For example, fine grain sizes offer best resistance to crack initiation and small crack growth in many alloys (e.g., ref. 51), yet in these same materials it is the coarse grain structures which promote the roughest crack paths and hence provide greatest resistance to long crack growth (through crack deflection and roughness-induced closure) (e.g., ref. 74).

In essence, the ideal alloy design approach is to clean-up the material for optimum resistance to crack initiation, incorporate small, randomly oriented grains to inhibit small crack growth, and then to add microstructural "crack stoppers" through shielding mechanisms to impede long crack growth. It may also be possible to minimize the small crack problem by incorporating texture, so that as few grains as possible are oriented for easy crack extension relative to a known uniaxial loading axis.

7.10 Conclusions

1. Small fatigue cracks can be characterized as mechanically-small (comparable with the extent of local plasticity), microstructurally-small (comparable with the scale of microstructure), physically-small (typically less than 1 mm in size), or chemically-small. Their common property is that they can propagate at rates which differ from, and generally exceed, those of

long cracks at the same nominal stress intensity factor, leading to potentially non-conservative damage-tolerant lifetime predictions.

2. The primary factors responsible for differences in behavior between long and mechanically- and physically-small flaws are, respectively, extensive plasticity ahead of the tip, and crack tip shielding from crack closure behind the tip. Such differences may be in part normalized through characterization in terms of ΔK_{eff}, or an equivalent elastic-plastic field parameter.

3. The behavior of microstructurally-small flaws differs from long cracks because of several factors, including excess crack tip plasticity, crack closure, crack shape and deflection, retardation at grain boundaries, and enhanced crack tip plastic strains. Such flaws may not be amenable to characterization in terms of a global field parameter, as their dimensions lie below continuum size-scales.

4. Approaches to apply small crack methodology to fatigue life prediction are suggested in terms of i) the use of ΔK_{eff}, or equivalent elastic-plastic parameter, to extend damage-tolerant procedures into the physically-small crack regime, and ii) probabilistic analyses of the initiation and early growth of microstructurally-small flaws.

5. In life prediction, the concern is with predicting the growth of the most rapidly growing, ultimately fatal, small crack. To design alloys which are resistant to such behavior, the approach must be to eliminate such maverick flaws, by creating microstructures to arrest the microstructurally-small cracks which are able to

nucleate. Thus, for optimum fatigue resistance, the approach may involve using clean materials to inhibit crack initiation, small randomly oriented grains to inhibit small crack growth, and employing crack tip shielding (i.e., microstructural "crack stoppers") to impede the growth of long cracks.

8. BRIEF SUMMARY OF FUTURE WORK

Studies planned for the coming year will be primarily directed towards characterizing the behavior of microstructurally-small (naturally-occurring) surface flaws, of sizes ranging from 5 to 400 µm, and the comparison of such results with the short, through-thickness flaws (a $\sim$ 40 to 400 µm) and long flaws ($\sim$ 20 mm) described in the current report. Studies on through-thickness short cracks have the disadvantage that the flaws are created artificially (see Section 3), yet they do offer the possibility of measuring the development of crack closure with initial small crack extension. With the exception of laser inferometry techniques,[35] it is not possible to monitor similarly the closure generated with small surface flaws. However, such cracks nucleate at the local preferential growth sites ("soft spots") in the microstructure, and therefore are a far better simulation of service conditions. Accordingly, it is planned to complete the study of the growth and closure characteristics of the through-thickness flaws in overaged 2124 and in 2090-T8E41, and then microstructurally-small surface

cracks in four-point bend samples of underaged and overaged 2124 and in 2090-T8E41.

Due to the strong anisotropy of the 2090 aluminum-lithium alloy, both with respect to microstructure and mechanical properties, attempts will be made to gather small crack data in the longitudinal, transverse and short-transverse directions. Because of the limited plate thickness (i.e., 13 mm), the evaluation of short-transverse properties will be performed using double-cantelever beam (DCB) specimens of dimensions 51 mm x 13 mm x 6.4 mm. Crack growth data will be analyzed in terms of the Newman and Raju stress intensity solutions[75] for small surface cracks, and will be considered in terms of a full fractographic evaluation of the fatigue surfaces.

Studies on the role of compression cycling will be continued with particular attention to the aluminum-lithium alloy. In order to study the effect with a well-defined stress field, center-crack panel-type specimens will be used with a set of specially designed friction grips. Single compression cycle tests, as well as negative load ratio tests, will be performed to fully understand the effect of compression cycling in the fatigue crack propagation. It is expected that the use of compression will decrease the amount of closure generated during crack growth. Consequently, it is anticipated that higher growth rates will be observed for tests with negative-R ratios than tests with positive-R ratios at comparable values of applied stress intensity range.

9. ACKNOWLEDGEMENTS

10. REFERENCES

1. R. O. Ritchie: International Metals Reviews, 1979, vol. 20, p. 205.

2. M. E. Fine and R. O. Ritchie: in Fatigue and Microstructure, p. 245, American Society for Metals, Metals Park, OH, 1979.

3. S. J. Hudak: J. Eng. Matls. Tech., Trans. ASME Series H, 1981, vol. 103, p. 26.

4. S. Pearson: Eng. Fract. Mech., 1975, vol. 7, p. 235.

5. H. Kitagawa and S. Takahashi: Proc. 2nd Intl. Conf. on Mech. Beh. of Materials, p. 627, American Society for Metals, Metals Park, OH, 1976.

6. Y. H. Kim, T. Mura and M. E. Fine: Eng. Fract. Mech., 1978, vol. 11, p. 1697.

7. N. E. Dowling: ASTM Spec. Tech. Publ. 637, American Society for Testing and Materials, Philadelphia, PA, 1978, p. 97.

8. M. H. El Haddad, N. E. Dowling, T. H. Topper and K. N. Smith: Int. J. Fract., 1980, vol. 16, p. 15.

9. R. A. Smith and K. J. Miller: Int. J. Mech. Sci., 1977, vol. 19, p. 11.

10. W. L. Morris: Met. Trans. A, 1980, vol. 11A, p. 1117.

11. ⁻. N. Leis and T. . Forte: ASTM Spec. Tech. Publ. 743, American Society for Testing and Materials, Philadelphia, PA, 1982, p. 100.

12. S. Usami and S. Shida: Fat. Eng. Matls. Struct., 1979, vol. 1, p. 471.

13. K. Tanaka and Y. Nakai: Fat. Eng. Matls. Struct., 1983, vol. 5, p. 315.

14. G. P. Sheldon, T. S. Cook, T. W. Jones and J. Lankford: Fat. Eng. Matls. Struct., 1981, vol. 3, p. 219.

15. R. P. Gangloff: Res. Mech. Letters, 1981, vol. 1, p. 299.

16. J. F. McCarver and R. O. Ritchie: Mater. Sci. Eng., 1982, vol. 55, p. 63.

17. J. Lankford: Fat. Eng. Matls. Struct., 1982, vol. 5, p. 223.

18. R. P. Gangloff: Met. Trans. A, 1985, vol. 16A, p. 953.

19. S. Suresh and R. O. Ritchie: International Metals Reviews, 1984, vol. 29, p. 445.

20. R. P. Gangloff and R. O. Ritchie: in Fundamentals of Deformation and Fracture, Eshelby Memorial Symp., B. A. Bilby, K. J. Miller and J. R. Willis, eds., Cambridge University Press, U.K., p. 529, 1985.

21. E. Zaiken and R. O. Ritchie: Mater. Sci. Eng., 1985, vol. 70, p. 151.

22. E. Zaiken and R. O. Ritchie: Scripta Met., 1984, vol. 8, p. 847.

23. E. Zaiken and R. O. Ritchie: Met. Trans. A, 1985, vol. 16A, p. 1467.

24. E. Zaiken and R. O. Ritchie: Eng. Fract. Mech., 1985, vol. 22, p. 35.

25. P. Donehoo, W. Yu and R. O. Ritchie: Mater. Sci. Eng., 1985, vol. 74, p. 11.

26. R. O. Ritchie, E. Zaiken and A. F. Blom: in Basic Questions in Fatigue, ASTM ST⁻, J. T. Fong and R. J. Fields, eds., American Society for Testing and Materials, Philadelphia, PA, 1986, in press.

27. R. J. Rioja and E. A. Ludwiczak: in Aluminum-Lithium Alloys III, C. Baker et al., eds., The Institute of Metals, London, U.K., 1986, p. 471.

28. W. F. Deans and C. E. Richards: J. Test. Eval., 1979, vol. 7, p. 147.

29. C. E. Richards and W. F. Deans: in The Measurement of Crack Length and Shape during Fracture and Fatigue, C. J. Beevers, ed., EMAS Ltd., Warley, U.K., 1980, p. 28.

30. M. Kikukawa, M. Jono and K. Tanaka: in Proc. 2nd Intl. Conf. on Mechanical Behavior of Materials, ASM, Metals Park, OH, 1976, p. 254.

31. V. B. Dutta, S. Suresh and R. O. Ritchie: Metall. Trans. A, 1984, vol. 15A, p. 1193.

32. M. N. James and J. F. Knott: Mater. Sci. Eng., 1985, vol. 72, p. L1.

33. W. Elber: Eng. Fract. Mech., 1970, vol. 2, p. 37.

34. K. Minakawa, J. C. Newman and A. J. McEvily: Fat. Eng. Matl. Struct., 1983, vol. 6, p. 359.

35. J. M. Larsen, T. Nicholas, A. W. Thompson and J. C. Williams: in Small Fatigue Cracks, R. O. Ritchie and J. Lankford, eds., TMS-AIME, Warrendale, PA, 1986.

36. K. D. Unangst, T. T. Shih and R. P. Wei: Eng. Fract. Mech., 1977, vol. 9, p. 725.

37. S. Suresh, D. M. Parks and R. O. Ritchie: in Fatigue Thresholds, J. Bäcklund, A. Blom and C. J. Beevers, eds., EMAS Ltd., Warley, U.K., 1982, vol. 1, p. 391.

38. C. M. Hudson and J. T. Scardina: Eng. Fract. Mech., 1969, vol. 1, p. 429.

39. P. Au, T. H. Topper and M. L. El Haddad: in Behavior of Short Cracks in Airframe Components, AGARD Conf. Proc. No. 328, AGARD, France, 1983, p. 11.1.

40. M. T. Yu, T. H. Topper and P. Au: in Fatigue '84, C. J. Beevers, ed., EMAS Ltd., Warley. U.K., 1984, vol. 1, p. 179.

41. T. M. Hsu and W. M. McGee: in Effect of Load Spectrum Variables in Fatigue Crack Initiation and Propagation, ASTM STP 714, American Society for Testing and Materials, 1980, p. 79.

42. D. Gan and J. Weertman: Eng. Fract. Mech., 1981, vol. 15, p. 87.

43. J. Schijve and D. Broek: Aircraft Engineering, 1962, vol. 34, p. 314.

44. S. Suresh, T. Christman and M. Bull: in Small Fatigue Cracks, R. O. Ritchie and J. Lankford, eds., TMS-AIME, Warrendale, PA, 1986.

45. R. Marissen, K. H. Trautmann and H. Nowack: Eng. Fract. Mech., 1984, vol. 19, p. 863.

46. R. O. Ritchie and W. Yu: in Small Fatigue Cracks, R. O. Ritchie and J. Lankford, eds., TMS-AIME, Warrendale, PA, 1986.

47. A. K. Vasudévan, P. E. Bretz, A. C. Miller and S. Suresh: Mater. Sci. Eng., 1984, vol. 64, p. 113.

48. K. V. Jata and E. A. Starke: in Aluminium-Lithium Alloys III, C. Baker et al., eds., The Metals Society, London, U.K., 1986, p. 247.

49. J. Lankford: Fat. Fract. Eng. Mat. Struct., 1985, vol. 8, p. 161.

50. K. J. Miller: Fat. Eng. Mat. Struct., 1982, vol. 5, p. 223.

51. C. W. Brown and J. E. King: in Small Fatigue Cracks, R. O. Ritchie and J. Lankford, eds., TMS-AIME, Warrendale, PA, 1986.

52. M. M. Hammouda and K. J. Miller: in Elastic-Plastic Fracture, ASTM STP 668, American Society for Testing and Materials, Philadelphia, PA, 1979, p. 703.

53. A. Pineau: in Small Fatigue Cracks, R. O. Ritchie and J. Lankford, eds., TMS-AIME, Warrendale, PA, 1986.

54. L. Wagner, J. K. Gregory, A. Gysler and G. Lütjering: in Small Fatigue Cracks, R. O. Ritchie and J. Lankford, eds., TMS-AIME, Warrendale, PA, 1986.

55. P. Clément, J. P. Angéli and A. Pineau: Fat. Eng. Mat. Struct., 1984, vol. 7, p. 251.

56. J. Lankford and D. L. Davidson: in Small Fatigue Cracks, R. O. Ritchie and J. Lankford, eds., TMS-AIME, Warrendale, PA, 1986.

57. R. O. Ritchie and S. Suresh: Mater. Sci. Eng., 1983, vol. 57, p. L27.

58. M. R. James and W. L. Morris: Metall. Trans. A, 1983, vol. 14A, p. 153.

59. J. Lankford: Fat. Eng. Mat. Struct., 1982, vol. 5, p. 233.

60. J. C. Newman, Jr.: in Behaviour of Short Cracks in Airframe Components, ARARD Conf. Proc. No. 328, Advisory Group for Aerospace Research and Development, Neuilly sur Seine, 1983, p. 6.1.

61. A. F. Blom, A. Fathulla, A. Hedlund, R. Stickler, B. Weiss and W. Zhao: in Proc. Intl. Conf. on "Crack Initiation/Short Cracks", E. R. de los Rios and K. J. Miller, eds., Mech. Eng. Publ. Ltd., Bury St. Edmunds, U.K., 1986.

62. F. Heubaum and M. E. Fine: Scripta Met., 1984, vol. 18, p. 1235.

63. K. Minakawa, H. Nakamura and A. J. McEvily: Scripta Met., 1984, vol. 18, p. 1371.

64. J. L. Bréat, F. Mudry and A. Pineau: Fat. Eng. Mat. Struct., 1983, vol. 6, p. 349.

65. J. Lankford and D. L. Davidson: in Fatigue Crack Threshold Concepts, D. L. Davidson and S. Suresh, eds., TMS-AIME, Warrendale, PA, 1984, p. 447.

66. J. Lankford: Eng. Fract. Mech., 1977, vol. 9, p. 617.

67. O. N. Romaniv, V. N. Siminkovich and A. N. Tkach: in Fatigue Thresholds, J. Bäcklund, A. F. Blom and C. J. Beevers, eds., EMAS Ltd., Warley, U.K., 1982, vol. 2, p. 799.

68. W. L. Morris, B. N. Cox and M. R. James: in Small Fatigue Cracks, R. O. Ritchie and J. Lankford, eds., TMS-AIME, Warrendale, PA, 1986.

69. K. Tanaka: in *Small Fatigue Cracks*, R. O. Ritchie and J. Lankford, eds., TMS-AIME, Warrendale, PA, 1986.

70. R. P. Gangloff and R. P. Wei: in *Small Fatigue Cracks*, R. O. Ritchie and J. Lankford, eds., TMS-AIME, Warrendale, PA, 1986.

71. R. S. Vecchio and R. W. Hertzberg: *Eng. Fract. Mech.*, 1985, vol. 22, p. 1049.

72. J. Schijve: in *Fatigue Thresholds*, J. Bäcklund, A. F. Blom and C. J. Beevers, eds., EMAS Ltd., Warley, U.K., 1982, vol. 2, p. 881.

73. S. Suresh: *Metall. Trans. A*, 1983, vol. 14A, p. 2375.

74. S. Suresh and R. O. Ritchie: in *Fatigue Crack Growth Threshold Concepts*, D. L. Davidson and S. Suresh, eds., TMS-AIME, Warrendale, PA, 1984, p. 227.

75. J. C. Newman and I. S. Raju: *Eng. Fract. Mech.*, 1981, vol. 15, p. 185.

11. PROGRAM ORGANIZATION AND PERSONNEL

The work described was performed in the Department of Materials Science and Mineral Engineering, University of California in Berkeley, under the supervision of Dr. R. O. Ritchie, Professor of Metallurgy, aided by research engineer, Dr. W. Yu, graduate student research assistant J. Miwa, and undergraduate research helpers. The individual personnel are listed below:

i) Professor R. O. Ritchie, Principal Investigator
    (Department of Materials Science and Mineral
    Engineering)

ii) Dr. W. Yu, Post-Graduate Research Engineer
     (Department of Materials Science and Mineral
     Engineering)

iii) J. Miwa, Graduate Student Research Assistant
      (Department of Materials Science and Mineral
      Engineering)

iv) H. Hayashigatani, Undergraduate Engineering Aide
     (Department of Materials Science and Mineral
     Engineering)

12. PUBLICATIONS

1983

1. R. O. Ritchie and S. Suresh: "The Fracture Mechanics Similitude Concept: Questions Concerning its Application to the Behavior of Short Fatigue Cracks," Materials Science and Engineering, 1983, vol. 57, pp. L27-L30.

2. R. O. Ritchie and S. Suresh: "Mechanics and Physics of the Growth of Small Cracks," in Behavior of Short Cracks in Airframe Components, AGARD, vol. CP328, pp. 1.1-1.14, North Atlantic Treaty Organization, AGARD, France, 1983.

3. S. Suresh: "Crack Deflection: Implications for the Growth of Long and Short Cracks," Metallurgical Transactions A, 1983, vol. 14A, pp. 2375-2385.

1984

4. S. Suresh and R. O. Ritchie: "Propagation of Short Fatigue Cracks," International Metals Reviews, 1984, vol. 29, pp. 445-476.

5. E. Zaiken and R. O. Ritchie: "On the Location of Crack Closure and the Threshold Condition for Fatigue Crack Growth," Scripta Metallurgica, 1984, vol. 8, pp. 847-850.

1985

6. E. Zaiken and R. O. Ritchie: "Effects of Microstructure on Fatigue Crack Propagation and Crack Closure Behavior in Aluminum Alloy 7150," Materials Science and Engineering, 1985, vol. 70, pp. 151-160.

7. R. P. Gangloff and R. O. Ritchie: "Environmental Effects Novel to the Propagation of Short Fatigue Cracks," in Fundamentals of Deformation and Fracture, roc. Eshelby Memorial Symp., B. A. Bilby, K. J. Miller and J. R. Willis, eds., Cambridge University Press, 1985, pp. 529-558.

8. E. Zaiken and R. O. Ritchie: "On the Development of Crack Closure at the Threshold Condition for Long and Short Cracks in 7150 Aluminum Alloys," Metallurgical Transactions A, 1985, vol. 16A, pp. 1467-1477.

9. E. Zaiken and R. O. Ritchie: "On the Role of Compression Overloads in Influencing Crack Closure and the Threshold Condition for Fatigue Crack Growth in 7150 Aluminum Alloy," Engineering Fracture Mechanics, 1985, vol. 22, pp. 35-48.

10. P. Donehoo, W. Yu and R. O. Ritchie: "On the Growth of Cracks at the Fatigue Threshold Following Compression Overloads: Role of Load Ratio," Materials Science and Engineering, 1985, vol. 75, pp. 11-17.

1986

11. R. O. Ritchie, E. Zaiken and A. F. Blom: "Is the Concept of a Fatigue Threshold Meaningful in the Presence of Compression Cycles?," in Basic Questions in Fatigue, Volume I, ASTM STP 924, J. T. Fong and R. J. Fields, eds., American Society for Testing and Materials, Philadelphia, PA, 1986, in press.

12. R. O. Ritchie and W. Yu: "Short Crack Effects in Fatigue: A Consequence of Crack Tip Shielding," in Small Fatigue Cracks, R. O. Ritchie and J. Lankford, eds., TMS-AIME, Warrendale, PA, 1986, in press.

13. R. O. Ritchie and J. Lankford: "Small Fatigue Cracks: A Statement of the Problem and Potential Solutions," accepted for publication in Materials Science and Engineering, 1986.

14. W. Yu and R. O. Ritchie: "Fatigue Crack Propagation in 2090 Aluminum-Lithium Alloy: Effect of Compression Overload Cycles," Journal of Engineering Materials and Technology, Transactions of ASME, Series H, submitted May 1986.

13. DISTRIBUTION LIST

AFOSR/NE
ATTN: Dr. A. H. Rosenstein
Bldg. #410
Bolling AFB
Washington, DC   20332

AFWAL/MLLM
ATTN: Branch Chief
Wright-Patterson AFB
Dayton, OH   45433

AFWAL/MLLS
ATTN: Branch Chief
Wright-Patterson AFB
Dayton, OH   45433

AFWAL/MLLN
ATTN: Branch Chief
Wright-Patterson AFB
Dayton, OH   45433

Dr. Hugh R. Gray
NASA Lewis Research Center
Materials and Structures Division
21000 Brookpark Rd.
Cleveland, OH   44135

Drs. R. J. Bucci, P. E. Bretz, and J. T. Staley
Alcoa Technical Center
Alcoa Laboratories
Alcoa Center, PA   15069

APPENDIX

Effects of Microstructure on Fatigue Crack Propagation and Crack Closure Behavior in Aluminum Alloy 7150

E. ZAIKEN* and R. O. RITCHIE

Department of Materials Science and Mineral Engineering, University of California, Berkeley, CA 94720 (U.S.A.)

ABSTRACT

A study has been made of the role of aging treatment in influencing fatigue crack propagation and crack closure behavior in a high purity ingot metallurgy aluminum alloy 7150, with specific reference to crack growth at low and high load ratios in the near-threshold regime. A trend of increasing growth rates and decreasing threshold stress intensity ΔK_{th} values with increased aging was seen to be consistent with lower measured levels of crack closure and a decreasing tortuosity in crack path. On the basis of crack growth measurements in moist room air, where closure due to corrosion product formation was found to be negligible in this alloy, the superior fatigue resistance of underaged microstructures (compared with overaged structures of similar strength and peak-aged structures of higher strength) was attributed to greater slip reversibility and to enhanced roughness-induced crack closure and deflection from the more tortuous crack paths. Such factors are promoted in alloy systems hardened by coherent shearable precipitates where the mode of deformation is one of non-homogeneous planar slip.

1. INTRODUCTION

Recent studies into the mechanics and mechanisms of fatigue have identified a prominent role of crack closure in influencing crack propagation behavior (see for example refs. 1–26). This is particularly apparent at low growth rates (*i.e.* below about 10^{-6} mm cycle^{-1}) near the fatigue threshold stress intensity range ΔK_{th} for no crack growth. In

*Present address: Shiley Incorporated, Irvine, CA 92714, U.S.A.

this regime the origin of such closure has been associated with mechanisms such as crack surface corrosion deposits [3–6], irregular fracture morphologies coupled with crack tip shear displacements [7–9] and fluid-induced pressure [12], in addition to conventional mechanisms relying on cyclic plasticity [1] (Fig. 1). The effect of the closure, which induces contact between mating fracture surfaces at positive stress intensities K_{cl} during the loading cycle, is to reduce the local driving force for crack advance from nominally applied levels, *e.g.* $\Delta K = K_{max} - K_{min}$, to some near-tip effective level $\Delta K_{eff} = K_{max} - K_{cl}$ [1] where K_{max}, K_{min}, K_{cl} and ΔK are the maximum stress intensity, minimum stress intensity, closure stress intensity and range of stress intensities respectively.

On the basis mainly of data in steels, the effects of variable-amplitude loading, frequency, load ratio, microstructure, environment and temperature have all been associated with closure phenomena (for a review see ref. 26). In non-ferrous alloys, however, less information exists. Elber [1] and Schmidt and Paris [2] first applied the concept of (plasticity-induced) closure to cyclic behavior in aluminum alloys in an attempt to explain variable-amplitude loading and load ratio effects in these alloys. Subsequent studies in this system have focused largely on effects of microstructure and environment [13–22]. Petit and Zeghoul [13] and Vasudévan and Suresh [14] identified a role of oxide-induced closure, although enhanced crack surface oxide films were only detected in overaged aluminum alloy 7075 and, unlike behavior in steels [4–6], were not consistent with lower growth rates. The more important mechanism in aluminum alloys appears to be associated with roughness-induced closure, where it has been suggested that the strongly crystal-
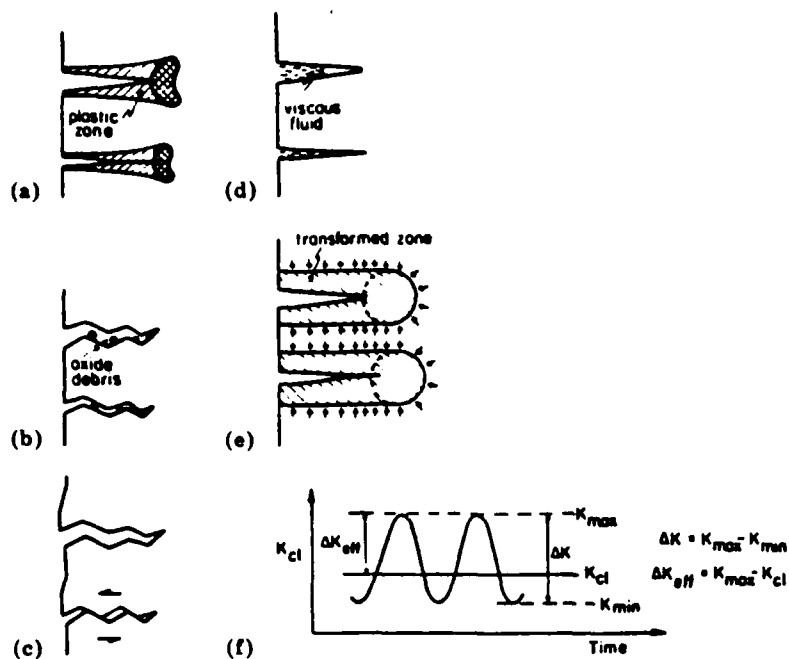
Fig. 1. (a)–(e) Schematic illustration of the primary mechanisms of fatigue crack closure ((a) plasticity-induced closure; (b) oxide-induced closure; (c) roughness-induced closure; (d) viscous-fluid-induced closure; (e) phase-transformation-induced closure) and (f) the nomenclature required in the definition of stress intensities representative of the fatigue cycle.

lographic nature of crack paths [27–32], particularly in underaged structures, promotes closure [17–20] and crack deflection [19, 20, 33] and thus reduces near-threshold growth rates. Recently, these concepts of deflection and closure have been applied to rationalize the microstructural effects on fatigue crack growth in aluminum alloy 7075 [19]. The decreasing threshold stress intensity ΔK_{th} values with increasing aging treatment were attributed to a smaller influence of closure associated with less crystallographic crack paths although, apart from oxide thickness measurements, detailed crack closure measurements were not made.

In the present work, effects of microstructure during precipitation hardening are examined on fatigue crack propagation in a high purity aluminum alloy 7150 in the light of quantitative measurements of oxide film thickness, fracture surface roughness and closure stress intensity values. It is shown that near-threshold growth rates are slowest in underaged structures, consistent with the highest measured closure loads, and the most deflected crack paths. No evidence of oxide-induced closure could be detected.

2. EXPERIMENTAL PROCEDURES

Conventionally cast ingot metallurgy aluminum alloy 7150 was supplied by Alcoa with the composition shown in Table 1. The Al–Zn–Mg–Cu alloy, which is a high purity version of aluminum alloy 7050 (with lower silicon and iron contents), was received as plate 25 mm thick in the solution-treated and 2% stretched (W51) condition. Samples for fatigue and tensile testing were machined at quarter-thickness and three-quarters-thickness locations and tempered to produce underaged, peak-aged (T6) and overaged (T7) structures. The specific heat treatments and resulting room temperature uniaxial tensile properties are shown in Tables 2 and 3 respectively. The underaged and overaged heat treatments were designed to produce structures with approximately similar yield strength. Transmission electron micrographs of the three microstructures are shown in Fig. 2. Underaged structures are characterized by coherent Guinier–Preston zones roughly 4–8 nm in diameter, which on further aging are replaced by semicoherent intermetallic η' precipitates ($MgZn_2$–$Mg(CuAl)_2$) in the peak-

TABLE 1

Nominal chemical composition

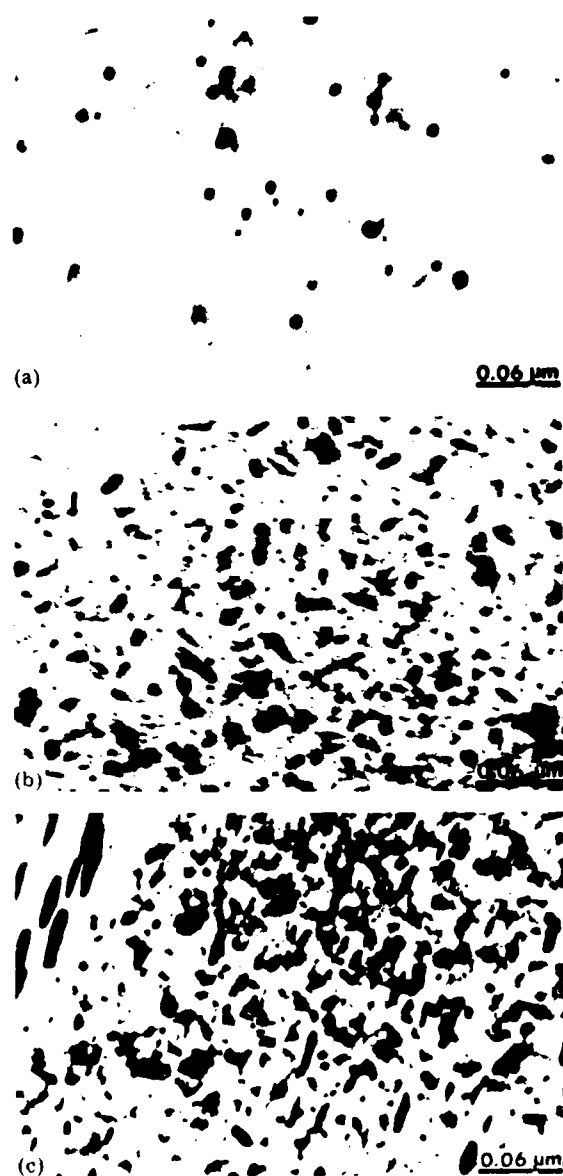| Element	Si	Fe	Cu	Mg	Zn	Ti	Zr	Al
Amount (wt.%) of element in alloy 7150	0.07	0.11	2.10	2.16	6.16	0.02	0.13	Balance

(a) 0.06 μm

(b)

(c) 0.06 μm.

Fig. 2. Transmission electron micrographs of (a) underaged, (b) peak-aged (T6) and (c) overaged (T7) ingot metallurgy aluminum alloy 7150.

aged condition. In overaged structures, predominately incoherent η phase precipitates ($MgZn_2$ compounds) are found in both the matrix and the grain boundaries (with small

TABLE 2

Heat treatments utilized for tests on alloy 7150

Condition	Heat treatment
Underaged	$ST^a + 1\frac{1}{2}$ h at 121 °C
Peak aged (T6)	$ST^a + 100$ h at 121 °C
Overaged (T7)	$ST^a + 24$ h at 121 °C + 40 h at 163 °C

^{a}ST, solution treated, quenched and stretched 2% (W51 condition).

precipitate-free zones of half-width about 30 nm), together with coarsened η' in the matrix. There is also evidence of small dispersoid particles (e.g. Al_3Zr) of less than 10 nm in diameter. Grains were somewhat elongated along the rolling direction with an approximate size of 15 μm by 5 μm.

Fatigue crack growth tests were performed in controlled room temperature air (22 °C; relative humidity, 45%) on compact tension test pieces 6.4 mm thick machined in the TL orientation (i.e. the load was applied in the long transverse direction and the crack propagated in the longitudinal direction). Using d.c. electrical potential techniques to monitor crack growth, tests were performed under load control at 50 Hz (sine wave) frequency with load ratios R ($= K_{min}/K_{max}$) of 0.10 and 0.75. Near-threshold crack propagation rates were determined under manual load-shedding (decreasing ΔK) conditions and checked under increasing ΔK conditions. The threshold level ΔK_{th} was defined as the highest ΔK level giving growth rates less than 10^{-8} mm cycle^{-1} [34], with the majority of tests duplicated.

Macroscopic crack closure measurements to determine K_{cl} values were performed in situ with the back-face strain technique using two strain gauges to record strain both parallel and perpendicular to the loading axis (Fig. 3) [22, 24]. Mean closure loads were deduced from the point during the loading cycle where the resulting elastic compliance curves of load versus relative strain deviated from linearity. Crack surface corrosion deposits were mea-

154

TABLE 3

Room temperature mechanical properties of alloy 7150

Condition	Yield strength (MPa)	Ultimate tensile strength (MPa)	Elongation[a] (%)	Reduction in area (%)	Work-hardening exponent
Underaged	371	485	6.8	12.1	0.055
Peak aged (T6)	404	480	6.0	10.3	0.046
Overaged (T7)	372	478	7.1	12.5	0.058

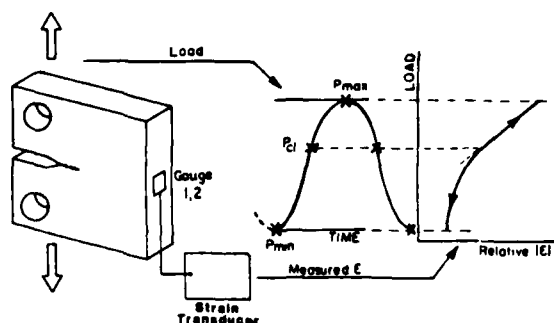[a]On a 32 mm gauge length.

Fig. 3. Schematic illustration of the back-face strain technique used to estimate closure stress intensity K_{cl} values. P_{max}, P_{min} and P_{cl} are the maximum, minimum and closure loads respectively.

sured by scanning Auger spectroscopy using an Ar^+ sputter rate of 45 Å min^{-1} [25]. The excess oxide thickness, representing the excess material inside the crack, was computed with a Pilling–Bedworth ratio of 1.3 for Al_2O_3, assuming oxide growth in only the thickness direction and equal thicknesses on each face. The degree of fracture surface roughness was assessed from scanning electron and optical micrographs of the crack paths in terms of the ratio of total length of the crack to the projected length on the plane of maximum tensile stress.

3. RESULTS

3.1. Growth rate behavior

The variation in fatigue crack propagation rates da/dN with stress intensity range ΔK for alloy 7150 in the underaged, peak-aged and overaged conditions is shown in Fig. 4 for load ratios of 0.10 and 0.75. Although growth rates above about 10^{-6} mm cycle^{-1} are similar at each load ratio for all three microstruc-

tures, at near-threshold levels it is evident that underaged structures show the highest fatigue resistance in terms of lowest growth rates and highest threshold ΔK_{th} values. Similar behavior has been reported for other aluminum alloys, including ingot metallurgy 7075 [15–19], 7475 [20, 31] and powder metallurgy 7091 [32]. Compared with those for the underaged structure, the threshold ΔK_{th} values in the present results are roughly 15% and 28% lower in the peak-aged and overaged structures respectively at $R = 0.10$ (Table 4). Thresholds are similarly reduced with increased aging at $R = 0.75$, although the absolute magnitude of the differences in ΔK_{th} values is much smaller.

3.2. Crack closure data

Corresponding crack closure data, in terms of back-face strain measurements of K_{cl}/K_{max} as a function of ΔK, are shown in Fig. 5 for the three microstructures at both $R = 0.10$ and $R = 0.75$. Similar to behavior reported for several ferrous and non-ferrous alloys at low load ratios (see for example refs. 20–24), the degree of crack closure at $R = 0.10$ increases sharply with decreasing ΔK level, approaching a maximum of K_{cl}/K_{max} close to unity at ΔK_{th}. Although no evidence of closure could be detected experimentally in any microstructure at $R = 0.75$, at low load ratios the underaged structures showed the highest closure levels, consistent with their highest thresholds.

3.3. Fractography

Scanning electron micrographs of the fatigue fracture surfaces close to ΔK_{th} in the three aging conditions are shown in Fig. 6. The fractography is transgranular in all cases with evidence of slip steps, ledges and facets. Such facets are particularly pronounced in
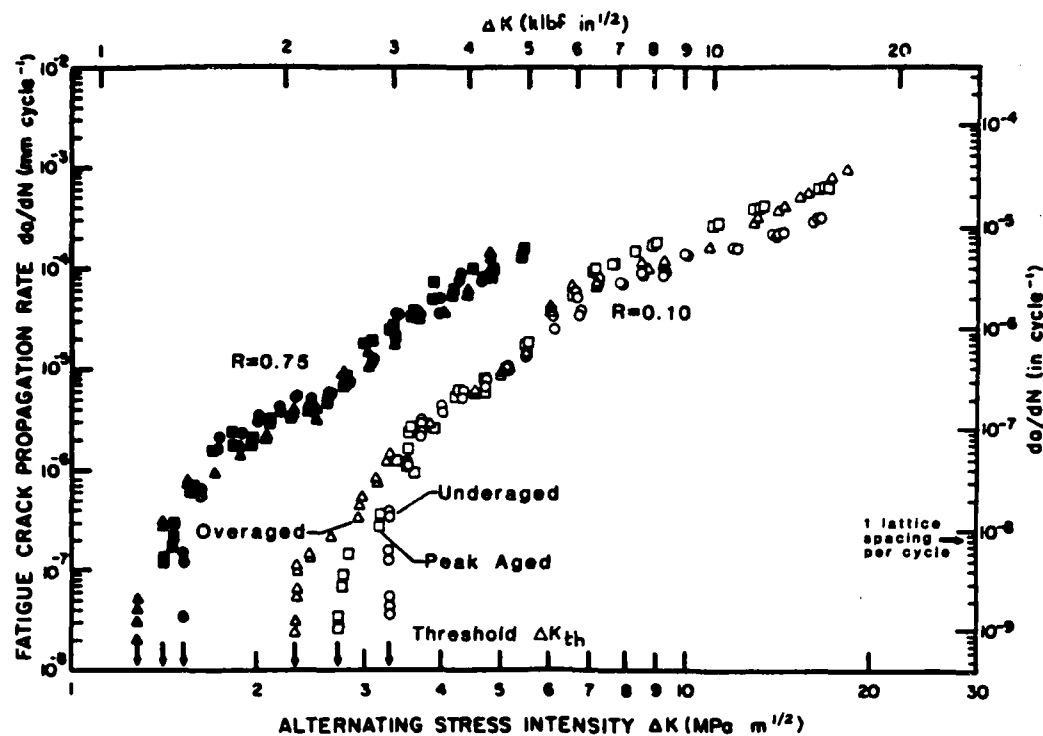
Fig. 4. Variation in fatigue crack growth rate da/dN as a function of stress intensity range ΔK for ingot metallurgy aluminum alloy 7150 tested at $R = 0.10$ and $R = 0.75$ in controlled moist air. Data are shown for underaged, peak-aged (T6) and overaged (T7) microstructures.

Condition	Symbol for the following load ratios	
	$R = 0.1$	$R = 0.75$
Underaged	○	●
Peak aged	□	■
Overaged	△	▲

TABLE 4

Threshold data for alloy 7150 at load ratios of 0.10 and 0.75

Condition	Load ratio K_{min}/K_{max}	ΔK_{th} (MPa m$^{1/2}$)	ΔCTOD[a] (nm)	Maximum K_{cl}/K_{th}[a]	Excess oxide thickness[a] (nm)	Degree of roughness[b]
Underaged	0.10	3.05-3.31	100	0.88	≈3	1.26
	0.75	1.5[1]	22	0	≈3	
Peak aged (T6)	0.10	2.44-2.94	65	0.85	≈3	1.21
	0.75	1.27	14	0	≈3	
Overaged (T7)	0.10	2.23-2.33	50	0.77	≈3	1.06
	0.75	1.16	13	0	≈3	

[a] At the threshold ΔK_{th}.
[b] The ratio of the total crack length to the projected length on the plane of maximum tensile stress.
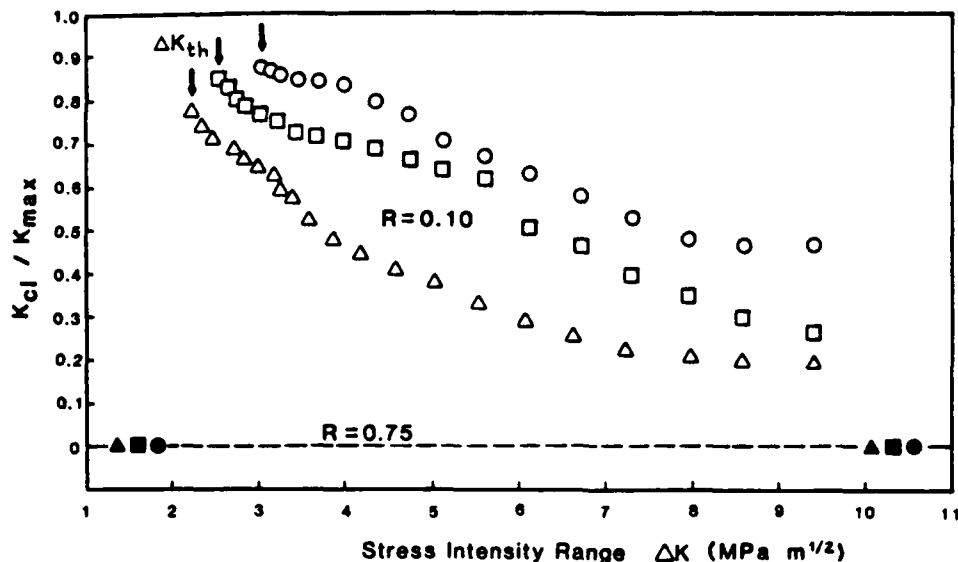
Fig. 5. Variation in crack closure, in terms of the ratio K_{cl}/K_{max} of closure stress intensity to maximum stress intensity, as a function of ΔK for underaged (O, ●), peak-aged (T6) (□, ■) and overaged (T7) (△, ▲) alloy 7150 at $R = 0.10$ and $R = 0.75$.

the underaged structure and have an appearance characteristic of crystallographic fatigue surfaces [27, 35, 36]. The rougher or more tortuous nature of the crack path in the underaged structures can be seen more clearly in Fig. 7 where crack profiles are shown for the three conditions. In contrast with the zigzag appearance of underaged fractures, crack paths in the overaged structures are predominately linear with far fewer crack deflections.

Associated Auger measurements of the extent of crack surface corrosion deposits are shown in Fig. 8. In marked contrast with behavior in lower strength steels [6, 25], there is no evidence in this present alloy of any pronounced oxide accumulation within the crack even at threshold levels. Oxide films were similar for all aging conditions at both load ratios with a measured thickness of the order of 3 nm, comparable with the limiting thickness of naturally occurring oxides in this alloy. Such results are similar to those reported for alloy 7075 in the underaged and peak-aged conditions. However, they are in contrast with those reported for overaged alloy 7075, where excess oxide thicknesses approached 100 nm at ΔK_{th} ($R = 0.33$) [14]. As listed in Table 4, the excess oxide film thicknesses in alloy 7150 are small compared with computed values of the cyclic crack-tip

opening displacements ΔCTOD, indicating that, for this alloy tested in room air environments, the contribution from oxide-induced crack closure is likely to be minimal.

4. DISCUSSION

Similar to other aluminum alloys [17–20, 27–33], the present results on a high purity ingot metallurgy alloy 7150 indicate clearly that underaged microstructures have superior near-threshold fatigue crack propagation resistance to overaged and peak-aged microstructures. This is seen in terms of lower growth rates below about 10^{-6} mm cycle^{-1} and higher threshold ΔK_{th} values at both low and high load ratios, although the magnitude of the effect is diminished at $R = 0.75$ (Fig. 4). The higher thresholds in the underaged structures are consistent with increased crack closure (Fig. 5), faceted and crystallographic fracture surfaces (Fig. 6) and more tortuous crack paths (Fig. 7), compared with the smoother more linear (undeflected) crack morphology in overaged structures. Data indicating this trend of lower thresholds with decreasing K_{cl}/K_{max} values and decreasing degrees of fracture surface roughness for increasing aging are listed in Table 4.
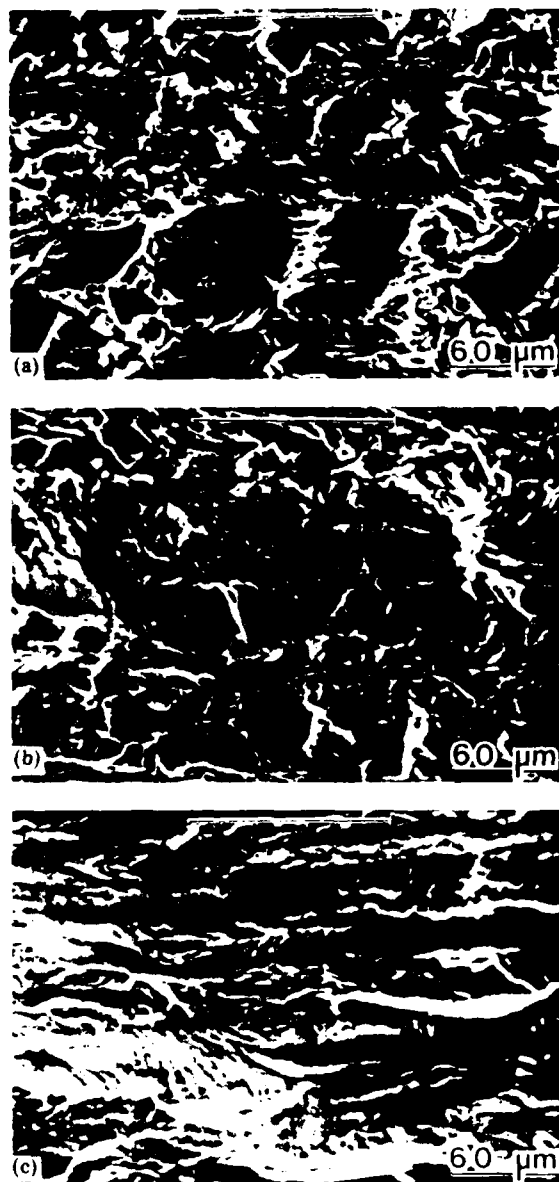
Fig. 6. Scanning electron micrographs of fatigue fracture surfaces close to ΔK_{th} ($R = 0.10$) in ingot metallurgy aluminum alloy 7150, showing the morphology in (a) underaged, (b) peak-aged (T6) and (c) overaged (T7) microstructures. Horizontal arrows indicate direction of crack growth.
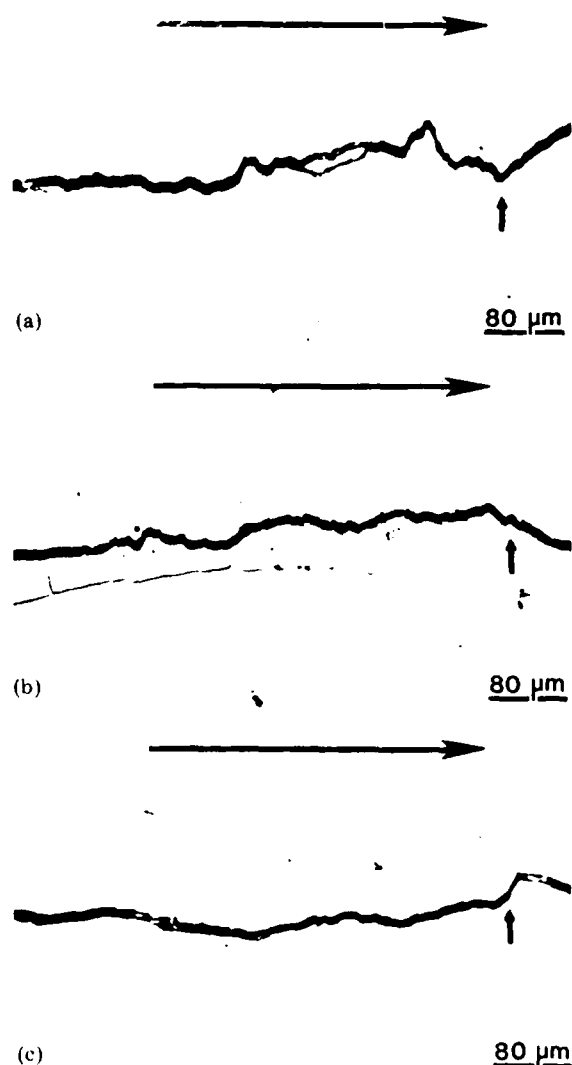

Fig. 7. Crack path morphology of near-threshold fatigue cracks in ingot metallurgy aluminum alloy 7150 in the (a) underaged, (b) peak-aged (T6) and (c) overaged (T7) conditions. Horizontal arrows indicate direction of crack growth; vertical arrows indicate the location of crack arrest at ΔK_{th}.

In keeping with current notions on the role of crack closure [26], this trend (which has been similarly rationalized in alloys 7075 [17, 19] and 7475 [20]) is to be expected. Akin to behavior in dual-phase steels [23, 24], β annealed titanium [37, 38] and Al-Li alloys [39], the generation of a meandering crack path (either by crack deflection at harder

phases [23, 24, 33] or in the present case by crystallographic deflection at grain boundaries) can lead to slower fatigue crack growth rates through a reduction in local crack driving force. This results from three major factors: (i) a lower effective da/dN due to a longer path length of the crack, (ii) lower effective stress intensities at the crack tip due to crack deflection from the plane of maximum tensile stress [33] and (iii) lower effective ranges of stress intensities at the crack tip due to the resulting production of increased crack
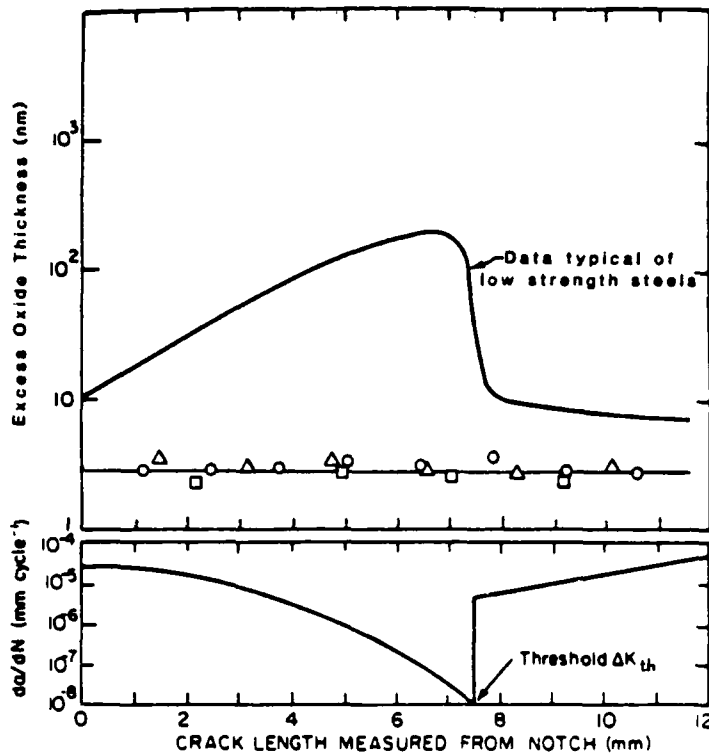
158

Fig. 8. Scanning Auger spectroscopy measurements of excess crack surface oxide deposits as a function of fatigue crack length and growth rate da/dN. Data points for ingot metallurgy aluminum alloy 7150 in the underaged, peak-aged and overaged microstructures ($R = 0.10$) are compared with prior data [6] on lower strength steels at low load ratios.

closure from asperity contact behind the crack tip [7-9]. Since the thicknesses of crack surface oxide films are so small compared with ΔCTOD values, it appears that the major contribution to this closure in the present alloy originates from the roughness-induced mechanism (Fig. 1) aided by the rough out-of-plane crack morphologies and the crack tip shear displacements [40] which result. These effects are far less pronounced in the overaged structures where crack paths are more linear (Fig. 7) such that corresponding crack growth rates are higher. Furthermore, at the high load ratios, differences between underaged and overaged microstructures are reduced because the role of crack closure is diminished at the larger crack-opening displacements (Fig. 5).

This argument is consistent with previous explanations based solely on microstructural factors [28]. In underaged precipitation-hardening systems, where the mode of alloy hardening is primarily the shearing of small coherent precipitates, the resulting hetero-

geneous deformation (i.e. coarse planar slip) promotes a crystallographic crack path. Because slip is occurring on fewer slip systems, the degree of slip reversibility is greater and hence the crack tip damage per cycle is less. Conversely, in overaged systems where the mode of hardening is now Orowan bypassing of semicoherent or incoherent larger non-shearable precipitates, the resulting homo-geneous deformation (i.e. wavy slip) generates a far more planar fracture surface because of the larger number of finer slip steps. This leads to greater slip irreversibility and more crack tip damage per cycle. Furthermore, as noted by Zedalis et al. [31], the larger pre-cipitate-free zones in overaged 7000 series aluminum alloys arising from the growth of incoherent grain boundary precipitates must contribute somewhat to the lower fatigue resistance in these microstructures.

Finally, it is interesting to note that the microstructures which show superior fatigue crack growth resistance at near-threshold

levels do not necessarily retain such resistance at higher growth rates [41, 42]. For example, although the effect is not apparent in alloy 7150 (Fig. 4), underaged microstructures in many aluminum alloys show faster growth rates above about 10^{-6} mm cycle^{-1} and slower growth rates close to ΔK_{th}, compared with overaged structures. Such observations tend to support explanations based on crack closure since at higher growth rates, with associated larger crack-tip-opening displacements, the effect of closure mechanisms relying on asperity contact (*i.e.* roughness-induced mechanisms) would be reduced. Conversely, where crack closure and deflection mechanisms are important (*e.g.* for transient crack growth behavior under variable-amplitude loading conditions), underaged structures clearly show the longest post-overload retardations and the highest general resistance to crack growth [42]. However, these planar slip characteristics of coherent particle precipitation-hardened systems, which are so important in generating superior-fatigue crack growth resistance through inhomogeneous deformation, rough crystallographic crack paths and enhanced closure and deflection, can lead simultaneously to inferior crack initiation toughness from a greater tendency for strain localization. This is particularly evident in Al–Li alloys where the increased coherency between lithium-containing intermetallics and the matrix can result in exceptionally good fatigue crack propagation resistance [43] through enhanced crack path tortuosity [39] and yet at the same time can produce extremely low fracture toughness values [44].

5. CONCLUSIONS

Based on a study of fatigue crack propagation behavior in high purity ingot metallurgy aluminum alloy 7150 tested at high and low load ratios in moist air with underaged, peak-aged and overaged microstructures, the following conclusions can be made.

(i) With increased aging, resistance to fatigue crack extension is decreased, in the form of faster near-threshold growth rates and lower fatigue threshold ΔK_{th} values, consistent with reduced measured levels of crack closure and a decreasing tortuosity in crack path.

(ii) The superior fatigue crack growth resistance of the underaged structures is attributed to greater slip reversibility and to enhanced roughness-induced crack closure and deflection from more tortuous crack paths, factors which result from the non-homogeneous planar slip characteristics of deformation in microstructures hardened by coherent (shearable) precipitates.

(iii) Crack flank corrosion deposits in all microstructures were small compared with near-threshold crack-tip-opening displacements at both load ratios, indicating that the contribution from oxide-induced crack closure in this alloy is minimal.

REFERENCES

1 W. Elber, *Damage Tolerance in Aircraft Structures, ASTM Spec. Tech. Publ. 486,* 1981, p. 230.
2 R. A. Schmidt and P. C. Paris, *Progress in Flaw Growth and Fracture Toughness Testing, ASTM Spec. Tech. Publ. 536,* 1973, p. 79.
3 P. C. Paris, R. J. Bucci, E. T. Wessel, W. G. Clark and T. R. Mager, *Stress Analysis and Growth of Cracks, Proc. Natl. Symp. on Fracture Mechanics, 1981,* in *ASTM Spec. Tech. Publ. 513,* 1972, p. 141.
4 R. O. Ritchie, S. Suresh and C. M. Moss, *J. Eng. Mater. Technol., 102* (1980) 293.
5 A. T. Stewart, *Eng. Fract. Mech., 13* (1980) 463.
6 S. Suresh, G. F. Zamiski and R. O. Ritchie, *Metall. Trans. A, 12* (1981) 1435.
7 N. Walker and C. J. Beevers, *Fatigue Eng. Mater. Struct., 1* (1979) 135.
8 K. Minakawa and A. J. McEvily, *Scr. Metall., 15* (1981) 937.
9 S. Suresh and R. O. Ritchie, *Metall. Trans. A, 13* (1982) 1627.
10 P. K. Liaw, T. R. Leax, R. S. Williams and M. G. Peck, *Metall. Trans. A, 13* (1982) 1607.
11 W. W. Gerberich, W. Yu and K. Esaklul, *Metall. Trans. A, 15* (1984) 875.

160

12 J.-L. Tzou, S. Suresh and R. O. Ritchie, *Acta Metall.*, 32 (1984), in the press.

13 J. Petit and A. Zeghoul, in J. Bäcklund, A. Blom and C. J. Beevers (eds.), *Proc. 1st Int. Conf. on Fatigue Thresholds, Stockholm, June 1-3, 1981*, Vol. 1, Engineering Materials Advisory Services, Warley, 1982, p. 563.

14 A. K. Vasudévan and S. Suresh, *Metall. Trans. A*, 13 (1982) 2271.

15 K. Schulte, H. Nowack and K. H. Trautmann, *Z. Werkstofftech.*, 11 (1980) 287.

16 J. Petit, P. Renaud and P. Violan, *Proc. 14th Eur. Conf. on Fracture, Leoben, 1982*, Engineering Materials Advisory Services, Warley, 1982, p. 426.

17 M. C. Lafarie-Frenot and C. Gasc, *Fatigue Eng. Mater. Struct.*, 6 (1983) 329.

18 J. Petit, in D. L. Davidson and S. Suresh (eds.), *Proc. Int. Symp. on Fatigue Crack Growth Threshold Concepts*, Metallurgical Society of AIME, Warrendale, PA, 1984, p. 3.

19 S. Suresh, A. K. Vasudévan and P. E. Bretz, *Metall. Trans. A*, 15 (1984) 369.

20 R. D. Carter, E. W. Lee, E. A. Starke and C. J. Beevers, *Metall. Trans. A*, 15 (1984) 555.

21 R. J. Asaro, L. Hermann and J. M. Baik, *Metall. Trans. A*, 12 (1981) 1133.

22 E. Zaiken and R. O. Ritchie, *Scr. Metall.*, 18 (1984) 847.

23 K. Minakawa, Y. Matsuo and A. J. McEvily, *Metall. Trans. A*, 13 (1982) 439.

24 V. B. Dutta, S. Suresh and R. O. Ritchie, *Metall. Trans. A*, 15 (1984) 1193.

25 S. Suresh, D. M. Parks and R. O. Ritchie, in J. Bäcklund, A. Blom and C. J. Beevers (ed), *Proc. 1st Int. Conf. on Fatigue Thresholds, Stockholm, June 1-3, 1981*, Vol. 1, Engineering Materials Advisory Services, Warley, 1982, p. 391.

26 S. Suresh and R. O. Ritchie, in D. L. Davidson and S. Suresh (eds.), *Proc. Int. Symp. on Fatigue Crack Growth Threshold Concepts*, Metallurgical Society of AIME, Warrendale, PA, 1984, p. 227.

27 G. G. Garrett and J. F. Knott, *Acta Metall.*, 23 (1975) 841.

28 E. Hornbogen and K. H. Zum Gahr, *Acta Metall.*, 24 (1976) 581.

29 J. Lindgkeit, A. Gysler and G. Lütjering, *Metall. Trans. A*, 12 (1981) 1 3.

30 F. S. Lin and E. A. Starke, in I. M. Bernstein and A. W. Thompson (eds.), *Proc. Int. Conf. on Hydrogen Effects in Metals, Moran, 1980*, Metallurgical Society of AIME, Warrendale, PA, 1981, p. 485.

31 M. Zedalis, L. Filler and M. E. Fine, *Scr. Metall.*, 16 (1982) 471.

32 M. Zedalis and M. E. Fine, *Scr. Metall.*, 16 (1982) 1411.

33 S. Suresh, *Metall. Trans. A*, 14 (1983) 2375.

34 R. O. Ritchie, *Int. Metall. Rev.*, 20 (1979) 205.

35 M. Gell and G. R. Leverant, *Acta Metall.*, 16 (1968) 553.

36 J. F. McCarver and R. O. Ritchie, *Mater. Sci. Eng.*, 55 (1982) 63.

37 G. R. Yoder, L. A. Cooley and T. W. Crooker, *Metall. Trans. A*, 8 (1977) 1737.

38 G. R. Yoder, L. A. Cooley and T. W. Crooker, *Metall. Trans. A*, 9 (1978) 1413.

39 A. K. Vasudévan, P. E. Bretz, A. C. Miller and S. Suresh, *Mater. Sci. Eng.*, 64 (1984) 113.

40 D. L. Davidson, *Fatigue Eng. Mater. Struct.*, 3 (1981) 229.

41 R. J. Bucci, A. B. Thakker, T. H. Saunders, R. R. Sawtell and J. T. Staley, in D. F. Bryan and J. M. Potter (eds.), *Effect of Load Variables on Fatigue Crack Initiation and Propagation, ASTM Spec. Tech. Publ. 714*, 1980, p. 41.

42 S. Suresh and A. K. Vasudévan, in D. L. Davidson and S. Suresh (eds.), *Proc. Int. Symp. on Fatigue Crack Growth Threshold Concepts*, Metallurgical Society of AIME, Warrendale, PA, 1984, p. 361.

43 E. J. Coyne, T. H. Sanders, Jr., and E. A. Starke, Jr., in T. H. Sanders, Jr., and E. A. Starke, Jr. (eds.), *Proc. 1st Int. Conf. on Aluminium-Lithium Alloys, Stone Mountain, GA, 1981*, Metallurgical Society of AIME, Warrendale, PA, 1981, p. 293.

44 E. S. Balmuth and R. Schmidt, in T. H. Sanders, Jr., and E. A. Starke, Jr. (eds.), *Proc. 1st Int. Conf. on Aluminium-Lithium Alloys, Stone Mountain, GA, 1981*, Metallurgical Society of AIME, Warrendale, PA, 1981, p. 69.

On the Development of Crack Closure and the Threshold Condition for Short and Long Fatigue Cracks in 7150 Aluminum Alloy

E. ZAIKEN and R. O. RITCHIE

In an attempt to analyze the behavior of physically "short" cracks, a study has been made of the development, location, and effect of crack closure on the behavior of fatigue cracks arrested at the "long" crack threshold stress intensity range, ΔK_{TH}, in underaged, peak aged, and overaged microstructures in a 7150 aluminum alloy. By monitoring the change in closure stress intensity, K_{cl}, during the *in situ* removal of material left in the wake of arrested threshold cracks, approximately 50 pct of the closure was found to be confined to a region within ~500 μm of the crack tip. Following wake removal, previously arrested threshold cracks recommenced to propagate at low load ratios even though nominal stress intensity ranges did *not* exceed ΔK_{TH}, representing the behavior of physically short cracks emanating from notches. No such crack extension at ΔK_{TH} was seen at high load ratios. With subsequent crack extension, crack closure was observed to redevelop leading to a deceleration in growth rates. The development of such closure was found to occur over crack extensions comparable with microstructural dimensions, rather than those associated with local crack tip plasticity. Such results provide further confirmation that the existence of a fatigue threshold and the growth of physically short cracks are controlled primarily by crack closure, and the data are discussed in terms of the micro-mechanisms of closure in precipitation hardened alloy systems.

I. INTRODUCTION

IN recent years the existence of a fatigue threshold, representing a stress intensity range ΔK_{TH} below which long cracks appear dormant, has been shown to be intimately associated with the development of crack closure in the wake of the crack tip (*e.g.*, References 1 through 16). Such closure, which results from interference between mating fracture surfaces, acts to reduce the local "crack driving force" from nominal levels, based on global measurements of applied loads and crack size, *e.g.*, $\Delta K = K_{max} - K_{min}$, to some lower effective near-tip level, *e.g.*, $\Delta K_{eff} = K_{max} - K_{cl}$, where K_{cl} is the stress intensity at first contact of the crack surfaces during unloading.[17] There is also a growing body of evidence that suggests that the "anomalous" behavior of short cracks, which are small compared to microstructural size-scales or the extent of local plasticity or simply physically small (≤ 1 mm), is linked similarly to the development of closure,[11,16,18-21] as such cracks can initiate and grow at progressively decreasing growth rates *below* the threshold before arresting or merging with long crack behavior[11,16,18-23] (Figure 1). Specifically, short cracks by virtue of their limited wake are presumed initially to be only marginally influenced by closure[18-21] such that, compared to equivalent long cracks at the same nominal "driving force", their effective "driving force" is higher, implying violation of K or J-based similitude.[19] With increasing length, the corresponding development of closure can compensate initially for the increase in nominal ΔK, such that the effective "driving force" can pass through a minimum, with a corre-

sponding minimum in growth rates. If this minimum "driving force" approaches the effective stress intensity range at the threshold, then the short crack can arrest leading to the phenomenon of nonpropagating cracks.[16] Otherwise, the small crack continues to grow and will merge with long crack behavior. Crack closure, however, is only one of several mechanisms which may contribute to discrepancies between long and short crack behavior although, in the absence of major electrochemical effects, it appears to be the most significant.[16]

Evidence to support such hypotheses is still comparatively limited, due possibly to theoretical difficulties with the mechanics of cracks of limiting continuum dimensions and experimental difficulties in monitoring their crack propagation and closure behavior. Studies in lower strength steels have claimed a direct correspondence between short crack and conventional long crack growth rate data when closure is accounted for through characterization with ΔK_{eff}, based on experimental K_{cl} measurements.[11,21] Mechanistically, this is difficult to rationalize as current models for crack closure, which rely on mechanisms involving cyclic wake plasticity,[17] crack surface corrosion product formation,[3,4,5] fracture surface roughness[6,7,8] and deflection,[24] fluid pressure within the crack,[25,26,27] and metallurgical phase transformations,[15] in general do not define a crack size dependence of closure forces. However, analytical modeling of fluid-induced closure[27] and experimental measurements of roughness-induced closure in titanium alloys[28] do show increasing closure with increasing crack length until "saturation" long crack levels are reached. Moreover, recent measurements on small cracks in notched and unnotched HSLA steel samples, where the mechanism of closure was undefined, clearly show this development of closure with short crack extension.[29]

One promising experimental approach to describe this role of crack closure in influencing near-threshold long cracks and sub-threshold short cracks has been to monitor

E. ZAIKEN, formerly Graduate Student with the Department of Mechanical Engineering, University of California, Berkeley, is now with Shiley Incorporated, Irvine, CA 92714. R. O. RITCHIE is Professor, Department of Materials Science and Mineral Engineering, University of California, Berkeley, CA 94720.
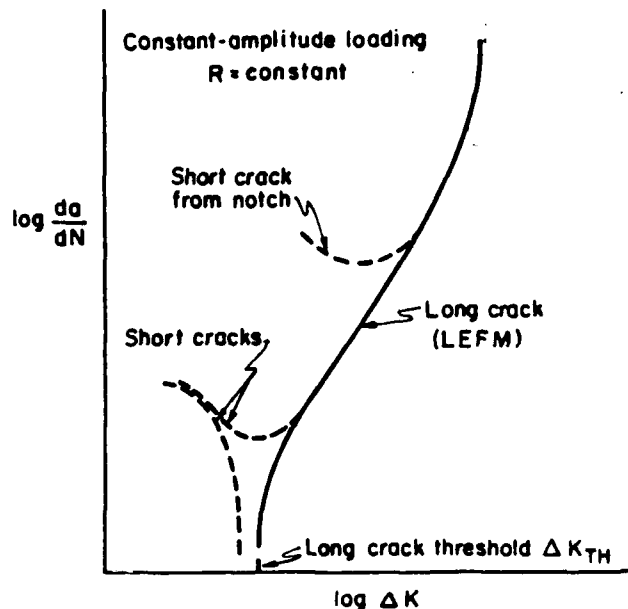Manuscript submitted July 19, 1984.

Fig. 1—Schematic representation of typical variation in fatigue crack propagation rates (da/dN) with stress intensity range (ΔK) for "long" and "short" cracks. Note how at near-threshold levels short flaws grow at progressively decreasing growth rates, either to arrest as nonpropagating cracks or to merge with long crack behavior.[16] LEFM refers to characterization in terms of linear elastic fracture mechanics.

behavior following the physical removal of closure forces. This has been achieved principally through the micro-machining of material left in the wake of the crack tip,[11,12,14,30] although one study has em[l]oyed single compression overloads.[31] Early attempts in nickel-based super-alloys (WASPALOY*), where a single 0.31 mm diameter

---
*WASPALOY is a trademark of United Technologies Corporation.
---

hole was drilled a short distance (within 0.31 mm) behind the tip of a threshold crack, did not reveal any substantial changes in closure.[30] However, more recent work[11,12,14] employing machined slots to remove wake material have shown (i) that long cracks previously arrested at the threshold ΔK_{TH} behave as short cracks and recommence to propagate at threshold levels after removal of the wake, and (ii) that closure well behind the crack tip is relatively less important compared to near-tip closure (i.e., within 1 mm or so from the tip).

The objective of the present investigation is to utilize this technique to examine the development, location, and effect of crack closure on arrested threshold fatigue cracks in underaged, peak aged, and overaged microstructures in a 7150 aluminum alloy, where the salient mechanisms of closure are a strong function of the degree of precipitation hardening.

Table II. Heat Treatments Utilized for Tests on 7150 Alloy

Underaged	ST* + 1.5 hr at 121 °C
Peak Aged (T6)	ST* + 100 hr at 121 °C
Overaged (T7)	ST* + 24 hr at 121 °C + 40 hr at 163 °C

*ST—solution treated, quenched, and stretched 2 pct (W51 condition)

II. EXPERIMENTAL PROCEDURES

A. Material

The material studied was a conventionally-cast 7150 aluminum alloy, supplied by ALCOA as 25 mm thick plate in the solution treated and 2 pct stretched (W51) condition. This material, of composition shown in Table I, is a high purity version of 7050 with lower levels of Si and Fe. Samples were machined at quarter and three-quarter thickness locations and tempered to produce underaged, peak aged (T6), and overaged (T7) microstructures, with underaged and overaged structures designed to have similar yield strengths. Specific heat treatment schedules and room temperature mechanical properties are listed in Tables II and III, respectively. The nature of these microstructures has been discussed elsewhere.[31,39] Briefly, underaged structures were characterized by coherent GP zones ($\sim$4 to 8 nm diameter), which were replaced in the T6 condition by semi-coherent η' precipitates (Figure 2). T7 structures were hardened by coarsened η' in the matrix and by predominately incoherent η precipitates in both matrix and grain boundaries, the latter resulting in small precipitate-free zones ($\sim$30 nm half width), as shown in Figure 2(c). Grains were pancake-shaped with an approximate size of 15 by 5 μm.

B. Fatigue Testing

Fatigue crack propagation tests were conducted in controlled room-temperature air (22 °C, 45 pct relative humidity) using 6.4 mm thick compact-type C(T) specimens machined in the T-L orientation. Tests were performed under load control with a frequency of 50 Hz (sine wave) at load ratios ($R = K_{min}/K_{max}$) of 0.10 and 0.75. D.C. electrical potential techniques were used to monitor crack extension. This method can be considered to have a resolution of at least 0.1 mm on absolute crack length and can detect changes in crack length of the order of 10 μm.[32] Periodically, macroscopic crack closure measurements were made in situ to determine K_{cl} values, using a back-face strain technique. As described elsewhere,[33] two strain gauges were affixed to the back face of the specimen to record strain both parallel and perpendicular to the loading axis. Mean closure loads were deduced from the point during the loading cycle where the resulting elastic compliance curves of load vs relative strain deviated from linearity.

Table I. Nominal Chemical Composition in Wt Pct

	Si	Fe	Cu	Mg	Zn	Ti	Zr	Al
7150	0.07	0.11	2.10	2.16	6.16	0.02	0.13	balance

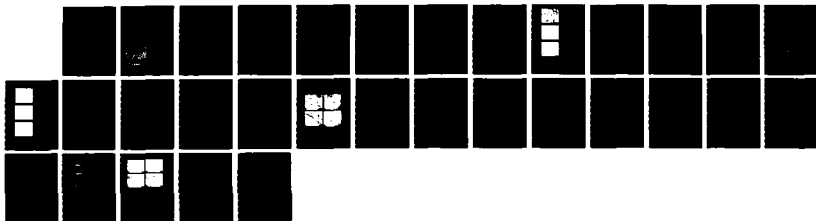AD-A169 980   FATIGUE BEHAVIOR OF LONG AND SHORT CRACKS IN WROUGHT   2/2
              AND POWDER ALUMINUM.. (U) CALIFORNIA UNIV BERKELEY DEPT
              OF MATERIALS SCIENCE AND MINERA..   R O RITCHIE ET AL.
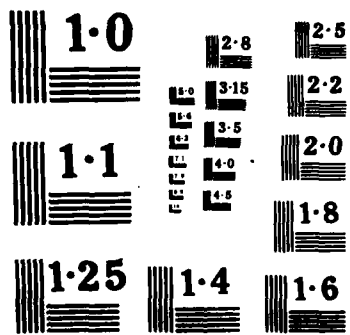UNCLASSIFIED 01 MAY 86 UCB/RP/86/A1040 AFOSR-TR-86-0447 F/G 11/6   NL

Table I. Room Temperature Mechanical Properties of 7150 Alloy

	Yield Strength (MPa)	U.T.S. (MPa)	Elong.* (Pct)	Redn. Area (Pct)	Work Hardening Exponent
Underaged	371	485	6.8	12.1	0.055
Peak Aged (T6)	404	480	6.0	10.3	0.046
Overaged (T7)	372	478	7.1	12.5	0.058

*On 32 mm gauge length

a. Long Crack Threshold Test

b. Removal of Wake

Fig. 3—Procedures used in the experiments to examine the effect of removing material left in the wake of long cracks arrested at the fatigue threshold.
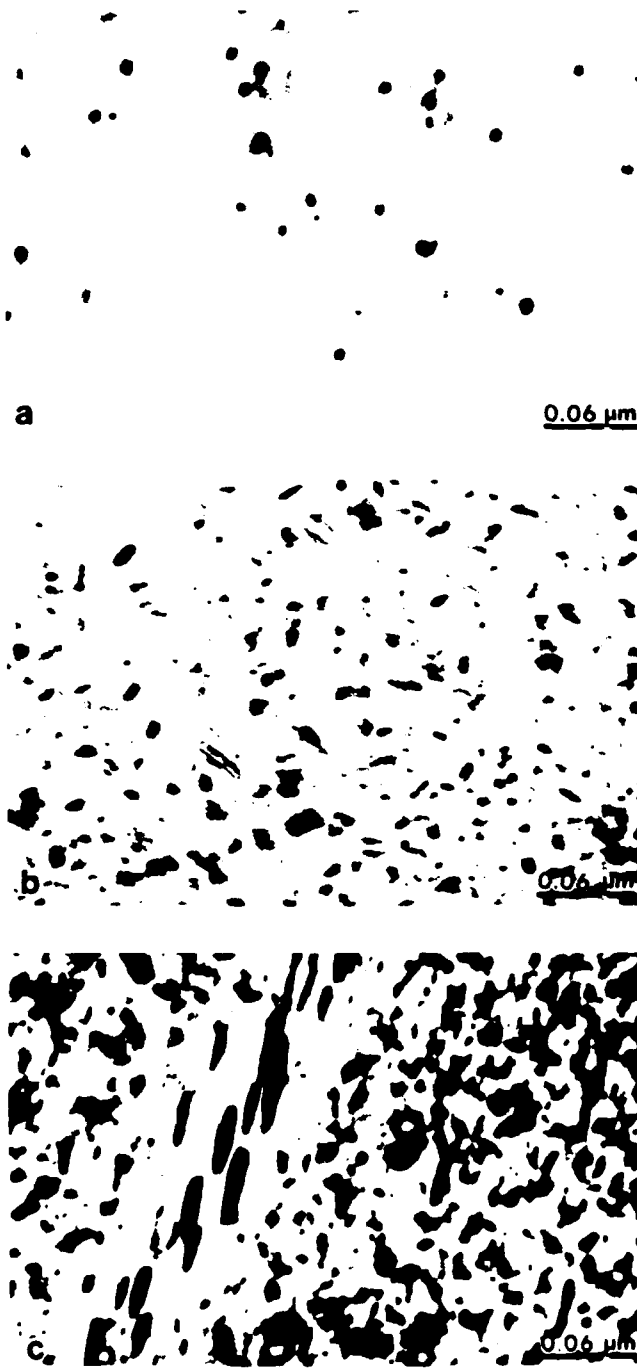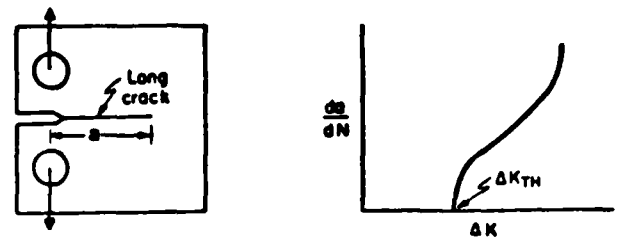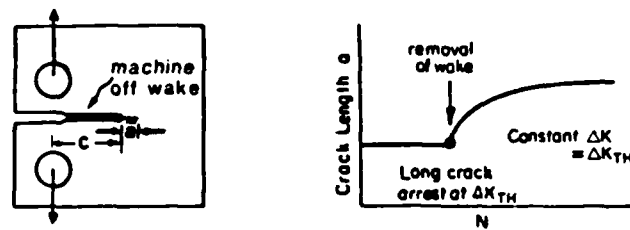

Fig. 2—Transmission electron micrographs of the microstructure of (a) underaged, (b) peak aged (T6), and (c) overaged (T7) 7150 aluminum alloy (from Ref. 39).

Constant amplitude crack growth data were obtained between $\sim 10^{-3}$ and 10^{-8} mm/cycle under both decreasing and increasing ΔK conditions, with the threshold ΔK_{TH} operationally defined as the highest stress intensity range giving growth rates less than 10^{-8} mm/cycle.[34] Procedures involved in the wake removal experiments are shown schematically in Figure 3. A threshold long crack, with total length (including notch) typically of the order 23 to 25 mm, was produced by manual load shedding until arrest at ΔK_{TH}. Material in the wake of the crack tip was then removed progressively in steps of roughly 0.5 to 1 mm, or less, while the specimen was maintained at mean load, using a fine jeweler's saw with a width of cut of approximately 300 μm. The micro-machining was conducted extremely slowly to minimize heating effects. Closure measurements to determine K_{cl} values were performed after each machining step, until the remaining fatigue crack was of a length $\bar{a} \sim$ 0.5 mm. Following removal of material to within 500 μm of the tip, cyclic loads were reapplied at ΔK_{TH}, and subsequent crack extension and closure behavior closely monitored. Although constant load cycling was employed, due to the small magnitude of both the crack extension and loads, conditions were effectively constant ΔK (ΔK varying by less than 0.02 MPa$\sqrt{m}$) over the first 0.1 to 0.15 mm of growth where the principal measurements were made.
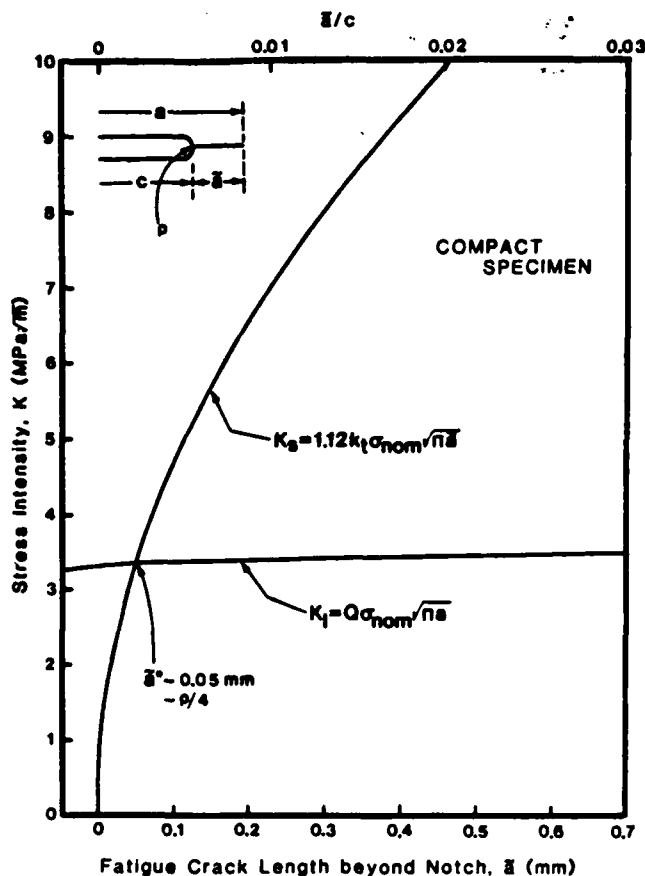
Fig. 4—Long and short crack limiting stress intensity solutions, K_l and K_s, respectively, for a small flaw (length $\bar{a}$) emanating from a notch (length c, root radius ρ) in the compact C(T) geometry. K calculations are relevant to current experimental conditions after wake machining at threshold levels, *i.e.*, with an applied load P of 0.55 kN and $c = 23$ mm.

C. Stress Intensity Computations

To compute the stress intensity K for the fatigue crack at the tip of the machined slot, we consider a small flaw, of length $\bar{a}$, emanating from a notch of length c, *i.e.*, total length $a = c + \bar{a}$, where the limiting K solutions for the short and long crack, K_s and K_l, respectively, are given in terms of the nominal stress σ_{nom}, and the stress concentration of the notch k_t, as:[35]

$$K_s = 1.12 \, k_t \sigma_{nom} \sqrt{\pi \bar{a}}, \qquad [1]$$

and

$$K_l = Q \sigma_{nom} \sqrt{\pi a}, \qquad [2]$$

where Q is the geometrical factor,[36] and the nominal stress for the compact specimen is given in terms of applied load P, specimen width W, and thickness B, as:

$$\sigma_{nom} = \frac{2P(2W + c)}{B(W - c)^2} \qquad [3]$$

These K solutions are plotted in Figure 4 as a function of $\bar{a}$ for the present experimental conditions at ΔK_{TH} of $P \sim 0.55$ kN and a total notch length (including the micromachined slot) of $c \approx 23$ mm. With the compact geometry of $W = 50$ mm and $B = 6.4$ mm, k_t for the machined

notch, with root radius $\rho \sim 0.2$ mm, was taken to be of the order of 8 from the numerical calculations of Wilson.[37] It is apparent that the notch field is felt only for flaw sizes below $\bar{a} \approx 50 \, \mu$m (*i.e.*, $\bar{a} \sim \rho/4$). As the minimum length of the remaining fatigue crack, $\bar{a}$, in the current experiments was a factor of 10 larger than this, *i.e.*, ~2.5 times the root radius of the notch, Eq. [2] (for the C(T) geometry) was utilized for all K computations with no notch correction factors incorporated. Furthermore, crack growth was assumed to be beyond any mechanically damaged zone due to the machining.

D. Fracture Surface Analysis

The thickness of crack surface corrosion deposits was estimated with scanning Auger spectroscopy using an argon ion sputtering rate of 45 Å per minute, as described elsewhere.[38,39] Fracture surfaces were examined with scanning electron microscopy and the degree of roughness assessed from crack path profiles in terms of the lineal roughness parameter, *i.e.*, the ratio of total length of the crack to the projected length on the plane of maximum tensile stress.

III. RESULTS

The effect of stress intensity range (ΔK) on crack growth rates (da/dN) and corresponding crack closure is shown in Figures 5 and 6, respectively, for 7150 alloy as a function of load ratio and aging treatment. Although behavior is similar at high load ratios, at $R = 0.10$ near-threshold growth rates are slowest and threshold values highest in the underaged microstructures, consistent with their highest measured levels of closure. Relevant threshold data for these microstructures, including the extent of crack surface oxidation and degree of fracture surface roughness, are listed in Table IV. As described in detail elsewhere,[39] the extent of closure at $R = 0.10$ in all three structures, expressed in Figure 6 as the ratio of closure stress intensity to maximum stress intensity, K_{cl}/K_{max}, progressively increases with decreasing ΔK as the threshold is approached, with $K_{cl}/K_{max} \rightarrow 0.8$ to 0.9 as $\Delta K \rightarrow \Delta K_{TH}$. No closure above K_{min} could be detected experimentally at $R = 0.75$.

The specific location of such closure can be inferred from the wake machining experiments. Shown in Figure 7 is the variation in closure plotted as a function of remaining fatigue crack length during removal of the wake of cracks arrested at ΔK_{TH}. Results for all three microstructures are plotted in the form of the ratio of K_{cl}/K_{max} as a function of the remaining fatigue crack length, $\bar{a}$, normalized by the initial length of the threshold crack, $\bar{a}_{TH}$. Similar to observations on T6 alloys,[12,14] the extent of closure is evenly distributed over the crack length to within ~500 μm of the crack tip at $R = 0.10$. However, after wake removal, approximately 50 pct of the closure still remains within this near tip region. For example, at ΔK_{TH} in the peak aged alloy, the arrested fatigue crack, of length $\bar{a} \approx 7.5$ mm, has a closure stress intensity $K_{cl} \approx 2.5$ MPa$\sqrt{m}$ ($\Delta K_{cl} \approx 0.4$ MPa$\sqrt{m}$) at the nominal threshold of $\Delta K_{TH} = 2.6$ MPa$\sqrt{m}$ ($R = 0.10$). After removal of ~7.0 mm of wake, closure is reduced, *i.e.*, $K_{cl} \approx 1.1$ MPa$\sqrt{m}$ ($\Delta K_{eff} \approx 1.8$ MPa$\sqrt{m}$), and must be confined to the very near-tip region. It is
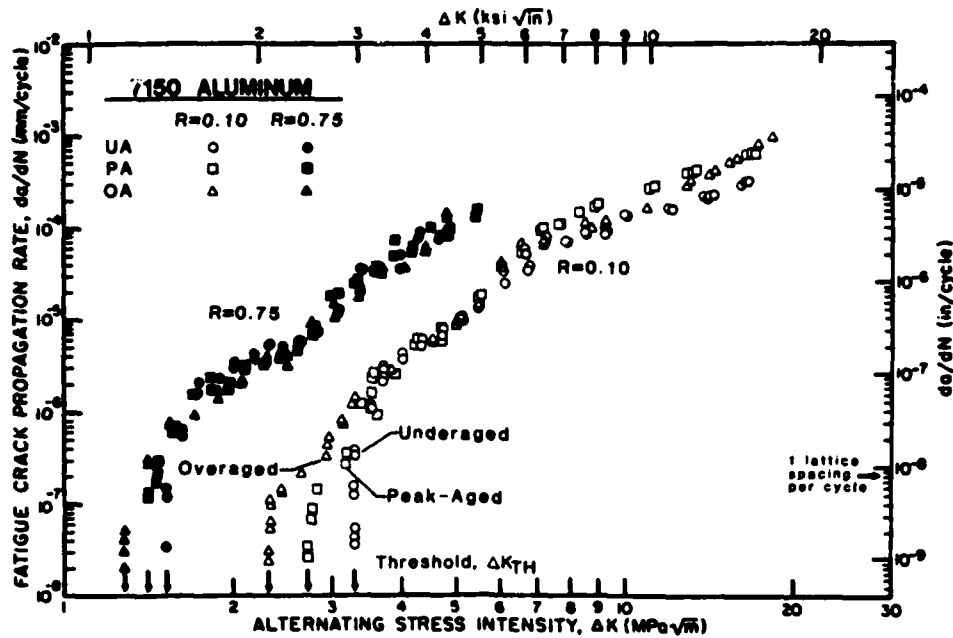
Fig. 5 — Variation in fatigue crack growth rate (da/dN) with stress intensity range (ΔK) for I/M 7150 aluminum alloy tested at R = 0.10 and 0.75 in controlled moist air. Data are shown for long cracks (a ~ 25 mm) in underaged (UA), peak aged (PA), and overaged (OA) microstructures.

noticeable, however, that the overaged condition, which develops the least closure overall at near-threshold stress intensities, also has the least closure removed by micro-machining of the wake material. As expected, the absence of detectable closure (above K_{min}) at high load ratios was not changed during subsequent removal of the wake of threshold cracks arrested at $R = 0.75$ (Figure 7).

The effect of the reduction in closure from micro-machining is readily apparent by immediate recycling of previously arrested threshold cracks, following wake removal, at the stress intensity range ΔK_{TH}. As shown in Figures 8 and 9, even though the initial ΔK level does not

exceed the threshold,* crack growth recommences in all

*Over the range of crack extension shown in Figure 8 for the initial crack growth behavior following wake machining, cycling conditions remain essentially constant ΔK, i.e., ΔK varies by less than 0.02 MPa√m. For example, for the data on the underaged condition, ΔK increases from 3.05 to 3.06 MPa√m over the 1.5×10^4 cycles plotted.

three microstructures at $R = 0.10$ with the locally increased ΔK_{eff}. After the reinitiation of crack growth, subsequent crack advance (Δa) proceeds initially at a decreasing growth rate consistent with a regeneration in closure, as can be seen in the K_{cl} values measured at an "apparent plateau" where the post-machining growth rates approach a minimum
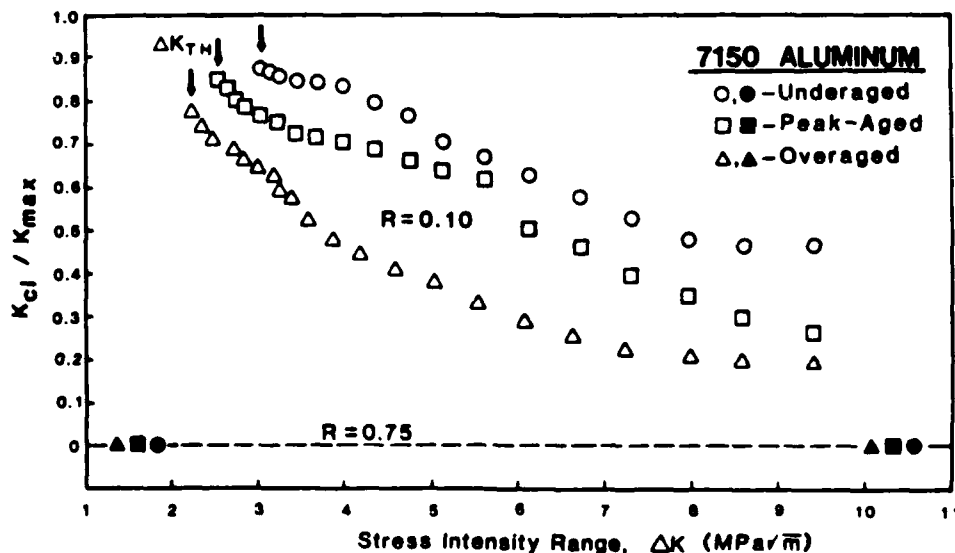

Fig. 6 — Variation in crack closure, in terms of the ratio of closure to maximum stress intensity, K_{cl}/K_{max}, as a function of ΔK, for underaged, peak aged, and overaged 7150 alloy. Data for long cracks at $R = 0.10$ and 0.75 correspond to growth rate results in Fig 5 (after Ref. 39).

| | Code | Load Ratio (K_{min}/K_{max}) | ΔK_{TH} (MP√m) | Plastic Zone Size[*][†] | | ΔCTOD[*][†] (nm) | Maximum K_{cl}/K_{max}[*] | Excess Oxide Thickness[*] (nm) | Lineal Roughness Parameter[**] |
				Cyclic (μm)	Maximum (μm)				
Underaged	UA	0.10	3.05 to 3.31	2.9	14.5	100	0.88	~ 3	1.26
		0.75	1.51	0.4	24.5	22	0	~ 3	
Peak Aged (T6)	PA	0.10	2.44 to 2.94	1.8	8.8	65	0.85	~ 3	1.21
		0.75	1.27	0.4	25.2	14	0	~ 3	
Overaged (T7)	OA	0.10	2.23 to 2.33	1.5	7.4	50	0.75	~ 3	1.06
		0.75	1.16	0.4	24.8	13	0	~ 3	

*At the threshold, ΔK_{TH}.

**Ratio of total crack length to projected length on plane of maximum tensile stress.

†Computed from $r_\Delta = \frac{1}{2\pi}(\Delta K/2\sigma_y)^2$, $r_{max} = \frac{1}{2\pi}(K_{max}/\sigma_y)^2$, and ΔCTOD $= \frac{1}{2}(\Delta K^2/2\sigma_y.E)$, where r_Δ and r_{max} are the cyclic and maximum plastic zone sizes, σ, the yield strength, and E Young's modulus.**

(Table V).** The deceleration occurs over a crack extension

**Short delays of ~5 × 10⁴ and ~3 × 10⁴ cycles were observed in under and peak aged structures, respectively, at the start of cycling following micro-machining (Figure 8). Such delayed reinitiation was conspicuously absent for overaged structures and is of unclear origin.

of the order of 20 μm (*i.e.*, ~2 times the maximum plastic zone size) in the underaged structure, less than in the peak and overaged structures where Δa is approximately 50 and 100 μm (*i.e.*, ~7 and 15 times the maximum plastic zone size), respectively. When plotted in terms of da/dN vs ΔK in Figure 9, such behavior resembles that of naturally short cracks (*cf.* Figure 1). Beyond the growth rate minimum, which does not lead here to complete arrest, small crack growth rates tend to merge with the long crack data (Figure 9).

In contrast to behavior at $R = 0.10$, for tests performed at high load ratios on the peak aged condition, where no closure could be measured, no development of closure or

further extension of the arrested threshold cracks could be detected on recycling at ΔK_{TH} (Figure 8(b)).

The near-threshold fractography associated with such behavior is summarized in Figure 10 and has been described elsewhere.[39] Briefly, fracture surfaces in the underaged microstructures at low ΔK levels are comparatively rough and faceted with a crack path morphology showing many examples of deflection. With increased aging, fracture surfaces become progressively smoother with an essentially linear profile in crack path.

IV.   DISCUSSION

The present study, whereby cracks arrested at ΔK_{TH} recommence to propagate due to a reduction in K_{cl} following wake removal, provides further confirmation that the existence of a fatigue threshold for the propagation of "long"
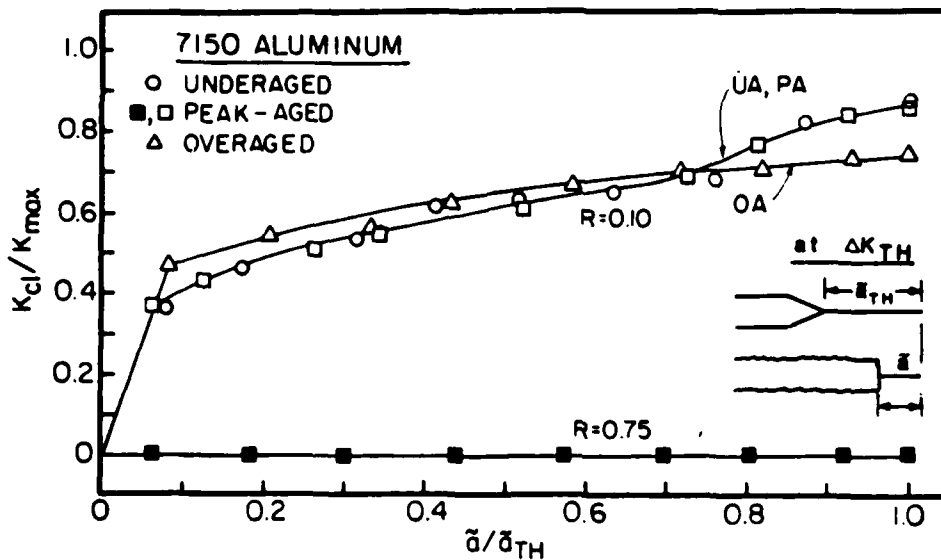

Fig. 7—Experimentally-measured variation in crack closure during progressive micro-machining of material left in the wake of long cracks arrested at the fatigue threshold at $R = 0.10$ and 0.75 in underaged, peak aged, and overaged 7150 alloy. Plotted is the ratio of closure to maximum stress intensity, K_{cl}/K_{max}, as a function of remaining length of fatigue crack, $\bar{a}$, normalized by its initial length at ΔK_{TH}, $\bar{a}_{TH}$. (Note: curves are extrapolated to zero as $\bar{a}/\bar{a}_{TH}$ tends to zero as there cannot be any closure at zero fatigue crack length.)

7150 UNDERAGED

MACHINE OFF WAKE

R = 0.10

(a)

7150 PEAK-AGED

R = 0.10

MACHINE OFF WAKE

R = 0.75

(b)

7150 OVERAGED

R = 0.10

MACHINE OFF WAKE

CONSTANT $\Delta K = \Delta K_{TH}$

(c)
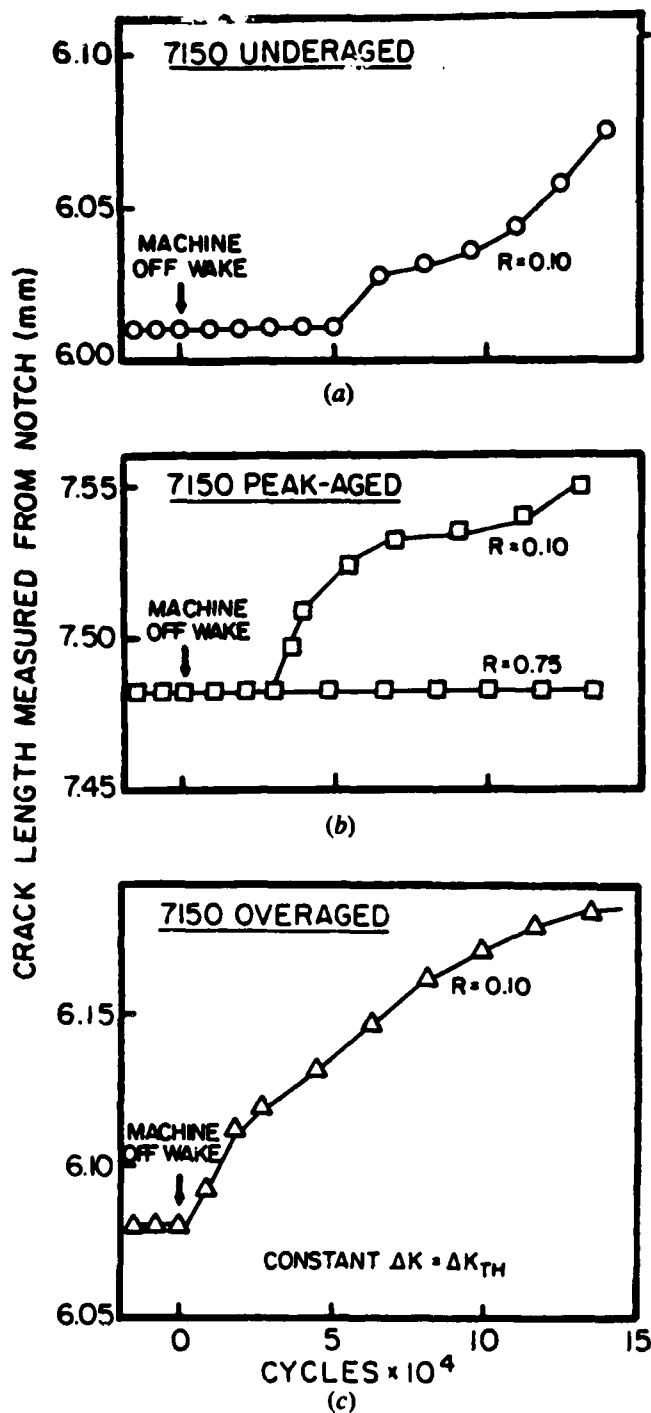
CRACK LENGTH MEASURED FROM NOTCH (mm)

CYCLES × 10^4

Fig. 8—Fatigue crack growth behavior, in terms of crack length (measured from the initial notch) vs number of cycles, in 7150 aluminum alloy cycled at the threshold ΔK_{TH}, before and immediately after removal of material in the wake of the tip of arrested crack (remaining fatigue crack length δ = 500 μm). Data are shown for (a) underaged structure at R = 0.10, (b) peak aged structure at R = 0.10 and 0.75, and (c) overaged structure at R = 0.10.

crack opening displacements. Further, by monitoring the reduction in K_{cl} during the removal process, it also is apparent that, although ~ 50 pct of the clc sure is distributed over most of the crack length, the remaining 50 pct is confined to the crack tip region within 500 μm or so from the tip.

Although values of K_{cl} are reduced by micro-machining of the wake causing crack propagation at ΔK_{TH}, closure redevelops on further crack extension to approach ~ 70 to 80 pct of previous (pre-machining) levels (Table V). This is manifest as a slowing down in post-machining growth rates (Figure 8) before the data merge with the long crack results (Figure 9). This minimum in growth rates is reached quite rapidly in the underaged structure after ~ 20 μm of crack extension, compared to ~ 50 and ~ 100 μm in the peak and overaged structures, respectively. The inference from this result is that significant crack closure can develop over smaller amounts of crack extension in the underaged structure compared to the more heavily aged conditions. Furthermore, the distances involved are comparable with microstructural dimensions and are far larger than the size-scales representative of local crack tip plasticity (cf. maximum and cyclic plastic zone sizes in Table IV).

Analogous behavior can be seen following the application of single compression overloads on similarly arrested cracks at ΔK_{TH}.[31] Experiments in the same 7150 alloy have shown that the reduction in closure, due primarily to the flattening of fracture surface asperities by the compressive loads, results in a local increase in ΔK_{eff} to again cause crack growth at the threshold. Unlike the present wake-machining experiments where closure is removed along the length of the crack, the compression overload principally affects near-tip closure with a resulting smaller decrease in K_{cl}. Accordingly, following the overload, growth rates progressively decelerate due to the redevelopment of closure with crack extension, but in this instance leading to complete crack arrest. The closure once more is regenerated most effectively in the underaged microstructure with the crack extension necessary to rearrest the crack increasing with increasing aging treatment.

Such results are consistent with the origin of crack closure mechanisms in precipitation hardened aluminum alloys, which tend to be based largely on microstructural rather than continuum plasticity factors.[39-44] Near-threshold crack growth in underaged structures, by virtue of the inhomogeneous mode of deformation (i.e., coarse planar slip) resulting from coherent (shearable) particle hardening, is generally far more crystallographic in nature than in peak aged and overaged structures.[45,46] This gives rise to a rougher, more faceted fracture surface (Figure 10). These fracture surface morphologies primarily enhance roughness-induced crack closure, as shown by the underaged 7150 alloy in Figure 6. Correspondingly, near-threshold growth rates are lower than in the more heavily aged micro-structures (Figure 5), where the more homogeneous mode of deformation (i.e., wavy slip) from incoherent (non-shearable) particle hardening promotes a more linear crack path (Figure 10).*

*Although closure is the primary effect, the increased near-threshold crack growth resistance of underaged structures is attributable additionally to the inhomogeneous mode of deformation, which increases slip reversibility to result in less crack tip damage per cycle; and the meandering crack paths, which reduce the local crack tip stress intensities from deflection of the crack from the normal crack propagation plane of maximum tensile stress.[39,41,44]

cracks at low load ratios is controlled primarily by a decrease in local "driving force" due to the development of crack closure in the wake of the crack tip. The lack of a similar effect at high load ratios is consistent with this notion as the role of closure is minimized there from the larger
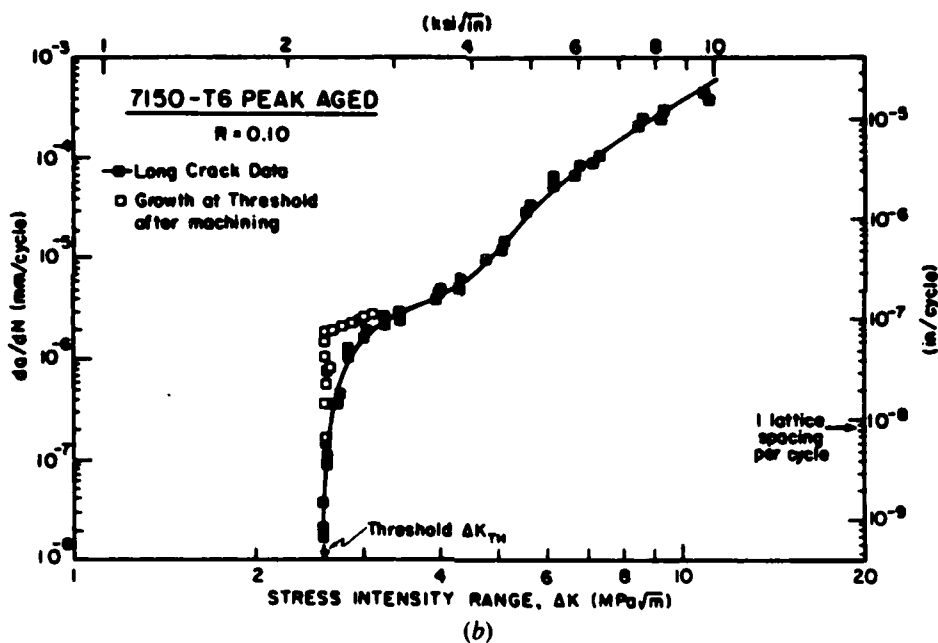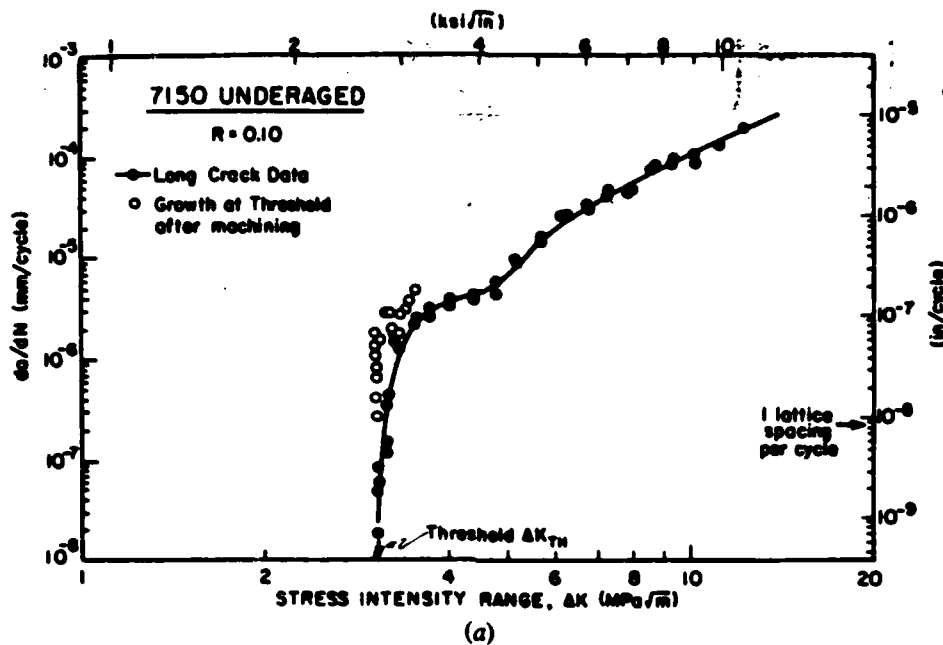
Fig. 9—Fatigue crack growth rate behavior of previously arrested threshold cracks following removal of material left in the wake to within 500 μm of the crack tip (open symbols). Data for 7150 aluminum alloy at R = 0.10 in (a) underaged, (b) peak aged, and (c) overaged conditions.

In the context of the present results, as fatigue crack closure clearly develops over microstructural dimensions in this alloy, it is promoted in the underaged structures where the roughness-induced mechanism is most potent due to the tortuous nature of the crack path (see also Reference 39). The formation of closure in the more heavily aged microstructures, where fracture surfaces are far smoother, is thus less efficient and correspondingly must involve larger amounts of crack extension to redevelop. Since the yield strengths of the underaged and overaged structures are

identical, their markedly different post-machining fatigue behavior strongly suggests that the above effects are microstructure and closure-related, rather than a sole function of notch or crack tip plasticity.[47]

Although the current experiments have not been performed on naturally-occurring short cracks, they do indicate that when fatigue cracks possess a limited wake, e.g., when they are short or emanating from a notch, they are subjected to a smaller influence from closure forces, which accounts for their ability to propagate at nominal stress intensities
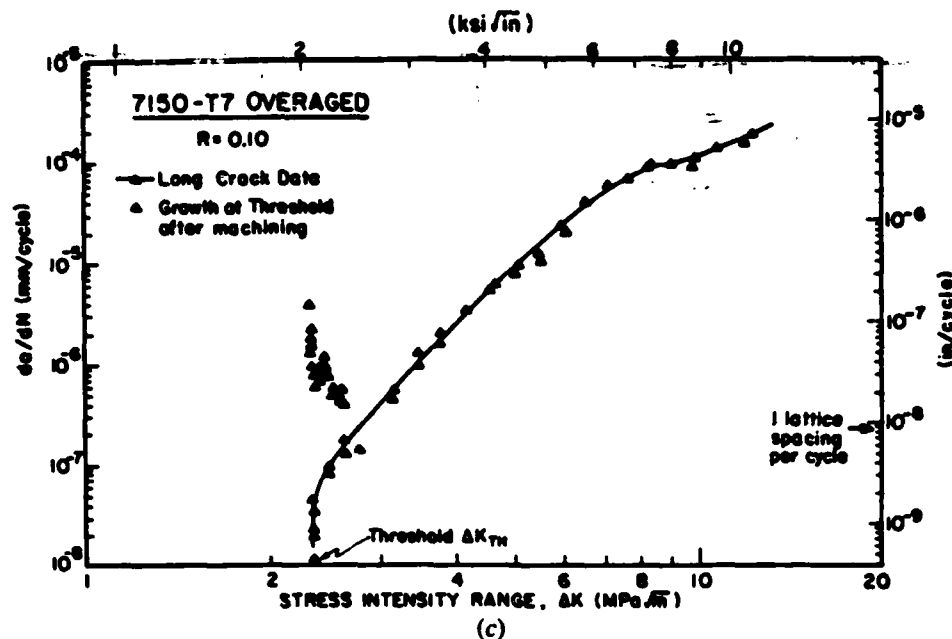
Fig. 9—Fatigue crack growth rate behavior of previously arrested threshold cracks following removal of material left in the wake to within 500 μm of the crack tip (open symbols). Data for 7150 aluminum alloy at $R = 0.10$ in (a) underaged, (b) peak aged, and (c) overaged conditions.

below the fatigue threshold. Moreover, their subsequent crack propagation will depend strongly on the generation of crack closure. As the effective crack driving force for this process, *e.g.*, ΔK_{eff}, must reflect both an increase in crack length (which increases ΔK_{eff}) and an increase in closure (which decreases ΔK_{eff}), subsequent behavior will depend predominately on the efficiency of developing new closure and the specific mechanisms involved. This can be governed by mechanical factors, such as the creation of a wake of plastically-deformed material; environmental factors, such as the oxidation of the crack surface; or microstructural factors, such as the interaction and deflection of the crack at phase or grain boundaries. This implies that growth rates in this regime will be nonunique with stress intensity range, *i.e.*, K-based similitude is violated,[19,48] as shown clearly in Reference 22. In the present case, where the contribution from roughness-induced closure varies with aging treatment, it is the microstructural factors which appear prominant. Thus, as illustrated in Figure 9, depending upon the particular aging condition, growth rates may increase or decrease with increasing crack length, before merging with the long crack constant amplitude data, similar to naturally-occurring short crack behavior.

V. CONCLUSIONS

Based on a study of the development, location, and effect of crack closure on near-threshold fatigue growth rate behavior in I/M 7150 aluminum alloy heat treated in the underaged, peak aged, and overaged conditions, the following conclusions can be made:

1. The existence of a threshold stress intensity range for the extension of long fatigue cracks appears to be controlled primarily by the level of crack closure.

2. Based on the measurement of closure stress intensities during the *in situ* removal of material left in the wake of threshold cracks arrested at ΔK_{TH}, approximately 50 pct of the closure was found to be confined to the immediate vicinity of the crack tip (*i.e.*, within 500 μm).

3. On removal of wake material to within 500 μm of the tip, previously-arrested cracks, at $R = 0.10$, recommenced to propagate even though nominal stress intensity ranges did *not* exceed threshold levels, representing the behavior of physically short cracks emanating from notches. In similar experiments performed at high load ratios ($R = 0.75$), threshold cracks remained dormant.

Table V. Crack Closure Data for 7150 Alloy at $\Delta K = \Delta K_{TH}$ ($R = 0.10$)

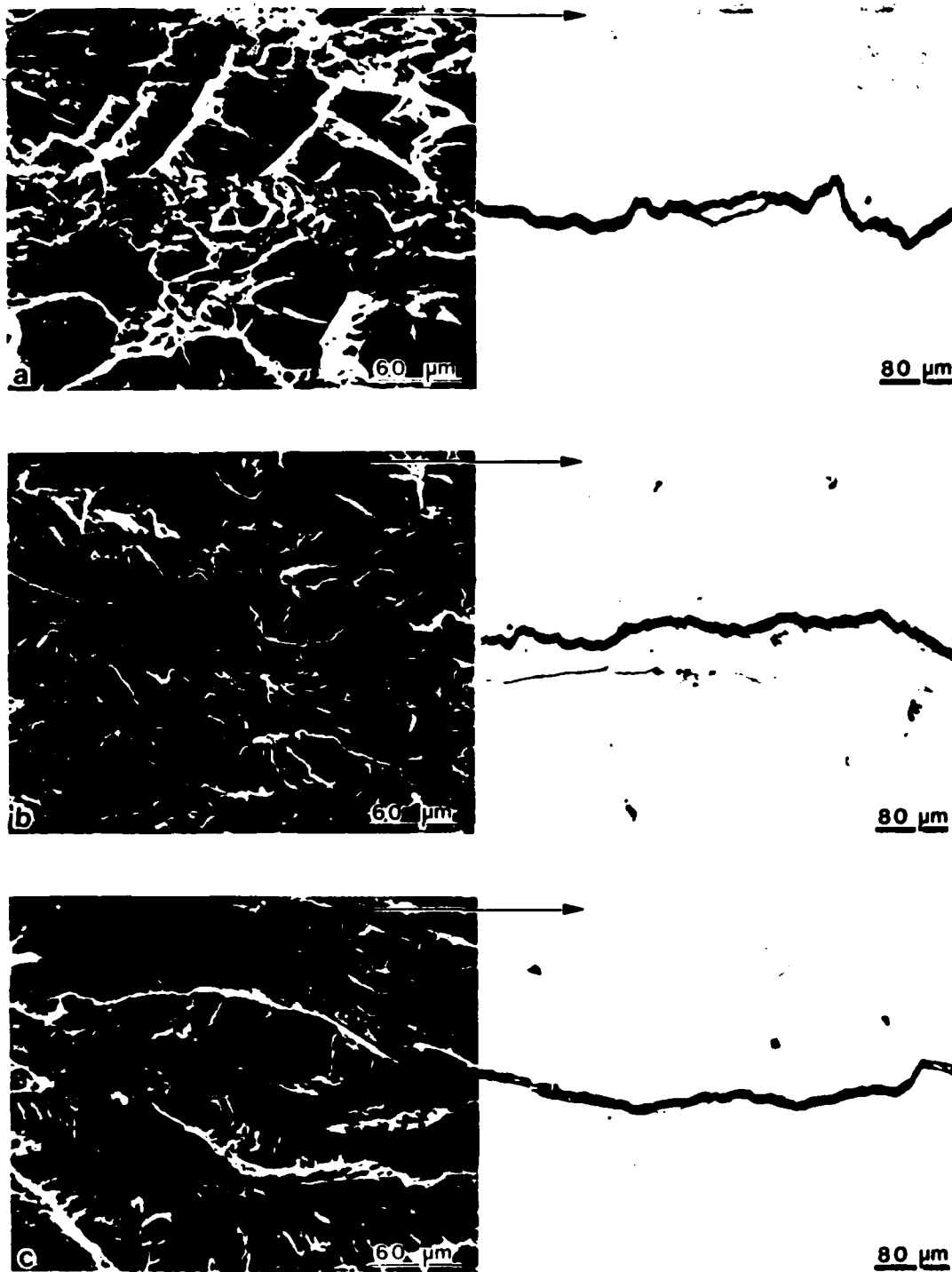|	Experimental K_{cl}/K_{max} Values at Threshold		
	At Initial Arrest	Following Wake Removal	Following Subsequent Growth
Underaged	0.88	0.37	0.61 at $\Delta a = 20$ μm
Peak Aged (T6)	0.85	0.36	0.59 at $\Delta a = 50$ μm
Overaged (T7)	0.75	0.48	0.57 at $\Delta a = 100$ μm

Fig. 10 — Fracture surface and crack path morphologies of near-threshold fatigue crack growth in underaged, peak aged, and overaged 7150 aluminum alloy (after Ref. 39)

4. At threshold levels, crack closure redeveloped on subsequent extension of the physically short cracks over distances comparable with microstructural dimensions, leading to a deceleration in growth rates. The development of closure was most efficient in the underaged microstructures where the inhomogeneous nature of deformation promoted faceted crack growth and hence roughness-induced crack closure.

ACKNOWLEDGMENTS

REFERENCES

1. P. C. Paris, R. J. Bucci, E. T. Wessel, W. G. Clark, and T. R. Mager: ASTM STP 513, Philadelphia, PA, 1972, pp. 141-76.
2. R. A. Schmidt and P. C. Paris: ASTM STP 536, Philadelphia, PA, 1973, pp. 79-93.
3. R. O. Ritchie, S. Suresh, and C. M. Moss: *J. Eng. Matls. Tech.*, Trans. ASME Ser. H, 1980, vol. 102, pp. 293-99.
4. A. T. Stewart: *Eng. Fract. Mech.*, 1980, vol. 13, pp. 463-78.
5. S. Suresh, G. F. Zamiski, and R. O. Ritchie: *Metall. Trans. A*, 1981, vol. 12A, pp. 1435-43.
6. N. Walker and C. J. Beevers: *Fat. Eng. Mat. Struct.*, 1979, vol. 1, pp. 135-48.
7. K. Minakawa and A. J. McEvily: *Scripta Met.*, 1981, vol. 15, pp. 633-36.
8. S. Suresh and R. O. Ritchie: *Metall. Trans. A*, 1982, vol. 13A, pp. 1627-31.
9. P. K. Liaw, T. R. Leax, R. S. Williams, and M. G. Peck: *Metall. Trans. A*, 1982, vol. 13A, pp. 1607-18.
10. M. Zedalis, L. Filler, and M. E. Fine: *Scripa Met.*, 1982, vol. 16, p. 471.
11. J. L. Breat, F. Mudry, and A. Pineau: *Fat. Eng. Mat. Struct.*, 1983, vol. 6, pp. 349-58.
12. K. Minakawa, J. C. Newman, Jr., and A. J. McEvily: *Fat. Eng. Mat. Struct.*, 1983, vol. 6, pp. 359-65.
13. W. W. Gerberich, W. Yu, and K. Esaklul: *Metall. Trans. A*, 1984, vol. 15A, pp. 875-88.
14. E. Zaiken and R. O. Ritchie: *Scripta Met.*, 1984, vol. 18, pp. 847-50.
15. S. Suresh and R. O. Ritchie: in *Fatigue Crack Growth Threshold Concepts*, D. L. Davidson and S. Suresh, eds., TMS-AIME, Warrendale, PA, 1984, pp. 227-61.
16. S. Suresh and R. O. Ritchie: *Int. Met. Rev.*, 1984, vol. 29, pp. 445-76.
17. W. Elber: *Eng. Fract. Mech.*, 1970, vol. 2, pp. 37-45.
18. J. Schijve: in *Fatigue Thresholds*, J. Bäcklund, A. Blom, and C. J. Beevers, eds., EMAS Ltd., Warley, U.K., 1982, vol. 2, pp. 881-908.
19. R. O. Ritchie and S. Suresh: *Mater. Sci. Eng.*, 1983, vol. 57, pp. L27-L30.
20. J. C. Newman, Jr.: in *Behavior of Short Cracks in Airframe Components*, AGARD Conf. Proc. No. 328, AGARD, France, 1983, pp. 6.1-6.26.
21. K. Tanaka and Y. Nakai: *Fat. Eng. Mat. Struct.*, 1983, vol. 6, pp. 315-27.
22. J. Lankford: *Fat. Eng. Mat. Struct.*, 1982, vol. 5, pp. 223-48.
23. D. Taylor and J. F. Knott: *Fat. Eng. Mat. Struct.*, 1981, vol. 4, pp. 147-55.
24. S. Suresh: *Metall. Trans. A*, 1983, vol. 14A, pp. 2375-85.
25. K. Endo, T. Okada, K. Komai, and M. Kiyota: *Bull. JSME*, 1972, vol. 15, pp. 1316-23.
26. J. -L. Tzou, S. Suresh, and R. O. Ritchie: *Acta Metall.*, 1985, vol. 33, pp. 105-16.
27. J. -L. Tzou, C. H. Hsueh, A. G. Evans, and R. O. Ritchie: *Acta Metall.*, 1985, vol. 33, pp. 117-27.
28. M. R. James and W. L. Morris: *Metall. Trans. A*, 1983, vol. 14A, pp. 153-55.
29. F. Heubaum and M. E. Fine: *Scripta Met.*, 1984, vol. 18, pp. 1235-40.
30. T. V. Duggan: in *Fatigue Thresholds*, J. Bäcklund, A. Blom, and C. J. Beevers, eds., EMAS Ltd., Warley, U.K., 1982, vol. 2, pp. 809-26.
31. E. Zaiken and R. O. Ritchie: *Eng. Fract. Mech.*, 1985, vol. 21, in press.
32. G. H. Aronson and R. O. Ritchie: *J. Test. Eval.*, 1979, vol. 7, pp. 208-15.
33. V. B. Dutta, S. Suresh, and R. O. Ritchie: *Metall. Trans. A*, 1984, vol. 15A, pp. 1193-207.
34. R. O. Ritchie: *Int. Met. Rev.*, 1979, vol. 20, pp. 205-30.
35. N. E. Dowling: *Fat. Eng. Mat. Struct.*, 1979, vol. 2, pp. 129-38.
36. H. Tada, P. C. Paris, and G. R. Irwin: *The Stress Analysis of Cracks Handbook*, Del Research Corp., St. Louis, MO, 1973.
37. W. K. Wilson: *J. Press. Ves. Tech.*, Trans. ASME, 1974, vol. 96, pp. 293-98.
38. S. Suresh, D. M. Parks, and R. O. Ritchie: in *Fatigue Thresholds*, J. Bäcklund, A. Blom, and C. J. Beevers, eds., EMAS Ltd., Warley, U.K., 1982, vol. 1, pp. 391-408.
39. E. Zaiken and R. O. Ritchie: *Mater. Sci. Eng.*, 1985, vol. 70, pp. 151-60.
40. K. Schulte, H. Nowack, and K. H. Trautmann: *Z. Werkstofftech*, 1980, vol. 11, p. 287.
41. J. Petit, P. Renaud, and P. Violan: *Proc. 14th European Conf. on Fracture*, Leoben, EMAS Ltd., Warley, U.K., 1982, pp. 426-33.
42. M. C. Lafarie-Frenot and C. Gasc: *Fat. Eng. Mat. Struct.*, 1983, vol. 6, pp. 329-44.
43. S. Suresh, A. K. Vasudévan, and P. E. Bretz: *Metall. Trans. A*, 1984, vol. 15A, pp. 369-79.
44. R. D. Carter, E. W. Lee, E. A. Starke, and C. J. Beevers: *Metall. Trans. A*, 1984, vol. 15A, pp. 555-63.
45. E. Hornbogen and K. H. Zum Gahr: *Acta Metall.*, 1976, vol. 24, pp. 581-92.
46. J. Lindgkeit, A. Gysler, and G. Lütjering: *Metall. Trans. A*, 1981, vol. 12A, pp. 1613-19.
47. M. M. Hammouda and K. J. Miller: ASTM STP 668, Philadelphia, PA, 1979, pp. 703-19.
48. R. P. Gangloff and R. O. Ritchie: in *Fundamentals of Deformation and Fracture*, Eshelby Memorial Symp., B. A. Bilby, K. J. Miller, and J. R. Willis, eds., Cambridge Univ. Press, Cambridge, U.K., 1985, pp. 529-58.
49. C. F. Shih: *J. Mech. Phys. Solids*, 1981, vol. 29, pp. 305-30.

ON THE ROLE OF COMPRESSION OVERLOADS IN INFLUENCING CRACK CLOSURE AND THE THRESHOLD CONDITION FOR FATIGUE CRACK GROWTH IN 7150 ALUMINUM ALLOY

E. ZAIKEN† and R. O. RITCHIE
Department of Materials Science and Mineral Engineering, University of California,
Berkeley, CA 94720, U.S.A.

Abstract—A study has been made of the effect of single compression cycles on near-threshold fatigue crack propagation in an *I/M* 7150 aluminum alloy. Based on experiments at a load ratio of $R = 0.10$ on cracks arrested at the fatigue threshold (ΔK_{TH}) in under-, peak and overaged microstructures, large compression overload cycles, of magnitude five times the peak tensile load, were found to cause immediate reinitiation of crack growth, even though the applied stress intensity range did not exceed ΔK_{TH}. Following an initial acceleration, subsequent crack advance was observed to take place at progressively decreasing growth rates until rearrest occurred. Such behavior is attributed to measured changes in crack closure which vary the effective near-tip driving force for crack extension (ΔK_{eff}). Specifically, roughness-induced closure primarily is reduced by the application of compressive cycles via a mechanism involving crack surface abrasion which causes flattening and cracking of fracture surface asperities. Closure, however, is regenerated on subsequent propagation resulting in the rearrest. Such observations provide further confirmation that the existence of a fatigue threshold is controlled principally by the development of crack closure and are discussed in terms of the mechanisms of closure in precipitation hardened alloys.

INTRODUCTION

THE GENERATION of fatigue crack closure, either from the presence of cyclic plasticity or through microstructural or environmental mechanisms, is now recognized as a major factor contributing to the development of a fatigue threshold, representing the stress intensity range ΔK_{TH} below which long cracks appear dormant (see, for example, Refs. [1–11]). Such closure, which results from interference between mating fracture surfaces, serves to reduce the near-tip driving force for crack advance from nominal levels, based on global measurements of applied loads and crack size, e.g. $\Delta K = K_{max} - K_{min}$, to some effective level actually experienced at the crack tip, e.g. $\Delta K_{eff} = K_{max} - K_{cl}$, where K_{cl} is the stress intensity on first contact of the crack surfaces during unloading [12]. Moreover, because of the nature of such contact which must occur in the wake of the crack tip, closure forces are limited at high load ratios ($R = K_{min}/K_{max}$) and at high stress intensity ranges due to the larger crack tip opening displacements, and at very small crack sizes due to the restricted wake [11]. The latter aspect appears to be one basis of the "anomalous" behavior of short cracks, which are small compared to the extent of local plasticity or microstructural size-scales or are simply physically small (i.e. ≤ 1 mm), as such cracks can initiate and grow, at progressively decreasing growth rates, *below* the long crack threshold with an associated smaller influence of closure [13, 14].

Recently, verification of this hypothesis, that both the existence of a threshold and the subthreshold propagation of short cracks are primarily related to closure phenomena, has been sought using experiments involving removal of material left in the wake of threshold fatigue cracks [15–18]. Through mechanical or electrodischarge machining of the wake of long cracks to within 0.5 to 1 mm of the tip, threshold cracks arrested at ΔK_{TH} in both steels [15] and aluminum alloys [16–18] were found to recommence to propagate at ΔK levels *not exceeding* ΔK_{TH}, consistent with a measured reduction in closure. Moreover, subsequent propagation rates, simulating the growth of short cracks emanating from a notch, were observed to be progressively decelerated consistent with a measured redevelopment of closure with increasing crack length [17, 18]. The location of the closure was determined by monitoring K_{cl} values during the micromachining process. Such measurements [16–18] indicated that closure far from

the crack tip was relatively less important and that approximately 50% of the closure was confined to within 500 μm or so from the tip.

In the present work, an alternative procedure is investigated for limiting crack closure in the wake of the crack tip. Specifically, the role of single compression overloads in influencing closure and near-threshold behavior of long cracks arrested at ΔK_{TH} is examined in under-, peak and overaged microstructures in an I/M 7150 aluminum alloy. Similar to prior experiments involving wake micromachining [18], compression overloads of sufficient magnitude were found to reduce the closure associated with arrested threshold cracks, resulting in an immediate recommencement of growth at ΔK_{TH}.

BACKGROUND

Whereas compression cycles are often a common occurrence in service, particularly for aerospace applications, and are known to be of importance in the process of crack initiation in smooth specimens, their effect on the propagation of (long) fatigue cracks, at least at intermediate to high ΔK levels, has long been considered to be minimal (e.g. Ref. [19]). This is in keeping with standard fracture mechanics concepts which imply that the crack will be closed during the compressive portion of the cycle, necessitating a stress intensity of zero at the tip, and the fact that tests invariably have been performed on long cracks where the magnitude of both tensile and compressive stresses are small. Although data are limited, several authors have found growth rates to be slightly faster at negative load ratios compared to $R = O$ in both steels and aluminum alloys [19–25], although the effect is negligible in certain alloys such as 7075-T6 [19]. Under variable amplitude fatigue loading, however, cyclic compressive stresses immediately following tensile overloads are known to lessen the post overload retardation in growth rates which usually accompanies single tensile overloads [26–28]. Moreover, under certain conditions of cracks initiating from notches, fatigue crack growth has been demonstrated under purely cyclic compressive loading [29–32]. In fact the technique has been used as a reliable means of producing small flaws for short crack experiments [30, 31].

Unlike behavior at higher growth rates where effects are small, recent studies at near-threshold levels have highlighted a significant role of compressive cycling on crack extension behavior [22–25]. Not only are threshold ΔK_{TH} values lower at $R = -1$ compared to $R = O$, but large periodic compressive cycles (of the order of one half the yield stress) applied during positive R cycling have been shown to dramatically reduce the threshold and to accelerate crack growth rates in both mild steel [25] and 2024-T3 aluminum [24]. Physical explanations for these effects remain unproven, although several suggestions have been proffered including redistribution of residual stresses *ahead* of the crack tip and reduced closure forces due to a diminished deformation zone left *behind* the crack tip [25]. In addition, periods of compression during the fatigue cycle are likely to result in a flattening of fracture surface asperities and a compacting of corrosion debris on crack faces, both processes leading to a reduction in closure via the roughness-induced [6–8] and oxide-induced [3–5] mechanisms, respectively.

The objectives of the current study were to investigate the role of single compression overload cycles on the propagation behavior of cracks arrested at the threshold, and specifically to monitor the variation in crack closure, both macroscopically in terms of K_{cl} measurements and microscopically in terms of changes in fracture surface morphology. A precipitation hardened aluminum alloy, 7150, was chosen for the study because in such systems the operative mechanisms of closure can be readily varied by heat treatment [33].

EXPERIMENTAL PROCEDURES

Material

Tests were performed on a conventionally-cast I/M 7150 aluminum alloy, supplied by ALCOA as 25-mm-thick plate in the solution treated and 2% stretched (W51) condition. The alloy, of composition shown in Table 1, is a high purity version of 7050 with lower levels of Si and Fe. Samples were machined from quarter and three-quarter plate thickness locations only and tempered to produce underaged, peak aged (T6) and overaged (T7) conditions. The specific heat treatments, which were designed to yield under- and overaged microstructures with iden-

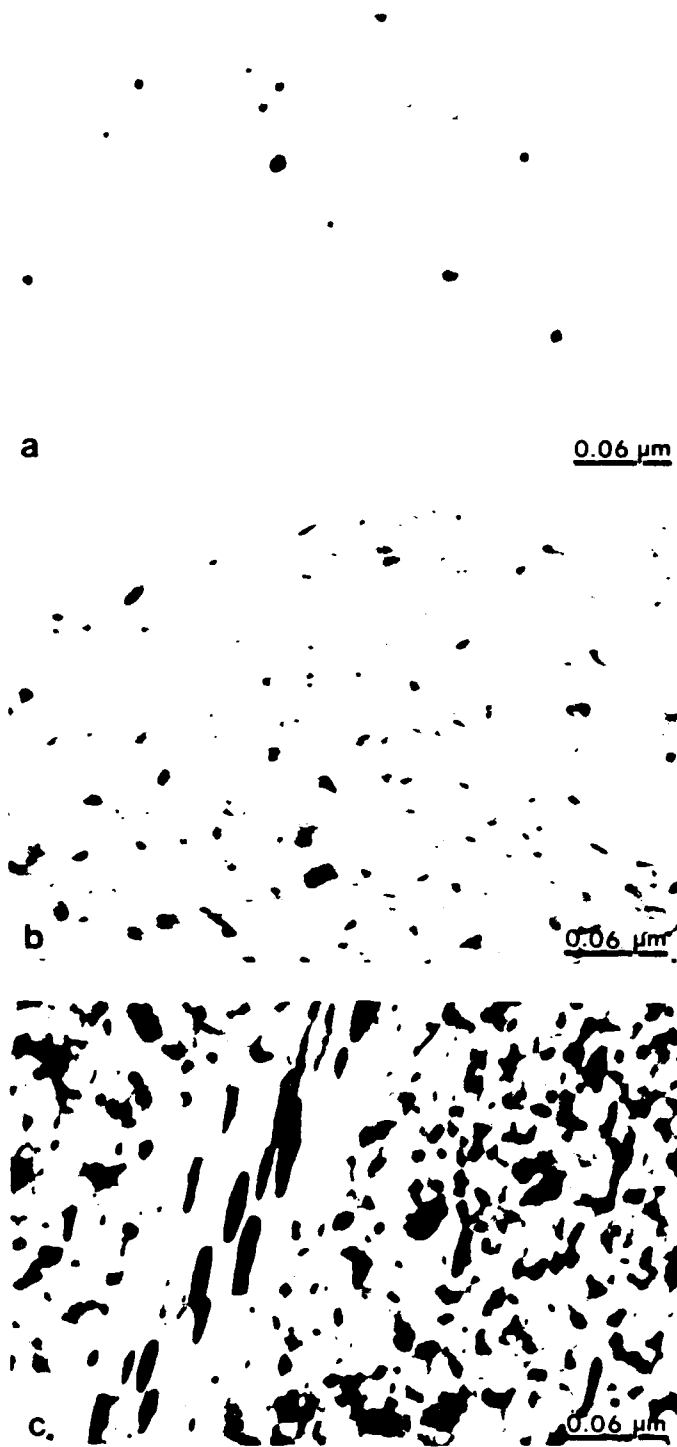Fig. 1. Transmission electron micrographs of (a) underaged, (b) peak aged (T6) and (c) overaged (T7) I/M 7150 aluminum alloy [33].
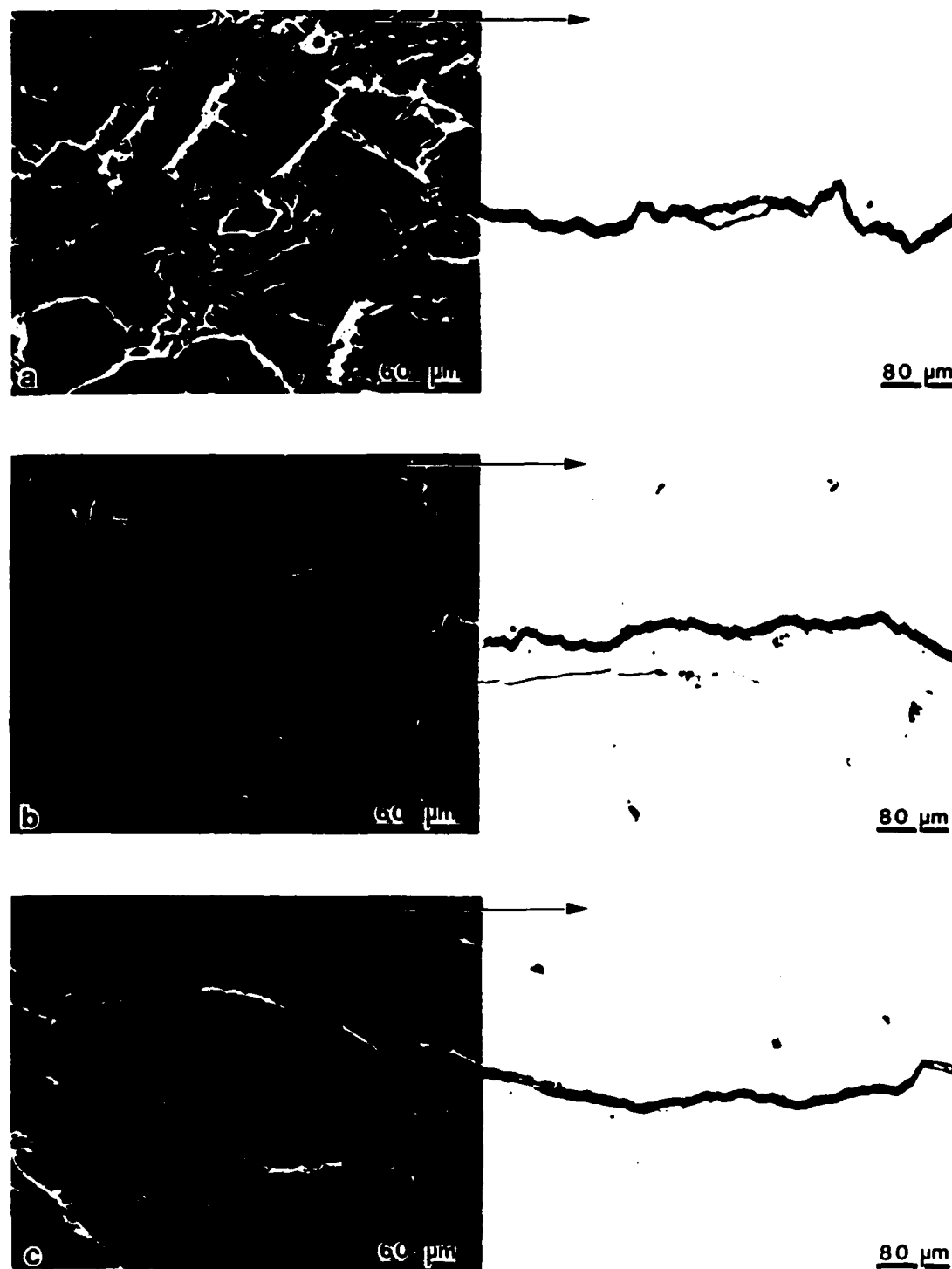
Fig. 6. Fracture surface and crack path morphologies for steady-state fatigue crack growth at near-threshold stress intensities in underaged, peak aged and overaged 7150 aluminum alloy [33]. Arrows indicate general direction of crack growth.

Table 1. Nominal chemical compositions in wt %

	Si	Fe	Cu	Mg	Zn	Ti	Zr	Al
7150	0.07	0.11	2.10	2.16	6.16	0.02	0.13	balance

tical strength levels, are listed in Table 2. Corresponding room temperature mechanical properties are shown in Table 3. Microstructures of the three aging conditions, shown in Fig. 1, have been described elsewhere [33]. Briefly, underaged structures were hardened by small coherent GP zones, roughly 4 to 8 nm in diameter, compared to hardening by semicoherent η' precipitates in peak aged structures. Overaged structures, conversely, showed evidence of coarsened η' precipitates in the matrix and predominately incoherent η precipitates in both matrix and grain boundaries, with small precipitate free zones of roughly 30 nm half-widths. Grains were elongated along the rolling direction with an approximate size of 15 by 5 μm.

Fatigue testing

Fatigue crack propagation testing was performed in controlled room temperature air (22°C, 45% relative humidity) using 6.4-mm-thick compact $C(T)$ test pieces machined in the T-L orientation. Tests were conducted under load control at a frequency of 50 Hz (sine wave) at a load ratio of 0.10. Direct current electrical potential methods were used to continuously monitor crack growth. Corresponding macroscopic crack closure measurements to determine K_{cl} values were carried out *in situ* using a back-face strain technique employing two strain gauges to record strain both parallel and perpendicular to the loading axis [34]. Mean closure loads were deduced from the point during the unloading cycle when the resulting elastic compliance curves of load versus relative strain first deviated from linearity.

Compression overload experiments were performed by first determining the long crack threshold using manual load shedding cycling, as described elsewhere [35]. In this manner, constant amplitude (steady-state) crack growth data between $\sim 10^{-6}$ and 10^{-11} m/cycle were obtained under decreasing ΔK conditions, with the threshold ΔK_{TH} operationally defined as the highest stress intensity range giving growth rates less than 10^{-11} m/cycle. Single (spike) compressive overloads were then applied to cracks arrested at ΔK_{TH}. The length of such arrested cracks was of the order 5 to 7 mm beyond the 17.5 mm initial notch in the compact specimen, i.e. $a \approx 23$ to 25 mm. With the applied loading conditions then maintained at a constant $\Delta K = \Delta K_{TH}$, subsequent growth rate and crack closure behavior were monitored closely. The magnitudes of the compression overload cycles were varied between one and five times the maximum tensile load in the fatigue cycle, i.e. up to a maximum compressive load between 1.8 and 2.8 kN corresponding to a fictitious "negative" stress intensity of 12 to 17 MPa√m.† The application of the single compression overloads at $\Delta K = \Delta K_{TH}$ was repeated two or three times on each specimen with at least 200 μm of crack extension between each event.

Fracture surface analysis

Fatigue fracture surfaces were examined using both optical and scanning electron microscopy. As described elsewhere [33], the degree of fracture surface roughness was assessed from

Table 2. Heat treatments utilized for tests on 7150 alloy

Underaged	ST† + 1½ hr at 121°C
Peak-aged (T6)	ST† + 100 hr at 121°C
Overaged (T7)	ST† + 24 hr at 121°C + 40 hr at 163°C

† ST — *solution treated, quenched and stretched 2% (WS1 condition)*

†As the compact specimen is not ideally suited for the application of compression cycles, such stress intensity values are very approximate and merely give an indication of magnitude of the overloads, i.e. ~ 5 times K_{max}. Current tests are being performed with center-cracked tension specimens where the magnitude of the compressive stresses and stress intensities are more readily ameanable to analysis.

Table 3. Room temperature mechanical properties of 7150 alloy

	Yield strength	U.T.S.	Elong.†	Redn. area	Work hardening exponent
	(MPa)	(MPa)	(%)	(%)	
Underaged	371	485	6.8	12.1	0.055
Peak-aged (T6)	404	480	6.0	10.3	0.046
Overaged (T7)	372	478	7.1	12.5	0.058

† On 32-mm-gauge length.

microstructural sections through crack paths, in terms of the ratio of total length of crack to projected length on the plane of maximum tensile stress. The thickness of crack surface corrosion deposits were measured in the scanning Auger spectroscopy using Ar^+ sputtering procedures [5, 33].

RESULTS

Steady-state fatigue behavior

The variation in fatigue crack propagation rate (da/dN) as a function of the nominal stress intensity range (ΔK), at $R = 0.10$ and 0.75, is shown in Fig. 2 for the under-, peak and overaged microstructures in 7150 alloy under steady-state (nonvariable amplitude) conditions. Data plotted in this figure represent mean values from at least three duplicate tests. Corresponding crack closure data have been presented elsewhere [33] and indicate that the progressively lower threshold values (and higher near-threshold growth rates), which are seen with increased aging, are consistent with less measured closure at $R = 0.10$. In all structures, K_{cl}/K_{max} values increased with decreasing ΔK, to approach unity at ΔK_{TH}. Relevant threshold data for these microstructures, including the extent of crack surface oxidation and degree of fracture surface roughness, are listed in Table 4 and are described in detail in Ref. [33].

Compression overload tests

Application of 100 to 300% single (spike) compression overloads (corresponding to one to three times the peak tensile loads) were observed to have no effect on crack closure or crack
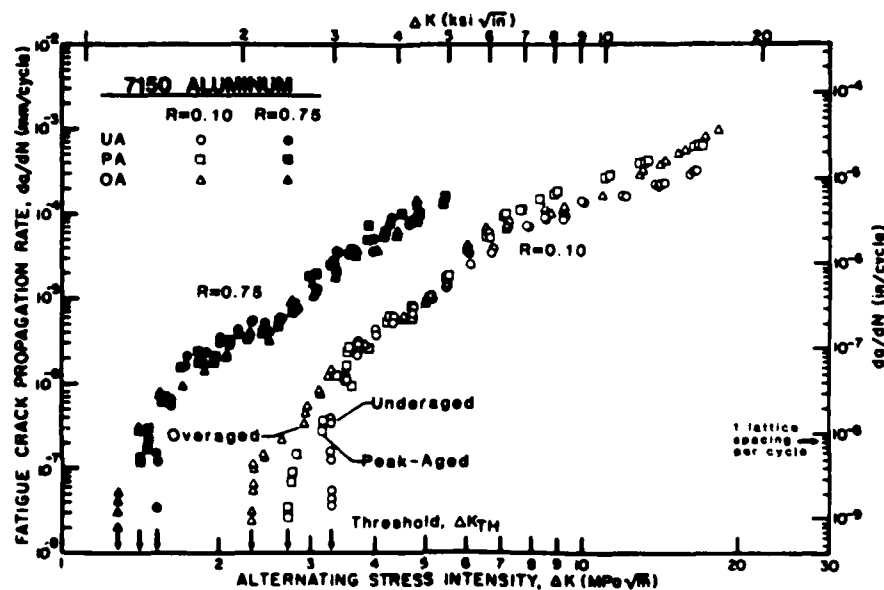

Fig. 2. Variation in steady-state fatigue crack propagation rates (da/dN) with stress intensity range (ΔK) for I/M 7150 aluminum alloy tested in controlled moist air at $R = 0.10$ and 0.75. Data represent the mean results for duplicate tests on long cracks $(a \approx 25$ mm) in underaged (UA), peak aged (PA) and overaged (OA) structures [33].

Table 4. Threshold data for 7150 alloy at R = 0.10

	Code	ΔK_{TH} (MPa $\sqrt{m}$)	Plastic zone size†,‡		Excess oxide thickness† (nm)	Degree of roughness§
			Cyclic (μm)	Maximum (μm)		
Underaged	UA	3.05–3.31	2.9	14.5	~3	1.26
Peak-aged (T6)	PA	2.44–2.94	1.8	8.8	~3	1.21
Overaged (T7)	OA	2.17–2.33	1.5	7.4	~3	1.06

† At the threshold, ΔK_{TH}.

‡ Computed from $r_\Delta = \frac{1}{6}\pi\,(\Delta K/2\sigma_y)^2$ and $r_{max} = \frac{1}{6}\pi(K_{max}/\sigma_y)^2$ and $\Delta CTOD = \frac{1}{4}(\Delta K^2/2\sigma_y,E)$, where r_Δ and r_{max} are the cyclic and maximum plastic zone sizes and σ_y the yield strength [36].

§ Ratio of total crack length to projected length on plane of maximum tensile stress (lineal roughness parameter).
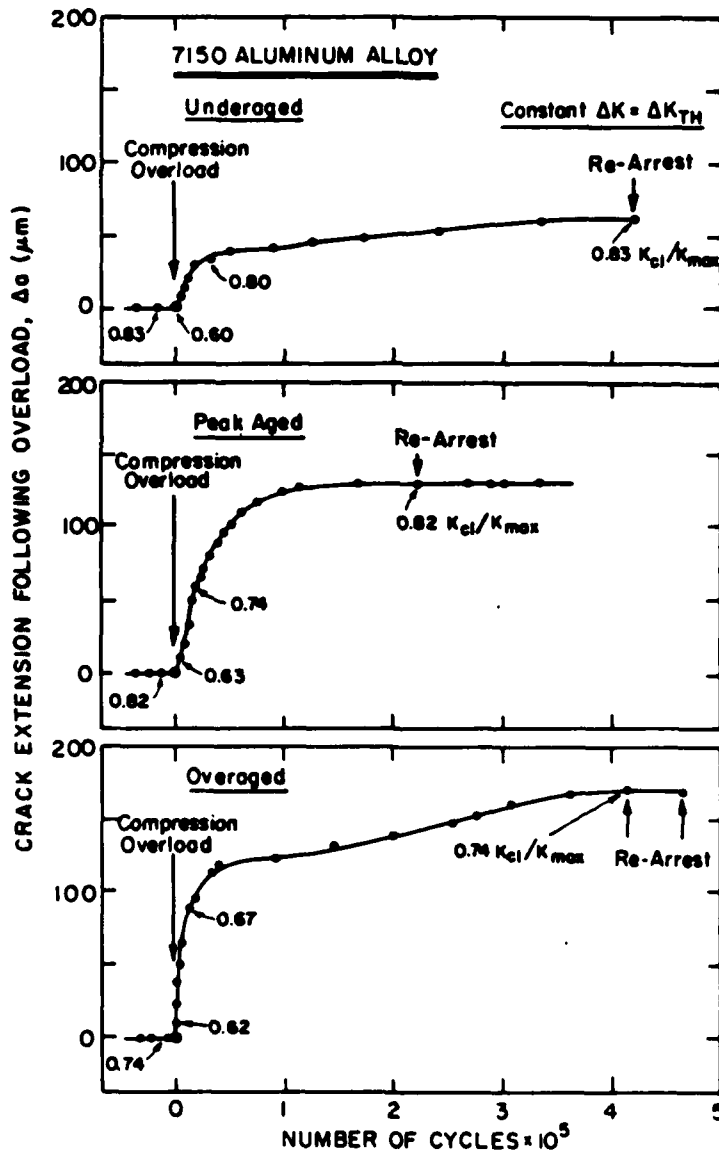

Fig. 3. Fatigue crack extension as a function of the number of cycles following application of 500% compression overloads on arrested threshold cracks in underaged, peak aged and overaged 7150 aluminum alloy. Data obtained under constant $\Delta K = \Delta K_{TH}$ cycling conditions at R = 0.10. K_{cl}/K_{max} closure data are listed beneath each curve.
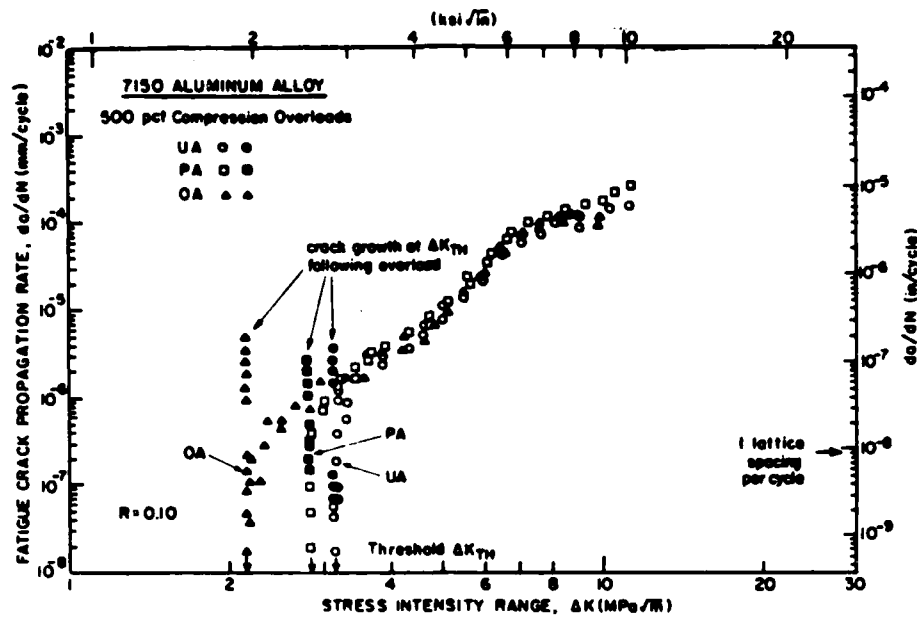
Fig. 4. Fatigue crack growth rate behavior, as a function of nominal stress intensity range (ΔK), for cracks previously arrested at the threshold (ΔK_{TH}) following the application of single 500% compression overloads (solid symbols). Data for underaged (UA), peak aged (PA) and overaged microstructures (OA) in 7150 aluminum alloy are compared with steady-state results from individual tests at $R = 0.10$ (open symbols).

growth of arrested cracks at the threshold. Crack growth behavior following the application of 500% compression overloads, however, is shown in Fig. 3 for the three microstructures. Here the compressive cycle has been applied and the subsequent closure and growth rates monitored under constant $\Delta K = \Delta K_{TH}$ cycling conditions. It is clearly apparent that the application of
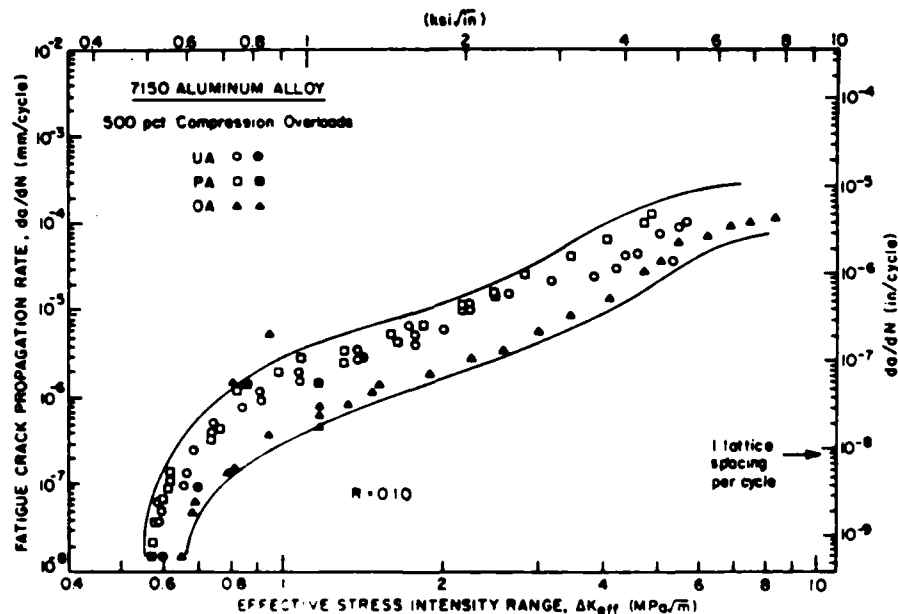

Fig. 5. Fatigue crack growth rates, as a function of the effective stress intensity range (ΔK_{eff}), for both steady-state behavior (open symbols) and following application of 500% compression overloads (solid symbols). Data from Fig. 3 for underaged (UA), peak aged (PA) and overaged (OA) microstructures in 7150 aluminum alloy. ΔK_{eff} calculations based on measured closure stress intensity data.
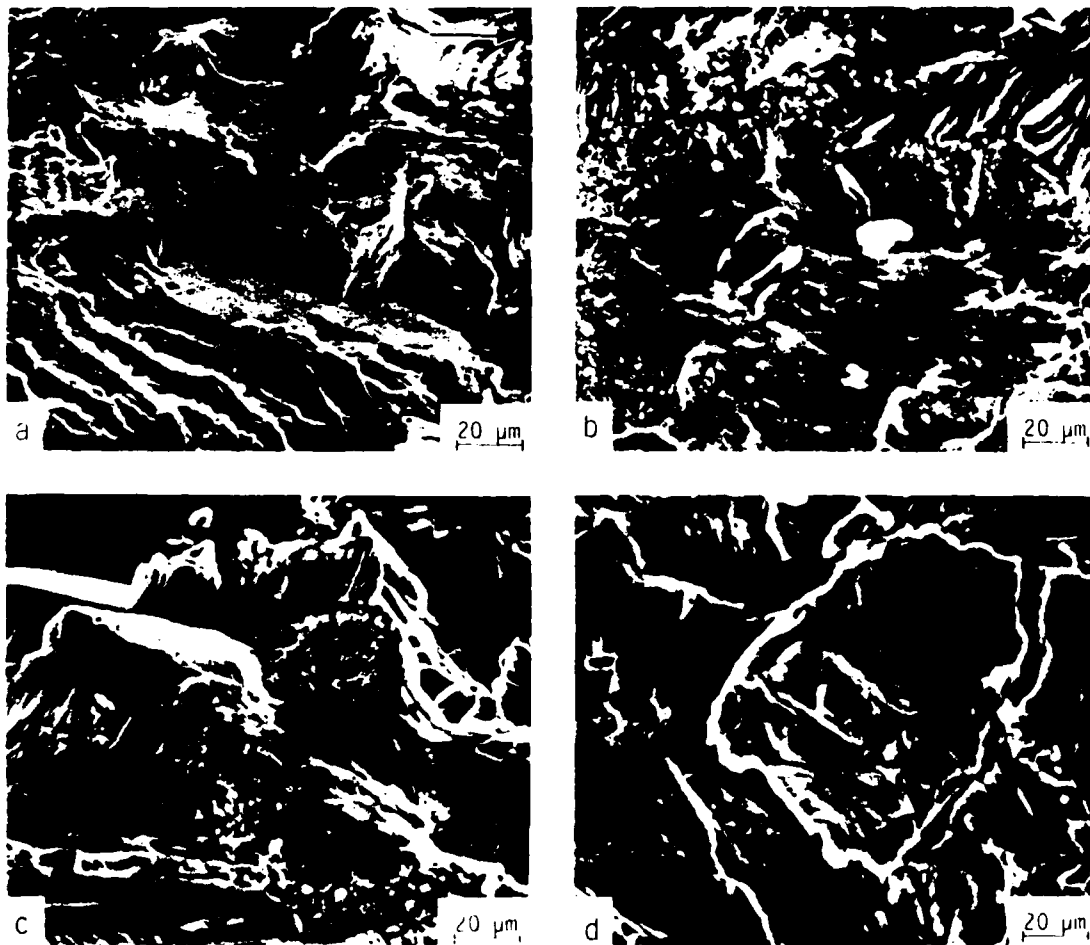
Fig. 7. Scanning electron micrographs of fatigue fracture morphology in underaged 7150 aluminum alloy directly behind the crack tip at the threshold ($\Delta K \approx 3.2$ MPa$\sqrt{m}$), showing (a) well-defined facets before the application of the compression overload, and (b) fretting oxide debris, (c) asperity flattening and (d) asperity cracking after the application of the overload. Arrow indicates general direction of crack growth.

Table 5. Closure, ΔK_{eff} and crack extension data at $\Delta K = \Delta K_{TH}$ before and after compression overloads on arrested cracks

Microstructure	ΔK_{TH}	At initial arrest		Following overload		At rearrest		Crack ext. to rearrest
	(MPa$\sqrt{m}$)	K_{cl}/K_{max}	ΔK_{eff} (MPa$\sqrt{m}$)	K_{cl}/K_{max}	ΔK_{eff} (MPa$\sqrt{m}$)	K_{cl}/K_{max}	ΔK_{eff} (MPa$\sqrt{m}$)	Δa (μm)
Underaged	3.14	0.83	0.59	0.60	1.40	0.83	0.59	60
Peak-aged (T6)	2.81	0.82	0.56	0.63	1.15	0.82	0.56	130
Overaged (T7)	2.17	0.74	0.63	0.62	0.92	0.74	0.63	170

the compressive overload causes immediate propagation of the arrested cracks, even though the stress intensity range does not exceed ΔK_{TH}. Moreover, under such constant ΔK conditions, the initial acceleration, to as high as $\sim 10^{-5}$ mm/cycle, is followed by a progressive deceleration in growth rates until rearrest. The extent of crack growth before rearrest occurs is of the order of 60 μm in the underaged structure, far smaller than in the peak and overaged structures where the crack extends a further 130 and 170 μm, respectively, before arrest. Application of a second single compression overload on the rearrested crack at this stage produced identical results. Such behavior was accompanied by significant changes in the magnitude of the crack closure. The initially high closure values which are associated with the original arrest at the threshold, i.e. K_{cl}/K_{max} values of the order of 0.75–0.85, were reduced

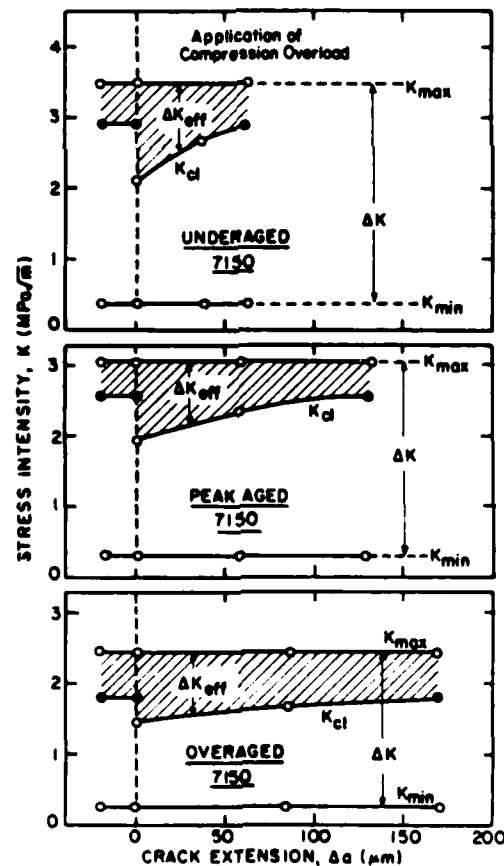Fig. 8. Variation in ΔK and ΔK_{eff} with crack extension, computed from measured K_{cl} closure data, for fatigue crack growth behavior in underaged, peak aged and overaged 7150 aluminum alloy following application of single compression overloads on arrested cracks at $\Delta K = \Delta K_{TH}$.

immediately by 16 to 28% to approximately 0.60 by the compressive overload. With further crack extension, however, the closure was regenerated until arrests again occurred at a $K_{cl}/$ K_{max} level similar to that of the original (pre-overload) threshold. Such closure measurements, together with the corresponding effective stress-intensity ranges, i.e. ΔK_{eff} values, are listed in Table 5. Plots of the pre- and post-overload growth rates as a function of both nominal and effective stress intensities, computed from these data for individual tests, are shown in Figs. 4 and 5, respectively. It can be seen that the "anomalously" high growth rates at ΔK_{TH}, resulting from the application of the compression cycles, fall within the scatterband for steady-state growth rates when characterized in terms of ΔK_{eff} rather than ΔK. This clearly implies a dominant role of closure.

Fractography

The fractography of steady-state near-threshold fatigue crack growth in this alloy is summarized in Fig. 6 and has been described in some detail elsewhere [33]. Briefly, at low ΔK levels, fracture surfaces show little evidence of corrosion debris and in underaged microstructures tend to be faceted and irregular, compared to the relatively smoother appearance of the peak and overaged structures. In terms of crack path morphology, this can be seen as many instances of crack deflection, in contrast to the more linear profiles in the more heavily aged microstructures. Following compression overload cycles, however, the well-defined features of these fracture surfaces become obscured somewhat. As shown in Fig. 7, there are clear indications of abrasion, compacted fretting oxide debris and the cracking and flattening of fracture surface asperities close behind the crack tip. These features, which always predominated in the immediate vicinity of the crack tip, were profuse in underaged structures where the asperities were most pronounced due to the faceted nature of the crack path.

DISCUSSION

The present results show a dramatic effect of compression overloads on the propagation behavior of "long" fatigue cracks. The application of a single compression cycle (of magnitude *five times the maximum fatigue tensile* load corresponding to a nominal bending stress of ~30% of the yield stress) was seen to result in the "removal" of the fatigue threshold. Moreover, previously arrested cracks at the threshold underwent an instantaneous acceleration in growth rates, to levels approaching ~ 10^{-5} mm/cycle, even though the applied stress intensity range was maintained constant at ΔK_{TH} (Figs. 3 and 4). Such phenomena were accompanied by a measured reduction in crack closure, in the form of decreased K_{cl} values, and hence can be related to an increase in near-tip crack driving force, ΔK_{eff}, following the compression cycle (Table 5).

Mechanistically, the increased local driving force can be attributed to two principal factors. In the present tests, the major effect appears to result from a reduction in roughness-induced closure from a flattening of fracture surface asperities during the compression, as shown in Fig. 7. The associated evidence of compacted fretting corrosion debris and a lack of fine detail on fracture surfaces, which have undergone compression cycles, both indicate marked abrasion between mating crack faces, consistent with such crushing of asperities. A second mechanism involves the residual stress distribution ahead of the crack tip, which must be altered by the large compressive loads. However, this effect of residual stresses *ahead* of the tip, as opposed to the associated closure *behind* the tip, is likely to be far more pronounced when cracks are small and propagating out of a notch (particularly in bend or compact geometries), due the fulcrum loading effect [32] of the notch in compression.

Following the initial post-overload acceleration of the previously arrested cracks at ΔK_{TH}, growth rates progressively decelerate until rearrest occurs (Fig. 3). This is accompanied by a measured build up in crack closure with crack extension, approaching pre-overload threshold levels at the rearrest (Table 5). Based on the K_{cl} measurements, the computed variation in ΔK_{eff} with crack extension (Δa), both prior to and following the overload, is shown in Fig. 8 for the three microstructures examined. Comparison of this figure with the crack length vs number of cycles data in Fig. 3 indicates that the reinitiation and rearrest of the threshold cracks is at least qualitatively consistent with closure-induced changes in the local driving force ΔK_{eff}.

Moreover, since the post-overload growth rate data can be brought into close correspondence with the steady-state fatigue data through characterization in terms of ΔK_{eff} instead of ΔK (c.f. Fig. 4 and Fig. 5), it would appear that this explanation is quantitatively consistent as well. These calculations imply that the actual threshold for no fatigue crack propagation in under-, peak and overaged 7150 can be defined in terms of a ΔK_{eff} value of approximately 0.6 MPa$\sqrt{m}$ (Table 5).

Comparison of behavior for the three aging treatments in Fig. 3 indicates that the redevelopment of closure with crack extension, following the application of the compression overload, is very dependent upon microstructure. Rearrest, which involves an increase in K_{cl} such that ΔK_{eff} is reduced to the threshold value of ~ 0.6 MPa$\sqrt{m}$, occurs after crack extensions between 60 and 170 μm, distances that are the order of 5 to 10 grain sizes and are far larger than the size-scales representative of local crack tip plasticity (c.f. maximum and cyclic plastic zone sites in Table 4). Furthermore, it is apparent that significant closure can develop over far smaller amounts of crack extension in the underaged microstructure compared to the more heavily aged conditions. Such results are consistent with the origins of closure in the 7150 alloy [33], which rely at near-threshold levels primarily on microstructural factors rather than on cyclic plasticity or environmental effects. Due to their inhomogeneous mode of deformation (i.e. coarse planar slip) resulting from hardening by coherent (shearable) particles, underaged structures tend to show crack paths which are more crystallographic in nature than in peak and overaged structures [33, 37–41]. This produces rough, faceted fracture surfaces (Fig. 6) which strongly promote roughness-induced closure in these microstructures [33, 37–39]. In contrast, the development of closure with crack extension in peak and overaged structures is far less efficient [18]. Since the roughness-induced mechanism is the principal source of closure in this alloy, the comparatively smoother crack paths, which result from the more homogeneous deformation mode (i.e. wavy slip) arising from incoherent particle hardening, significantly limit the development of closure in the more heavily aged structures [18, 33, 37–39].

The present experiments, on the role of compression overloads in the propagation and subsequent arrest of threshold fatigue cracks, are analogous to prior studies [17, 18] in 7150 on the effect of the mechanical removal of material left in the wake of threshold cracks. Here, the micro-machining away of wake material causes a similar reduction in closure, leading to a recommencement of growth of previously arrested cracks. Subsequent crack extension again is associated with progressively decreasing growth rates (but not in this case complete arrest) as closure is redeveloped over roughly 2 to 10 grain sizes. The difference in the two types of experiment appears to be in the location of the closure which is removed. Whereas micro-machining can only remove closure away from the crack tip vicinity (i.e. reliably no closer than 500 μm) [18], the nature of the fracture surface damage in Fig. 7 suggests that compression overloads may primarily limit the more important near-tip closure.

This study, as with prior studies [15–18] on the role of wake removal, clearly identifies the existence of a fatigue threshold with the phenomenon of crack closure. Furthermore, the results show that wherever closure is restricted, such as in the present case with the application of large compression cycles, steady-state propagation rate data *characterized in terms of* ΔK can no longer be relied upon to predict crack growth behavior in a given material.

CONCLUDING REMARKS

Despite early claims to the contrary [19, 27], compressive loading in the form of single (spike) overloads clearly can lead to dramatic increases in fatigue crack growth rates at low stress intensity ranges and most notably *to crack propagation at the threshold*. These results are consistent with the recent work of Topper and his co-workers [24, 25], who found a linear decrease in threshold values with increasing compressive peak stress, and an accentuation of the effect when the compressive overloads were applied more frequently. Such observations serve to highlight the inherent danger of utilizing low load ratio threshold ΔK_{TH} values in engineering design to predict the absence of fatigue cracking. The existence of the threshold is linked intimately to the degree of closure which controls the effective near-tip driving force, yet such considerations are not incorporated into nominal stress intensity calculations used in defect-tolerant life prediction analyses. Thus, wherever the extent of crack closure is restricted,

such as at high load ratios [2–5], with small flaws or cracks at notches [13–15], or in the presence of large compressive stresses, the consequent increase in near-tip crack driving force can lead to accelerated and nonunique [42] growth rate behavior and, more importantly, to *crack extension at* ΔK *levels at or below the* ΔK_{TH} *threshold.*

CONCLUSIONS

Based on a study on the effect on single (spike) compression overloads on near-threshold fatigue crack propagation at $R = 0.10$ in underaged, peak aged and overaged *I/M* 7150 aluminum alloy, the following conclusions can be made:

1. A single compression overload, of magnitude five times the tensile peak load, resulted in immediate reinitiation of growth of cracks arrested at the fatigue threshold even though the applied ΔK was maintained constant at ΔK_{TH}, consistent with a measured 16 to 28% reduction in crack closure.

2. The reduction in closure stress intensity (K_{cl}) following the compressive cycle was related primarily to a reduced contribution from roughness-induced crack closure arising from abrasion between mating crack surfaces, i.e. fractographically to the flattening and cracking of fracture surface asperities in the vicinity of the crack tip.

3. Crack growth at $\Delta K = \Delta K_{TH}$ following the application of the overload was characterized by a progressive deceleration until rearrest occurred within 60 to 170 μm. Such behavior was accompanied by a measured increase in crack closure back to original pre-overload threshold levels.

4. Compared to the more heavily aged structures, deceleration and rearrest occurred after far less crack extension in underaged microstructures, consistent with a larger magnitude, and more efficient redevelopment, of roughness-induced crack closure. This arises from the coherent particle hardening mechanism in this microstructure which induces a planar slip mode of deformation, thereby promoting rougher, more faceted crack path morphologies and the consequent generation of more pronounced fracture surface asperities.

REFERENCES

[1] P. C. Paris, R. J. Bucci, E. T. Wessel, W. G. Clark and T. R. Mager, Extensive study of low fatigue crack growth rates in A533B and A508 steels. *Stress Analysis and Growth of Cracks, ASTM STP* 513, 141–176 (1972).
[2] R. A. Schmidt and P. C. Paris, Threshold for fatigue crack propagation and effects of load ratio and frequency. *Progress in Flaw Growth and Fracture Toughness Testing, ASTM STP* 536, 79–93 (1973).
[3] R. O. Ritchie, S. Suresh and C. M. Moss, Near-threshold fatigue crack growth in 2¼Cr-1Mo pressure vessel steel in air and hydrogen. *J. Engng Mater. Technol. Ser. H* 102, 293–299 (1980).
[4] A. T. Stewart, The influence of environment and stress ratio on fatigue crack growth at near-threshold stress intensities in low-alloy steels. *Engng Fracture Mech.* 13, 463–478 (1980).
[5] S. Suresh, G. F. Zamiski and R. O. Ritchie, Oxide-induced crack closure: An explanation for near-threshold corrosion fatigue crack growth behavior. *Metall. Trans. A* 12A, 1435–1443 (1981).
[6] N. Walker and C. J. Beevers, A fatigue crack closure mechanism in titanium. *Fatigue Engng Mater. Struct.* 1, 135–148 (1979).
[7] K. Minakawa and A. J. McEvily, On crack closure in the near-threshold region. *Scripta Met.* 15, 633–636 (1981).
[8] S. Suresh and R. O. Ritchie, A geometric model for fatigue crack closure induced by fracture surface roughness. *Metall. Trans. A* 13A, 1627–1631 (1982).
[9] P. K. Liaw, T. R. Leax, R. S. Williams and M. G. Peck, Near-threshold fatigue crack growth behavior in copper. *Metall. Trans. A* 13A, 1607–1618 (1982).
[10] W. W. Gerberich, W. Yu and K. Esaklul, Fatigue threshold studies in Fe, Fe-Si and HSLA steel. I. Effect of strength and surface asperities on closure. *Metall. Trans. A* 15A, 875–888 (1984).
[11] S. Suresh and R. O. Ritchie, Near-threshold fatigue crack propagation: A perspective on the role of crack closure. in *Fatigue Crack Growth Threshold Concepts* (Edited by D. L. Davidson and S. Suresh), pp. 227–261. TMS-AIME, Warrendale, PA (1984).
[12] W. Elber, The significance of fatigue crack closure. *Damage Tolerance in Aircraft Structures, ASTM STP* 486, 230–242 (1971).
[13] J. Schijve, Differences between the growth of small and large fatigue cracks in relation to threshold K values, in *Fatigue Thresholds* (Edited by J. Backlund, A. Blom and C. J. Beevers), Vol. 2, pp. 391–408 EMAS Ltd., Warley, England (1982).

[14] S. Suresh and R. O. Ritchie, The propagation of short fatigue cracks. *Int. Met. Rev.* **25**, 445–476 (1984).

[15] J. L. Breat, F. Mudr and A. Pineau, Short crack propagation and closure effects in A508 steel. *Fatigue Engng Mater. Struct.* **6**, 349–358 (1982).

[16] K. Minakawa, J. C. Newman, Jr. and A. J. McEvily, A critical study of the crack closure effect on near-threshold fatigue crack growth. *Fatigue Engng Mater. Struct.* **6**, 359–365 (1983).

[17] E. Zaiken and R. O. Ritchie, On the location of crack closure and the threshold for fatigue crack growth. *Scripta Met.* **18**, 847–850 (1984).

[18] E. Zaiken and R. O. Ritchie, On the development of crack closure and the threshold condition for short and long fatigue cracks in 7150 aluminum alloy. *Metall. Trans. A* **16A**, in review.

[19] C. M. Hudson and J. T. Scardina, Effect of stress ratio on fatigue crack growth in 7075-T6 aluminum alloy sheet. *Engng Fracture Mech.* **1**, 429–446 (1969).

[20] T. R. Gurney, The effect of mean stress and material yield stress on fatigue crack propagation in steels. *Metal Constr.* **1**, 91–96 (1969).

[21] R. P. Skelton and J. R. Haigh, Fatigue crack growth rates and thresholds in steels under oxidizing conditions. *Mater. Sci. Engng* **36**, 17–25 (1978).

[22] S. Usami, Applications of threshold cyclic-plastic-zone-size criterion to some fatigue limit problems, in *Fatigue Thresholds* (Edited by J. Bäcklund, A. Blom and C. J. Beevers), Vol. 1, pp. 205–238. EMAS Ltd., Warley, England (1982).

[23] A. F. Blom, A. Hadrboletz and B. Weiss, Effect of crack closure on near-threshold crack growth behaviour in a high strength Al-alloy up to ultrasonic frequencies, in *Mechanical Behavior of Materials IV*, Proc. 4th Intl. Conf. (Edited by J. Carlsson and N. G. Olhsen), Vol. 2, pp. 755–763. Pergamon Press, Oxford (1984).

[24] P. Au, T. H. Topper and M. L. El Haddad, The effects of compressive overloads on the threshold stress intensity for short cracks, in *Behavior of Short Cracks in Airframe Components*, AGARD Conf. Proc. No. 328, pp. 11.1–11.17. AGARD, France (1983).

[25] T. H. Topper, M. T. Yu and P. Au, The effects of stress cycle on the threshold of a low carbon steel, in *Proc. VIII Inter-American Conf. on Materials Technology*, San Juan, Puerto Rico, pp. 26.15–26.22 (1984).

[26] J. Schijve and D. Broek, Crack-propagation tests based on a gust spectrum with variable amplitude loading. *Aircraft Engng* **34**, 314–316 (1962).

[27] T. M. Hsu and W. M. McGee, Effects of compressive loads on spectrum fatigue crack growth rate. *Effect of Load Spectrum Variables in Fatigue Crack Initiation and Propagation*, ASTM STP 714, 79–90 (1980).

[28] D. Gan and J. Weertman, Crack closure and crack propagation rates in 7050 aluminum. *Engng Fracture Mech.* **15**, 87–106 (1981).

[29] C. N. Reid, K. Williams and R. Hermann, Fatigue in compression. *Fatigue Engng Mater. Struct.* **1**, 267–270 (1979).

[30] S. Usami and S. Shida, Elastic-plastic analysis of the fatigue limit for a material with small flaws. *Fatigue Engng Mater. Struct.* **1**, 471–481 (1979).

[31] J. F. McCarver and R. O. Ritchie, Fatigue crack propagation thresholds for long and short cracks in René 95 nickel-base superalloy. *Mater. Sci. Engng* **55**, 63–67 (1982).

[32] S. Suresh, unpublished research, University of California, Berkeley (1983).

[33] E. Zaiken and R. O. Ritchie, Effects of microstructure on fatigue crack propagation and crack closure behavior in aluminum alloy 7150. *Mater. Sci. Engng*, **68**, (1985).

[34] V. B. Dutta, S. Suresh and R. O. Ritchie, Fatigue crack propagation in dual-phase steels: Effects of ferritic-martensitic microstructures on crack path morphology. *Metall. Trans. A* **15A**, 1193–1207 (1984).

[35] R. O. Ritchie, Near-threshold fatigue crack propagation in steels. *Int. Met. Rev.* **20**, 205–230 (1979).

[36] C. F. Shih, Relationships between the *J*-integral and the crack opening displacement for stationary and extending cracks. *J. Mech. Phys. Solids* **29**, 305–330 (1981).

[37] M. C. Lafarie-Frenot and C. Gasc, The influence of age-hardening on fatigue crack propagation behaviour in 7075 aluminum alloy in vacuum. *Fatigue Engng Mater. Struct.* **6**, 329–344 (1983).

[38] S. Suresh, A. K. Vasudévan and P. E. Bretz, Mechanisms of slow fatigue crack growth in high strength aluminum alloys: Role of microstructure and environment. *Metall. Trans. A* **15A**, 369–379 (1984).

[39] R. D. Carter, E. W. Lee, E. A. Starke and C. J. Beevers, The effect of microstructure and environment on fatigue crack closure of 7475 aluminum alloy. *Metall. Trans. A* **15A**, 555–563 (1984).

[40] E. Hornbogen and K.-H. Zum Gahr, Microstructure and fatigue crack growth in a γ-Fe-Ni-Al alloy. *Acta Metall.* **24**, 581–592 (1976).

[41] J. Lindgkeit, A. Gysler and G. Lutjering, The effect of microstructure on the fatigue crack propagation behavior of an Al-Zn-Mg-Cu alloy. *Metall. Trans. A* **12A**, 1613–1619 (1981).

[42] R. O. Ritchie and S. Suresh, The fracture mechanics similitude concept: Questions concerning its application to the behavior of short fatigue cracks. *Mater. Sci. Engng* **57**, L27–L30 (1983).

On the Growth of Cracks at the Fatigue Threshold following Compression Overloads: Role of Load Ratio

P. DONEHOO, W. YU and R. O. RITCHIE

Department of Materials Science and Mineral Engineering, University of California, Berkeley, CA 94720 (U.S.A.)

(Received December 17, 1984)

ABSTRACT

Studies have been performed on the effect of single compression overload cycles on the role of crack closure during near-threshold fatigue crack growth in ingot metallurgy aluminum alloy 7150-T7, specifically with respect to the role of mean stress or load ratio R ($= K_{min}/K_{max}$). It was found that large compression or simple unloading cycles, applied to cracks arrested at the fatigue threshold at R = 0.75, had no detectable effect on crack closure or crack growth behavior. This is in contrast with previous studies at R = 0.10 where arrested threshold cracks subjected to such compression cycles (of magnitude five times the maximum tensile load) were seen to recommence growth immediately, consistent with a measured reduction in closure. Such results are discussed in terms of the major origins of crack closure in this alloy.

1. INTRODUCTION

It is well known that compressive loads can have a marked effect on the initiation of fatigue cracks in smooth specimens (see for example ref. 1). Conversely, the effect on (constant-amplitude) fatigue crack propagation generally is considered to be minimal, since the crack is expected to be fully closed during the compressive portion of the cycle, necessitating a stress intensity of zero at the crack tip (see for example refs. 2 and 3). Similarly, under variable-amplitude loading, compressive overload cycles in general are found to have little effect, except when they immediately follow a tensile overload where they act to reduce the post-overload retardation (see for example refs. 4 and 5). Such tests, however, generally have been performed at relatively high growth rates (*e.g.* above about 10^{-8} m cycle^{-1}) on "long" fatigue cracks where the magnitude of both the tension and the compression stresses have been small.

In contrast with behavior at higher growth rates, recent work at lower near-threshold growth rates, employing somewhat larger compressive stresses (of the order of several times the maximum tensile stress in the fatigue cycle), have shown a marked influence of compression cycles on crack growth and closure behavior [6-12]. For example, the application of periodic compressive cycles during cycling at positive load ratios ($R = K_{min}/K_{max}$) has been shown to decrease fatigue threshold ΔK_{th} values markedly and to accelerate near-threshold propagation rates in both low strength steels and aluminum alloys [7, 8]. In 17-4 PH stainless steels and aluminum alloys 7150 and 7475 where single compressive cycles were applied to fatigue cracks arrested at the threshold, it was found that the cracks immediately recommenced to propagate (even though the applied stress intensity ranges did not exceed ΔK_{th}), concomitant with a measured decrease in crack closure [11, 12].

Explanations for these effects have been considered in terms of two mechanisms, namely (i) the redistribution of residual stresses ahead of the crack tip [7, 9], specifically involving a reduction in the magnitude of the compressive stresses within the cyclic plastic zone, which lowers the subsequent crack opening (or crack closure) load [9], and (ii) the crushing and compacting of fracture surface asperities during the compression cycle [11, 12], which decreases the contribution from roughness-induced crack closure [13-15]. The dominance of crack closure in these explanations has yet to be tested, however, as most experiments reported to date on the role of

12

TABLE 1

Composition of aluminum alloy 7150

Element	Si	Fe	Cu	Mg	Zn	Ti	Zr	Al
Amount (wt.%)	0.07	0.11	2.10	2.16	6.16	0.02	0.13	Balance

TABLE 2

Room temperature mechanical properties of aluminum alloy 7150-T7

Yield strength (MPa)	372
Ultimate tensile strength (MPa)	478
Elongation (%) in 32 mm	7.1
Reduction (%) in area	12.5
Work-hardening exponent	0.06

compression overloads have been performed at low load ratios where closure effects predominate.

The objective of the present paper is to examine the corresponding effects of compression overload cycles at high load ratios, where the influence of closure phenomena is far less dominant, and to compare behavior with that previously reported for $R = 0.10$ [11].

2. EXPERIMENTAL PROCEDURES

Tests were conducted on a conventionally cast ingot metallurgy aluminum alloy 7150 of composition shown in Table 1. The alloy was supplied by Alcoa as plate 25 mm thick in the solution-treated and 2% stretched (W51) condition. Specimen blanks were machined between quarter-thickness and three-quarters-thickness locations and were subsequently tempered for 24 h at 121 °C plus 40 h at 163 °C to produce an overaged (T7) structure. The T7 microstructure consisted of predominately incoherent η precipitates ($MgZn_2$ compounds) in both matrix and grain boundaries, with coarse semicoherent η' particles ($MgZn_2$-$Mg(CuAl)_2$) in the matrix [16]. The grain size was approximately 15 μm by 5 μm, with precipitate-free zones (about 30 nm half-width) visible at the boundaries. The room temperature mechanical properties are listed in Table 2 [16].

Conventional long crack threshold fatigue tests first were carried out using compact tension specimens 6.4 mm thick (TL orientation, i.e. the load was applied in the long traverse direction and the crack propagated in the longitudinal direction), cycled under load control in room temperature air (22 °C; relative humidity, 45%) at 50 Hz [11, 16]. Using d.c. electrical potential methods to monitor crack growth, thresholds were approached under manual load-shedding conditions, at load ratios of 0.10 and 0.75, with the value of ΔK_{th} defined as the highest stress intensity range giving growth rates less than 10^{-11} m cycle^{-1} [17]. Corresponding macroscopic crack closure measurements to determine the closure stress intensity K_{cl} were conducted in situ with the back-face strain technique [18]. The effective "crack driving force" was then computed as $\Delta K_{eff} = K_{max} - K_{cl}$.

Once the crack had arrested at ΔK_{th}, single (spike) compressive overloads or tensile underloads were applied and the subsequent crack extension and crack closure behavior closely monitored. The specific notation for the variable-amplitude loads is defined in Fig. 1. Compression overloads and tension underloads both involve a negative excursion of K_L from K_{max}. For the compression overloads, however, this load excursion includes a compressive portion, characterized by the fictitious stress intensity $|K_{cp}|$. Corresponding loads are referred to as P_L and P_{cp} respectively. Specific values of these loads, and associated stress intensities, for the compressive overload and tensile underload tests at R values of 0.10 and 0.75 are listed in Table 3.

3. RESULTS AND DISCUSSION

Fatigue crack propagation rates da/dN, under constant-amplitude loading conditions, are shown in Fig. 2 for the alloy 7150-T7 as a function of stress intensity range ΔK at $R =$
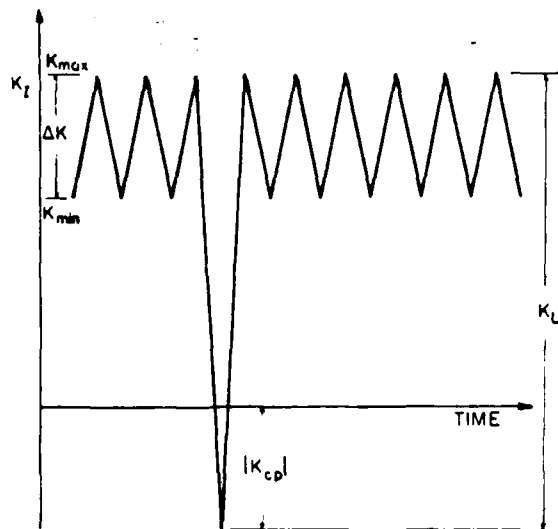
Fig. 1. Nomenclature used to define compression overload and tensile underload cycles applied at ΔK_{th}.

plication of a large compression overload (*i.e.* with an applied compressive load P_{cp} of 1.78 kN ($|K_{cp}| = 12$ MPa m$^{1/2}$) and a total overload P_L of 2.14 kN ($|K_L| = 14.4$ MPa m$^{1/2}$) to a crack arrested at ΔK_{th} was found to cause immediate recommencement of growth even though the applied stress intensity range did not exceed the threshold (Fig. 4(a)). Such behavior was concomitant with a measured reduction in closure; in the present case, the ratio K_{cl}/K_{max} was decreased from a value of 0.74 ($K_{cl} = 1.78$ MPa m$^{1/2}$) at the initial arrest to 0.62 ($K_{cl} = 1.49$ MPa m$^{1/2}$) following the compressive cycle, representing an effective increase in ΔK_{eff} from 0.63 to 0.92 MPa m$^{1/2}$. On subsequent crack extension, however, closure was re-generated, causing crack growth to decelerate progressively until re-arrest at a point where the magnitude of the closure had returned to the pre-overload threshold levels, *i.e.* $K_{cl}/K_{max} = 0.74$ with $\Delta K_{eff} = 0.63$ MPa m$^{1/2}$. The crack extension required for re-arrest in this alloy was found to be of the order of 170 μm, which is large compared with the scale of local plasticity at the threshold, *i.e.* large compared with a cyclic plastic zone size and a maximum plastic zone size of roughly 1.5 μm and 7.5 μm respectively.

Conversely, in the present tests, compression overloads applied to threshold cracks arrested at high load ratios, *i.e.* at $R = 0.75$, caused no such change in closure and no recommencement of cracking at ΔK_{th}. This is shown in Fig. 4(b) for a single overload cycle with an identical applied compressive load to the $R = 0.10$ test, *i.e.* for $P_{cp} = 1.78$ kN ($|K_{cp}| = 15.4$ MPa m$^{1/2}$) with $P_L = 2.3$ kN ($|K_L| = 20$ MPa m$^{1/2}$). Similar results were obtained for smaller compression overloads and for cycles where the crack was unloaded to zero load (*i.e.* tensile underloads in Fig. 4(c)), as listed in Table 3.

0.10 and $R = 0.75$. Threshold ΔK_{th} values were measured as 2.17 MPa m$^{1/2}$ and 1.06 MPa m$^{1/2}$ for R values of 0.10 and 0.75 respectively (Table 4). Corresponding crack closure measurements, plotted in terms of K_{cl}/K_{max} as a function of ΔK, are shown in Fig. 3. Characteristic of near-threshold behavior in many alloys (see for example ref. 19), the extent of closure at low load ratios was seen to increase progressively with decreasing ΔK as the threshold was approached, with K_{cl}/K_{max} increasing rapidly as ΔK approaches ΔK_{th}. No such closure above K_{min} could be detected at $R = 0.75$ (Table 4).

Corresponding near-threshold behavior under variable-amplitude loading conditions is illustrated in Fig. 4. As reported previously [11], at low load ratios, *i.e.* $R = 0.10$, the ap-

TABLE 3

Magnitude of overloads for tests performed at ΔK_{th}

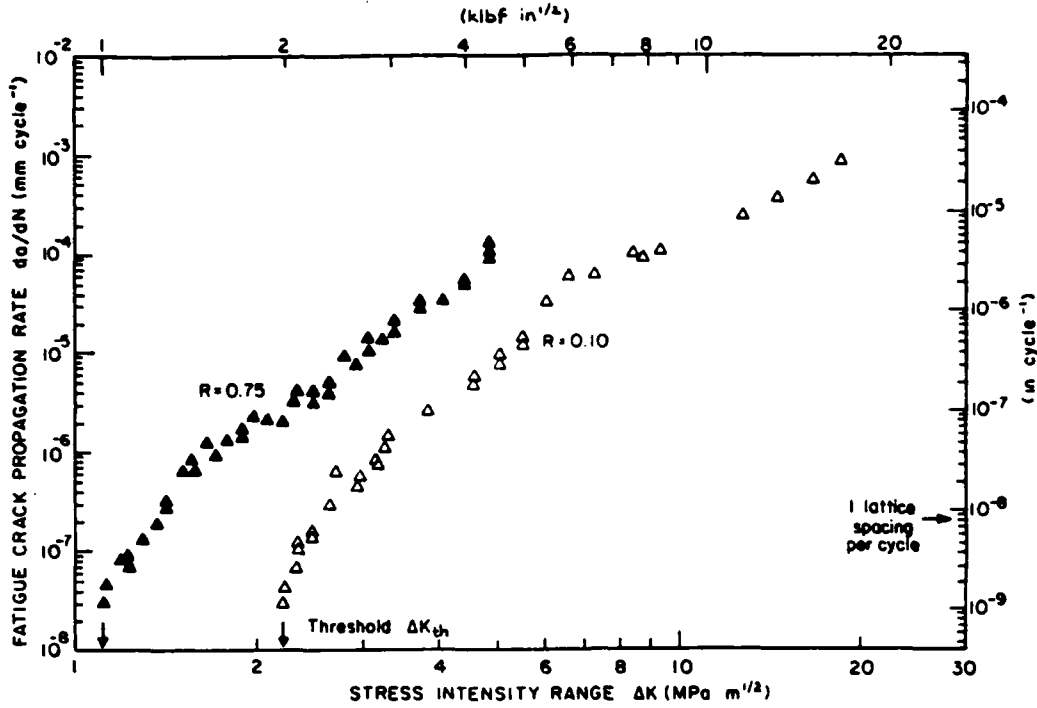| Test	R	Crack length (mm)	P_{cp} ($|K_{cp}|$) (kN (MPa m$^{1/2}$))	P_L ($|K_L|$) (kN (MPa m$^{1/2}$))	Result
Compression overload	0.10	25.1	1.78 (12.0)	2.14 (14.4)	Re-initiation
Compression overload	0.75	28.4	0.89 (7.7)	1.45 (12.0)	No effect
Compression overload	0.75	28.4	1.78 (15.4)	2.27 (20.0)	No effect
Tensile underload	0.75	26.4	0 (0)	0.56 (4.2)	No effect

14

Fig. 2. Steady state (constant-amplitude) fatigue crack propagation data for overaged aluminum alloy 7150-T7 tested in room air at R values of 0.10 and 0.75.

TABLE 4

Threshold data for tests on aluminum alloy 7150-T7

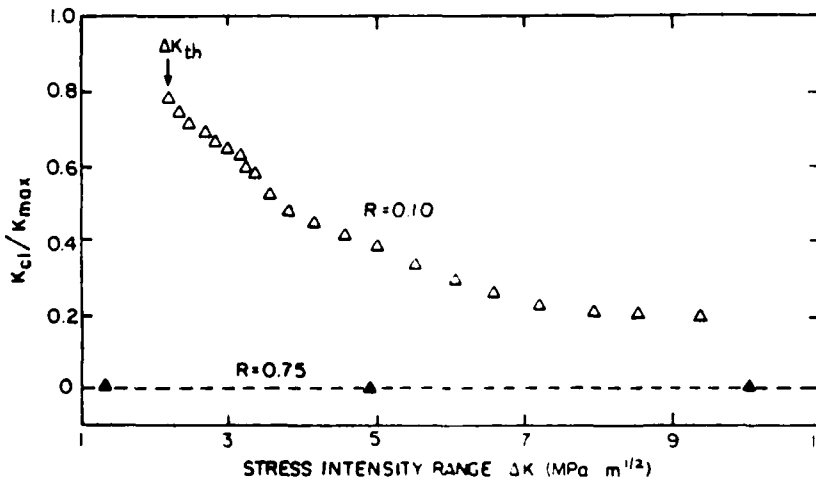| R	K_{max} (MPa m$^{1/2}$)	K_{min} (MPa m$^{1/2}$)	ΔK_{th} (MPa m$^{1/2}$)	K_{cl} (MPa m$^{1/2}$)	Plastic zone size (μm)	
					Cyclic	Monotonic
0.10	2.41	0.24	2.17	1.78	1.5	7.4
0.75	4.24	3.18	1.06	2.01	0.3	20.7

Fig. 3. Macroscopic crack closure data, plotted as the ratio K_{cl}/K_{max} of closure to maximum stress intensity as a function of nominal stress intensity range ΔK, for overaged aluminum alloy 7150-T7 tested at R values of 0.10 and 0.75. Data corresponds to growth rate results in Fig. 2 with $K_{cl} \gtrsim K_{min}$ [16].
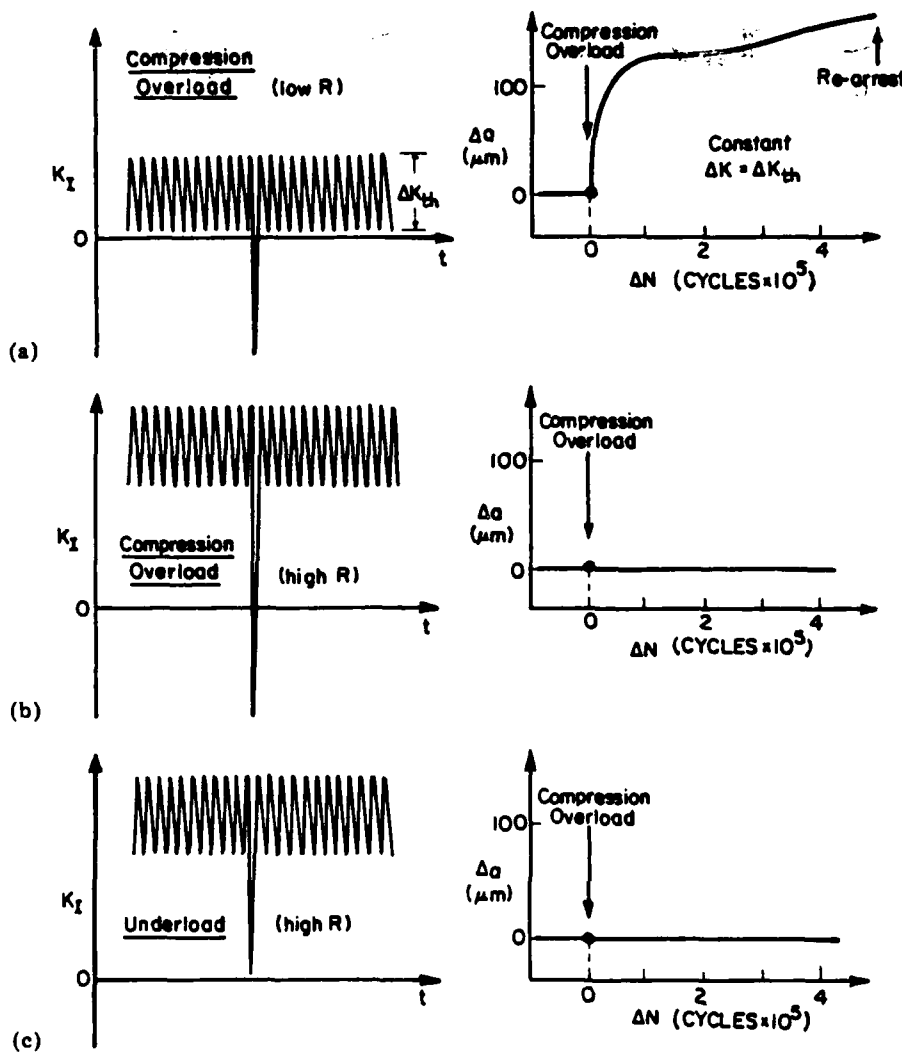
Fig. 4. Load spectra and corresponding crack extension Δa vs. number ΔN of cycles in aluminum alloy 7150-T7 following spike loads on arrested cracks at ΔK_{th}, showing (a) compression overload at $R = 0.10$, (b) compression overload at $R = 0.75$ and (c) tensile underload at $R = 0.75$.

Although crack closure loads were found to be unaffected by the overloads, K_{cl} values were measured at the threshold value ΔK_{th} of 1.06 MPa m$^{1/2}$ to be between 2.0 and 2.2 MPa m$^{1/2}$, i.e. less than K_{min} such that $\Delta K = \Delta K_{eff}$.

Such results are consistent with fractography which revealed marked evidence of abrasion and cracked asperities following the compression cycles, particularly at low load ratios. As shown in Fig. 5, compared with the distinct features of the pre-overload surfaces, fracture morphologies following the compressive cycles showed regions of compacted fretting oxide debris at low R, and crushed and broken fracture surface asperities at both $R = 0.10$ and $R = 0.75$. The extent of such "damage" to fracture surfaces, however, was far less apparent at high R. Since one of the major sources of crack closure in this microstructure arises from the wedging of fracture surface asperities [16], i.e. from roughness-induced closure, the effect of the compression can be reasoned to reduce the magnitude of closure at low load ratios primarily from this crushing action (see also refs. 11 and 12). Although a similar process appears to take place at high load ratios, the effect on the "crack driving force" is negligible as crack surface contact
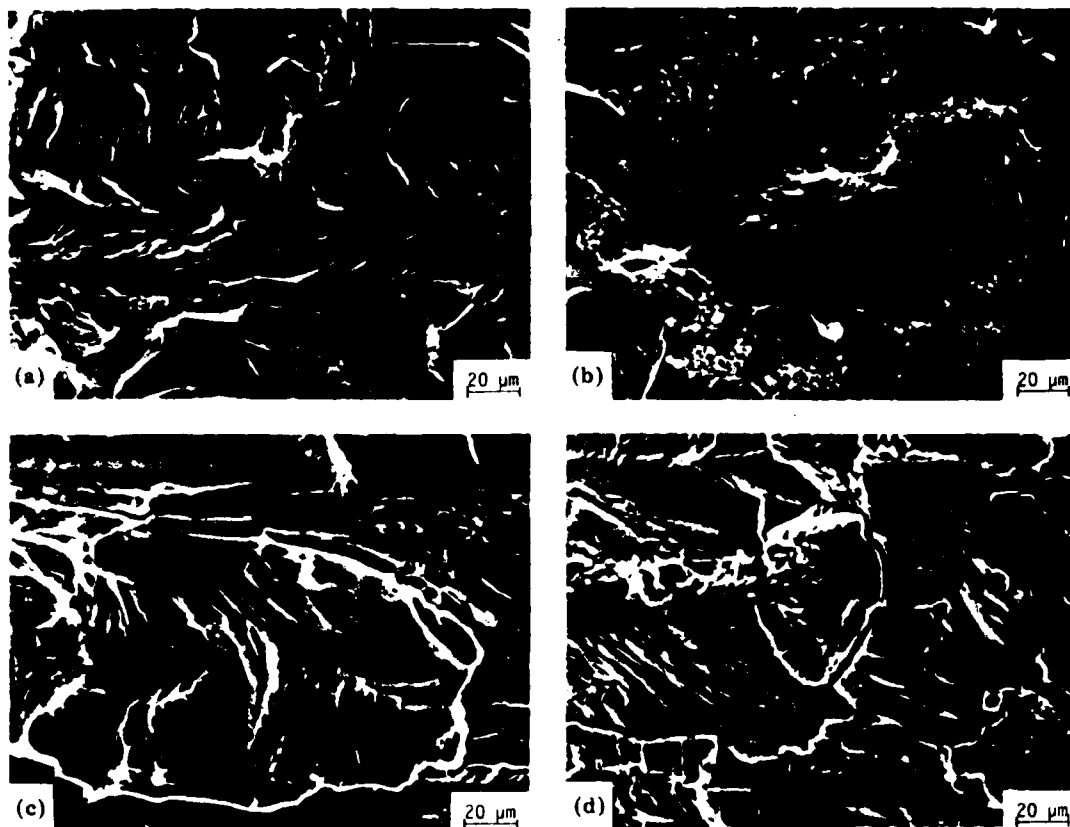
16

Fig. 5. Scanning electron micrographs of fatigue fracture morphology in overaged aluminum alloy 7150-T7 directly behind the crack tip at ΔK_{th}, showing (a) well-defined facets before application of compression overload, (b) fretting oxide debris at $R = 0.10$, (c) asperity cracking at $R = 0.10$ and (d) asperity cracking at $R = 0.75$, following application of overload. The arrow indicates the general direction of crack growth.

does not occur during the fatigue cycle owing to the much larger maximum crack opening displacements, i.e. K_{cl} remains less than K_{min}. Stress intensity calculations show this clearly in Fig. 6 where, at $R = 0.10$, the re-initiation in growth at ΔK_{th} can be attributed to a locally increased ΔK_{eff} from a reduction in K_{cl} whereas, at $R = 0.75$, any changes in K_{cl} can have no influence on ΔK_{eff} since $K_{cl} < K_{min}$.

4. CONCLUSIONS

Based on experiments on ingot metallurgy aluminum alloy 7150-T7 where single compression overload cycles were applied to fatigue cracks arrested at the fatigue threshold ΔK_{th} at both a low load ratio R (= 0.10) and a high load ratio ($R = 0.75$), the following conclusions can be made.

(1) As reported previously, large compression overloads applied at $R = 0.10$ caused an immediate recommencement in growth at ΔK_{th}, concomitant with a measured reduction in crack closure and evidence of abrasion on near-threshold fracture surfaces.

(2) Experiments at $R = 0.75$, employing either overload cycles with similar compressive loads or unloading cycles, were found to have no effect on arrested cracks at the threshold, consistent with measurements showing K_{cl} values to remain below K_{min}.

(3) Such results are consistent with the notion that the role of compression overload cycles in influencing near-threshold fatigue behavior in this alloy is related primarily to a reduction in roughness-induced crack closure from the compaction of fracture surface asperities.
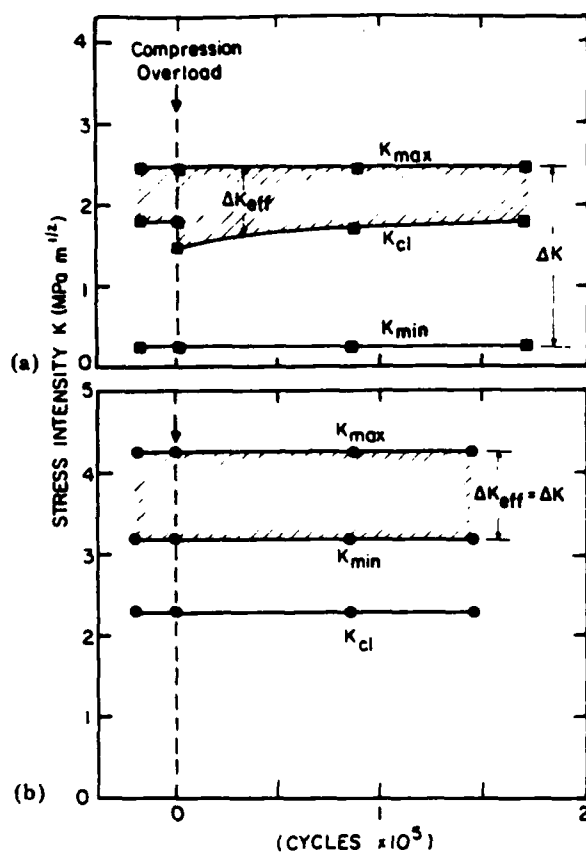
Fig. 6. Computation of the variation in the nominal stress intensity range ΔK and effective stress intensity range ΔK_{eff} for overaged aluminum alloy 7150-T7 following application of a single compression overload ($P_{cp} = 1.78$ kN) on arrested threshold cracks at (a) $R = 0.10$ and (b) $R = 0.75$. Calculations are based on K_{cl} values obtained from *in situ* back-face strain measurements.

REFERENCES

1 H. O. Fuchs and R. I. Stephens, *Metal Fatigue in Engineering*, Wiley-Interscience, New York, 1980.
2 C. M. Hudson and J. T. Scardina, *Eng. Fract. Mech., 1* (1969) 429.
3 T. M. Hsu and W. M. McGee, in D. F. Bryan and J. M. Potter (eds.), *Effect of Load Variables on Fatigue Crack Initiation and Propagation, ASTM Spec. Tech. Publ. 714*, 1974, p. 79.
4 J. Schijve and D. Broek, *Aircr. Eng., 34* (1962) 314.
5 R. I. Stephens, D. K. Chen and B. W. Hom, *Fatigue Crack Growth under Spectrum Loads, ASTM Spec. Tech. Publ. 595*, 1976, p. 27.
6 D. Gan and J. Weertman, *Eng. Fract. Mech., 15* (1981) 87.
7 P. Au, T. H. Topper and M. L. El Haddad, *Behavior of Short Cracks in Airframe Components*, in *AGARD Conf. Proc., 328* (1983) 11.1
8 M. Yu, T. H. Topper and P. Au, in C. J. Beevers (ed.), *Fatigue '84, Proc. 2nd Int. Conf. on Fatigue and Fatigue Thresholds*, Vol. 1, Engineering Materials Advisory Services, Warley, 1984, p. 179.
9 R. Marissen, K. H. Trautmann and H. Nowack, *Eng. Fract. Mech., 19* (1984) 863.
10 S. Suresh, *Eng. Fract. Mech., 20* (1984), in the press.
11 E. Zaiken and R. O. Ritchie, *Eng. Fract. Mech., 21* (1985), in the press.
12 R. O. Ritchie, E. Zaiken and A. F. Blom, in J. T. Fong (ed.), *Fundamental Questions and Critical Experiments on Fatigue, ASTM Spec. Tech. Publ.*, in the press.
13 N. Walker and C. J. Beevers, *Fatigue Eng. Mater. Struct., 1* (1979) 135.
14 K. Minakawa and A. J. McEvily, *Scr. Metall., 15* (1981) 633.
15 S. Suresh and R. O. Ritchie, *Metall. Trans. A, 13* (1982) 1627.
16 E. Zaiken and R. O. Ritchie, *Mater. Sci. Eng., 70* (1984) 151.
17 R. O. Ritchie, *Int. Metall. Rev., 20* (1979) 205.
18 V. B. Dutta, S. Suresh and R. O. Ritchie, *Metall. Trans. A, 15* (1984) 1193.
19 S. Suresh and R. O. Ritchie, in D. L. Davidson and S. Suresh (eds.), *Fatigue Crack Growth Threshold Concepts*, Metallurgical Society of AIME, Warrendale, PA, 1984, p. 227.

END
DTIC
9- 86